Supplementary Information

Spiroketal Formation and Modification in Avermectin Biosynthesis Involves a Dual Activity of AveC

Peng Sun,[†,‡] Qunfei Zhao,[†] Futao Yu,[†] Hua Zhang,[†] Zhuhua Wu,[†] Yinyan Wang,[†] Yan Wang,[†] Qinglin Zhang[†], and Wen Liu[†,*]

[†] State Key Laboratory of Bioorganic and Natural Products Chemistry, Shanghai Institute of Organic Chemistry, Chinese Academy of Sciences, 345 Lingling Road, Shanghai 200032, China;

[‡] Research Center for Marine Drugs, School of Pharmacy, Second Military Medical University, 325 Guo-He Road, Shanghai, 200433, China.

* To whom correspondence should be addressed: Shanghai Institute of Organic Chemistry, Chinese Academy of Sciences, 345 Lingling Rd., Shanghai 200032, China. Wen Liu, Email: wliu@mail.sioc.ac.cn, Tel: 86-21-54925111, Fax: 86-21-64166128

Table of Contents

5 Supplementary References

1. Supplementary Methods

1.1. General Materials and Methods

HPLC analysis was carried out on Agilent 1200 HPLC system (Agilent Technologies Inc., USA) with a Zorbax SB-C18 column (4.6 mm × 25 cm, 5 μm). Semipreparative HPLC was carried out on an Agilent 1100 system with a Zorbax SB-C18 column (9.4 mm × 25 cm, 5 μm). Preparative HPLC was carried out on an Agilent 1100 system with a Zorbax SB-C18 column (21.2 × 25 cm, 7 μm). Optical rotations were measured on an Autopol-IV polarimeter at the sodium D line (590 nm). UV absorption spectra were recorded on a Varian Cary 100 UV−vis spectrophotometer. NMR analysis was carried out on a Bruker AV-400, a Bruker AV-500 (Bruker Co. Ltd., Germany), or a Varian Unity Inova 600 (Varian Inc., USA) NMR spectrometer. Chemical shifts were reported in parts per million (δ); coupling constants (J) in Hz; assignments were supported by COSY, HSQC, HMBC, and NOESY experiments. Electrospray ionization MS (ESIMS) was performed on a Thermo Fisher LTQ Fleet ESIMS spectrometer (Thermo Fisher Scientific Inc., USA). High resolution ESIMS (HR-ESIMS) analysis was carried out on a Bruker APEXIII 7.0 Tesla FT-MS system (Bruker Co. Ltd., Germany). X-ray crystallographic analysis was carried out on a Bruker APEXII CCD diffractometer with Cu Kα radiation (λ = 1.54178 Å).

1.2. Gene Inactivation and Complementation

Inactivation of aveD. The genomic DNA of the *S. avermectinius* wild type strain serves as the template for PCR amplification. A 2.0 kb fragment obtained by using the primers aveD-L-for and aveD-L-rev and a 1.8 kb fragment obtained by using the primers aveD-R-for and aveD-R-rev were initially cloned into pMD19-T, giving pVL1001 and pVL1002, respectively. After sequencing to confirm the fidelity, the 2.0 kb EcoRI/HindIII and 1.8 kb HindIII/XbaI fragments were recovered and then co-ligated into the EcoRI/XbaI site of pKC1139, yielding the recombinant plasmid pVL1003, which encodes a G79L mutation for replacing the conserved motif DxGxGxG (of various methytransferases) by DxGxGxL and a S78K mutation for introducing a HindIII site. Introduction of pVL1003 into the AVE-producing strain *S. avermectinius* was carried out by *E.coli-Streptomyces*

conjugation, following the procedure described previously.[1] The colonies that were apramycin-resistant at 37□ were identified as the integrating mutants, in which a single-crosssover homologous recombination event took place. These mutants were further cultured on MS plates for several rounds in the absence of apramycin. The resulting strains that were apramycin-sensitive were subjected to PCR amplification (using the primers aveD-gt-for and aveD-gt-rev) to give a 2.0 kb product. HindIII digestion was then carried out on this PCR product to determine the genotype. For the recombinant strain VL1001, in which *aveD* was site-specific inactivated, HindIII digestion yielded the 0.6 kb and 1.4 kb fragments (Figure S7a).

Inactivation of aveC and aveCE, respectively, in VL1001. Considering that *aveC* is closely linked with *aveE* in the gene cluster (Figure 1), we carried out a two-step strategy to in-frame delete *aveC* in the *aveD* mutant strain VL1001.

To make the △*aveCDE* triple mutant strain, the genomic DNA of the *S. avermectinius* wild type strain serves as the template for PCR amplification. A 1.9 kb fragment obtained by using the primers aveCE-L-for and aveCE-L-rev and a 2.1 kb fragment obtained by using the primers aveCE-R-for and aveCE-R-rev were initially cloned into pMD19-T, giving pVL1004 and pVL1005, respectively. After sequencing to confirm the fidelity, the 1.9 kb EcoRI/PstI and 2.1 kb BglII/XbaI fragments were recovered, and then co-ligated with a 1.8 kb PstI/BglII erythromycin resistant gene-containing fragment into the EcoRI/XbaI site of pKC1139, yielding the recombinant plasmid pVL1006. Following the procedure described above, pVL1006 was introduced into VL1001 for double crossover recombination. The resulting strain VL1004, which is apramycin-sensitive but erythromycin-resistant, was then subjected to PCR amplification to validate the genotype. The amplification by using the primers aveCE-gt-for and aveCE-gt-rev yielded a desired 1.9 kb product (figure S7b). Further sequencing of this PCR product confirmed the genotype of VL1004, in which both *aveC* and *aveE* were replaced by the erythromycin resistant gene.

To make the △*aveCD* double mutant strain, a 1.9 kb fragment obtained from the genomic DNA of the wild type strain by using the primers aveC-R-for and aveC-R-rev was cloned into pMD19-T to yield pVL1007. The 1.9 kb EcoRI/PstI fragment from pVL1004 and the 1.9 kb PstI/XbaI fragment from pVL1007 were ligated into the EcoRI/XbaI sites of pKC1139 to yield pVL1008, in which a

756 bp in-frame coding region of *aveC* was deleted. Following the procedure described above, pVL1008 was introduced into VL1004 for double crossover recombination. The resulting strain VL1002, which is apramycin and erythromycin-sensitive, was then subjected to PCR amplification to validate the genotype. The amplification by using the primers aveCE-gt-for and aveCE-gt-rev yielded a desired 0.4 kb product (figure S7c). Further sequencing of this PCR product confirmed the genotype of VL1002, in which *aveC* was in-frame deleted.

Heterologous expression of meiC in VL1002. A 1.7 kb *meiC*-containing fragment was amplified from the genomic DNA of the MEI-producing strain *S. nanchangensis* by PCR using the primers meiC-c-for and meiC-c-rev, and then cloned into pMD19-T to yield pVL1009. After digestion with BamHI and XbaI, this 1.7 kb PCR product was recovered from pVL1009 and subsequently ligated with a 0.45 kb EcoRI/BamHII fragment from pWHM79 into the EcoRI/XbaI site of pSET152, yielding the recombinant plasmid pVL1010, in which *meiC* is under the control of the constitutive promoter *PermE**. pVL1010 was introduced into VL1002 (*aveCD* double mutant) by conjugation, generating the corresponding recombinant strain VL1003 for *meiC*-expressing.

Site-specific mutation of aveA1-M2-DH. The genomic DNA of the *S. avermectinius* wild type strain serves as the template for PCR amplification. A 1.1 kb fragment obtained by using the primers DH2-L-for and DH2-L-rev and a 1.1 kb fragment obtained by using the primers DH2-R-for and DH2-R-rev were initially cloned into pMD19-T, giving pVL1013 and pVL1014, respectively. After sequencing to confirm the fidelity, the 1.1 kb HindIII/KpnI fragment from pVL1013 and 1.1 kb KpnI/BamHI fragment from pVL1014 were recovered and then co-ligated into the HindIII/BamHI site of pKC1139, yielding the recombinant plasmid pVL1015, which encodes a H33G mutation for replacing the conserved motif HxxxGxxxxS by GxxxGxxxxS and has a mutation for replacing GGC ACG (encoding G37 and T38) to GGT ACC (without coding change) for introducing a KpnI site. Following the procedure described above, pVL1015 was introduced into the wild type strain for double crossover recombination. The resulting strains that were apramycin-sensitive were subjected to PCR amplification (using the primers DH2-gt-for and DH2-gt-rev) to give a 0.9 kb product. KpnI digestion was then carried out on this PCR product to determine the genotype. For the recombinant

strain VL1005, in which *aveA1-M2-DH* was site-specific inactivated, KpnI digestion yielded the 0.5 kb and 0.4 kb fragments (Figure S7d). This mutation was further confirmed by sequencing of the 0.9 kb PCR product.

Complementation of aveC in VL1002. A 1.2 kb *aveC*-containing fragment was amplified from the genomic DNA of the AVE-producing strain *S. avermectinius* by PCR using the primers aveC-c-for and aveC-c-rev, and then cloned into pMD19-T to yield pVL1011. After digestion with BamHI and XbaI, this 1.2 kb PCR product was recovered from pVL1011 and subsequently ligated with a 0.45 kb EcoRI/BamHII fragment from pWHM79 into the EcoRI/XbaI site of pSET152, yielding the recombinant plasmid pVL1012, in which *aveC* is under the control of the constitutive promoter *PermE**. pVL1012 was introduced into VL1002 (*aveCD* double mutant) by conjugation, generating the corresponding recombinant strain VL1006 for *aveC*-expressing.

Inactivation of aveE in VL1001. The genomic DNA of the *S. avermectinius* wild type strain serves as the template for PCR amplification. A 2.1 kb EcoRI/XbaI fragment obtained by using the primers aveE-L-for and aveE-L-rev was cloned into pOJ260, yielding pVL1016. A 2.3 kb XbaI/HindIII fragment obtained by using the primers aveE-R-for and aveE-R-rev was cloned into pVL1016 to give pVL1017. After this, a 1.9 kb XbaI fragment, which encodes the erythromycin resistance gene from *Saccharopolyspora erythraea* NRRL 2338, was amplified by primers ermE-S and ermE-A, and then inserted into the XbaI site of pVL1017, yielding the recombinant plasmid pVL1018. Following the procedure described above, pVL1018 was introduced into VL1001 for double crossover recombination. The resulting strain VL1008, which is apramycin-sensitive but erythromycin-resistant, was then subjected to PCR amplification to validate the genotype. The amplification by using the primers aveE-gt-for and aveE-gt-rev yielded a desired 3.0 kb product (Figure S7e). Further sequencing of this PCR product confirmed the genotype of VL1008, in which *aveE* was replaced by the erythromycin resistant gene.

1.3. Compound Isolation and Derivatization

1.3.1. Compound characterization in the *ΔaveDC* double mutant stain VL1002

Isolation of 1 and 1'. Fr. 24 was fractionated by silica gel CC (petroleum ether/EtOAc, 70:30), and subsequently by semipreparative HPLC (75% MeOH/H_2O, 3.0 mL min^{-1}) to afford compound **1** (260.3 mg, t_R = 17.2 min). Fr. 11 was fractionated by silica gel CC (petroleum ether/EtOAc, 85:15), and subsequently by semipreparative HPLC (80% MeOH/H_2O, 3.0 mL min^{-1}) to give compound **1'** (100.1 mg, t_R = 20.4 min).

Isolation of 2 and 2' (with a ratio at around 2 : 1). Fr. 26 (3.5 g) contained compounds **2**, which was unstable and easily converted into and **2'** and into **1** and **1'** during the purification by silica gel CC, Sephadex LH-20 or semipreparative HPLC. A small amount of metabolites (4.9 mg) containing **2** and **2'** (around 2 : 1) was eventually purified by preparative HPLC eluting with 75% MeOH/H_2O at a flow rate of 18.0 mL min^{-1}. To slow down the degradation, the purification and evaporation were carried out rapidly at < 20 °C. The NMR spectra of **2** and **2'** were recorded by a Bruker Avance 500 spectrometer with a cryogenic probe.

Derivatization of 2 and 2' to generate 4 and 4'. Fr. 26 (100.0 mg) was dissolved in a solution of anhydrous CH_2Cl_2 (7 mL) and MeOH (7 mL) at -80 °C under nitrogen atmosphere and then stirred. $NaBH_4$ (0.05 g) was added slowly to the solution. The resulting mixture was stirred vigorously for additional 30 min and warmed to room temperature. The reaction mixture was cooled to 0 °C with ice water and then quenched by adding dropwise saturated NH_4Cl aqueous solution. The biphasic system was extracted with EtOAc (2 × 20 mL). The combined organic layers were washed with H_2O (10 mL) and then dried by evaporation in vacuum to give the crude product. Further purification of the resulting product was accomplished by semipreparative HPLC eluting with a flow rate of 2.0 mL min^{-1} gradient as follows: T = 0 min, 80% B; T = 10 min, 80% B; T = 15 min, 85% B; T = 20 min, 100% B; T = 27 min, 100% B, and T = 30 min, 65% B (phase A, H_2O; phase B, MeOH). Two compounds with the same molecular weight of 588, **4** (26.1 mg, t_R = 10.2 min) and **4'** (7.0 mg, t_R = 12.3 min), were obtained.

Derivatization of 2 and 2' to generate 5. Methylation of Fr. 26 containing compound **2** was carried out according to a method described previously.[2] To a stirred solution of Fr. 26 (100 mg) and 1,8-bis(dimethylamino)naphthalene (proton sponge, 0.5 g, 0.230 mmol) in anhydrous CH_2Cl_2 (10 mL) at room temperature under nitrogen atmosphere was added methyl triflate (MeOTf, 208 μL, 0.32 g, 0.192 mmol). The resulting mixture was stirred for 24 h and then the suspension was treated with concentrated NH_4OH (2 mL) before stirred for 30 min. The biphasic mixture was diluted with CH_2Cl_2 (10 mL) and H_2O (5 mL) and the layers were shaken well before separation. The aqueous phase was extracted with CH_2Cl_2 (2 × 10 mL) and the combined organic extracts were washed with H_2O (20 mL). The organic phase was dried (Na_2SO_4) and concentrated in vacuum. The resulting crude residue was fractionated by silica gel CC eluting with 25% EtOAc in petroleum ether to yield 7 sub-fractions. LC-MS analysis indicated that sub-fraction 4 contained the methylated adducts. Further purification was accomplished by semipreparative HPLC eluting with 90% MeOH/H_2O at a flow rate of 2.5 mL·min^{-1} to give compound **5** (5.3 mg, t_R=13.5 min).

Partial purification of 3 and 3'. Fr. 26 contained the minor and unstable compound **3**, which can be rapidly converted to **3'**, and after longer incubation into the major pair **2** and **2'** and the minor pair **7** and **7'**, and then into **1** and **1'**. Partial purification of **3** and **3'** were achieved by semipreparative HPLC eluting with 65% CH_3CN/H_2O (10 °C, 2.5 mL·min^{-1}). The fraction containing **3** and **3'** was used for HR-ESIMS analysis and for *in vitro* biotransformations.

Derivatization of 3 and 3' to generate 6 and 6'. Selective oximation of the carbonyls of **3** and **3'** was carried out according to a method described previously.[3] A solution of NH_2OH-HCl in water (20 mL, 0.2 mM, neutralized by saturated sodium carbonate to reach pH at 7.0) was added dropwise to a methanol solution of Fr. 26 (150 mg in 10 mL). The mixture was stirred at room temperature for 30 min and then concentrated under reduced pressure. The residue was extracted with EtOAc (2 × 20 mL) and the combined organic phase was washed with H_2O (10 mL), dried (Na_2SO_4), and concentrated in vacuum. The resulting product was analyzed by HPLC-MS to target the peaks with MWs of 634, which were supposed to be *di*-oxime derivatives of unstable intermediates **3** and **3'**. Further purification was achieved by preparative HPLC eluting with 70% MeOH-H_2O at a flow rate

of 15.0 mL min^{-1} to give sub-fractions 1-5. Sub-fraction 3 was further purified by semipreparative HPLC eluting with 45% CH_3CN/H_2O at a flow rate of 3.0 mL·min^{-1} to give compound **6** (6.7 mg, t_R = 9.9 min). Sub-fraction 5 was subjected to semipreparative HPLC eluting with 40% CH_3CN/H_2O at a flow rate of 3.0 mL·min^{-1} to give compound **6'** (4.4 mg, t_R = 10.2 min).

Isolation of 7 and 7'. Fr. 19 was fractionated by preparative HPLC eluting with 80% $MeOH/H_2O$ at a flow rate of 15.0 mL min^{-1} to afford 8 sub-fractions. Sub-fraction 3 was further purified by semipreparative HPLC with 85% $MeOH/H_2O$ at a flow rate of 2.0 mL min^{-1} to yield compound **7** (19.0 mg, t_R = 12.3 min). Fr. 13 was fractionated by preparative HPLC eluting with 85% $MeOH/H_2O$ at a flow rate of 15.0 mL min^{-1} to afford 5 sub-fractions. Sub-fraction 4 was further purified by semipreparative HPLC with 90% $MeOH/H_2O$ at a flow rate of 2.5 mL min^{-1} to yield compound **7'** (6.5 mg, t_R = 10.9 min).

1.3.2. Compound characterization in the *ΔaveDE* double mutant stain VL1008

Isolation of compound 8. VL1008 was cultivated to accumulate about 4 L of the fermentation broth, which was then centrifuged for 30 min at 4,000 rpm to collect the mycelia. The mycelia were extracted with acetone (1 L × 3 times) and the combined acetone extracts were evaporated under reduced pressure to afford the crude extract (1.2 g). The crude extracts were subjected to the separation by a silica gel CC, with a gradient elution of EtOAc in petroleum ether (0:100 → 100:0, v/v), to give 12 fractions. Fraction 4 was further purified by semipreparative HPLC (90% $MeOH/H_2O$, 2.5 mL min^{-1}) to afford compound **8** (6.3 mg, t_R=10.9 min).

2. Supplementary Results

2.1. Physico-Chemical Properties and Structural Elucidations of 1 and 1'.

Compound 1. white amorphorous powder; $[\alpha]_D^{23}$ +80.5 (*c* 0.84, MeOH); UV (MeOH) λ_{max} (log ε) 247 nm (4.61); ^1H and ^{13}C NMR (400 and 100 MHz, respectively, acetone-d_6) see Table S3; ESIMS

m/z 591 $[M + Na]^+$, *m/z* 1159 $[2M + Na]^+$, HRESIMS *m/z* 591.3279 $[M + Na]^+$ (calcd for $[C_{34}H_{48}NaO_7]^+$, 591.3292).

Compound 1'. white amorphorous powder; $[\alpha]_D^{23}$ +124.3 (*c* 0.60, MeOH); UV (MeOH) λ_{max} (log ε) 246 nm (4.51); ^1H and ^{13}C NMR (400 and 100 MHz, respectively, acetone-d_6) see Table S3; ESIMS *m/z* 591 $[M + Na]^+$, *m/z* 1159 $[2M + Na]^+$, HRESIMS *m/z* 591.3279 $[M + Na]^+$ (calcd for $[C_{34}H_{48}NaO_7]^+$, 591.3292).

Structural elucidation of 1 and 1'. Compounds **1** and **1'** were shown with the same molecular weight of 568 and their formulae were determined equally to be $C_{34}H_{48}O_7$ by HRESIMS. The ^{13}C NMR and DEPT spectra of **1** revealed seven methyl groups, five methylene groups, fourteen methine groups, and eight quaternary carbons. The presence of five oxygenated carbons (δ_C 79.4, 74.7, 70.5, 69.4, 69.1 ppm, CH) indicates the loss of sugar moieties of natural AVEs. In the ^{13}C NMR spectrum of **1**, the absence of the oxymethine carbon at C-6 and oxymethylene carbon at C-8a indicates the lack of the furan ring from C-6 to C-8a, which was confirmed by HMBC cross peaks between H_3-8Me and C-7, C-8, and C-9. Instead, the NMR signals at lower field of ^1H and ^{13}C spectra (δ_C 158.0, 144.7, 132.6, 123.9, 123.8, 114.7 ppm; δ_H 7.25, 6.69 ppm) suggests the presence of a *tetra*-substituted aromatic ring, which was further conformed by the HMBC correlations between H_3-4Me and C-3, C-4, and C-5. The planar structure of **1** was elucidated by detailed analysis of the 1D and 2D NMR spectra (^1H, ^{13}C, DEPT, HSQC, COSY, and HMBC) of **1** and by comparison with its ^1H and ^{13}C chemical shifts of the aglycone moiety of natural AVEs (Table S3).[4] In a similar way, the planar structure of **1'** was established (Table S3). **1** and **1'** were shown with the same planar structures. **1'** was further determined to be the 6,8a-seco-6,8a-deoxy-2,5-didehydro AVE-B2a aglycone by ^1H and ^{13}C NMR data comparison,[5] which was previously isolated from the *S. avermectinius* mutant strain K2057 *(ΔaveDE*, X)[6] and *S. avermectinius* NEAU1069[5].

The difference of **1** and **1'** is shown in their relative configurations, which can be observed in their NOESY spectra. In the NOESY spectrum of **1**, the NOE effect between H-17 and H-22b and between H-19 and H-22a indicates that the C21-C22 single bond is in an α-orientation, while the NOE correlation between H-20b and H-25 suggests that the C21-O25 single bond has a β-orientation.

In the NOESY spectrum of **1'**, the obvious NOE effect between H-17 and H-25, H-27, and H_3-28 indicates that C21-O25 single bond possesses a α-orientation. The β-orientation of C21-C22 single bond was proved by NOE correlations between H-20b and H-22a, and between H-23 and H-22a. The structures and absolute configurations of the two enantiomers were further confirmed by X-ray crystallographic analysis. Thus, the absolute configurations at the C-21 position of **1** and **1'** were assigned as (*S*) and (*R*), respectively. **1** was assigned as (21S)-6,8a-seco-6,8a-deoxy-2,5-didehydro AVE-B2a aglycone.

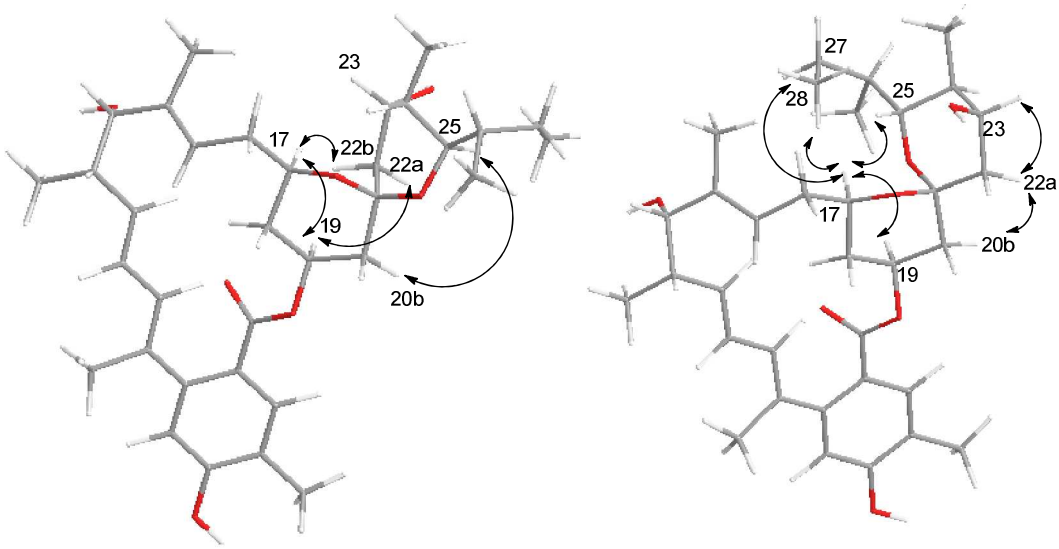

Key NOESY correlations of 1 (left) and 1' (right)

X-ray crystallographic analysis of 1 and 1'. Colorless crystal of **1** was obtained from toluene and hexane. Colorless crystal of **1'** was obtained from MeOH and hexane. The crystal diffraction data was collected at 296 K on a Bruker APEXII CCD diffractometer with Cu Kα radiation (λ=1.54178Å). The structures were solved by direct methods (SHELXS-97) and refined using full-matrix least-square difference Fourier techniques. All non-hydrogen atoms were refined anisotropically, and all hydrogen atoms were placed in geometrically idealized position and constrained to ride on their parent atoms.

Crystal data for **1** (CCDC 902276): $C_{34}H_{48}O_7$, *M*r = 568.72, orthorhombic, space group $P2_12_12_1$ with a = 10.780(2) Å, b = 14.083(3) Å, c = 22.105(4) Å, $\alpha = \beta = \gamma = 90°$, V =3356.0(12) Å^3, Z = 4, D_x = 1.126 mg/mm^3, μ (Cu Kα) = 0.622 mm^{-1}, and F(000) = 1232. Crystal dimensions: 0.10 × 0.18 ×

0.21mm^3. Independent reflections: 5837 (R_{int} = 0.0198). The final R_1 values were 0.0333, Flack parameter = 0.00(14), wR_2 = 0.0927 ($I > 2\sigma(I)$).

Crystal data for **1'** (CCDC 902279): $C_{34}H_{48}O_7 \bullet H_2O$, *M*r = 600.77, monoclinic, space group $P2_1$ with a = 12.806(3) Å, b = 9.263(2) Å, c = 14.377(3) Å, $\alpha = \gamma = 90°$, β = 93.38(3)°, V =1702.4(6) Å^3, Z = 2, D_x = 1.172 mg/mm^3, μ (Cu Kα) = 0.659 mm^{-1}, and F(000) = 652. Crystal dimensions: 0.11 × 0.13 × 0.16mm^3. Independent reflections: 5485 (R_{int} = 0.0248). The final R_1 values were 0.0418, Flack parameter = -0.01(17), wR_2 = 0.1164 ($I > 2\sigma(I)$).

2.2. Physico-Chemical Properties and Structural Elucidations of 2 and 2'.

Compound 2. white amorphorous powder; ^{1}H and ^{13}C NMR (500 and 125 MHz, respectively, acetone-d_6) see Table S4; ESIMS *m/z* 609 $[M + Na]^+$, *m/z* 1195 $[2M + Na]^+$, HRESIMS *m/z* 609.3387 $[M + Na]^+$ (calcd for $[C_{34}H_{50}NaO_8]^+$, 609.3398).

Compound 2'. white amorphorous powder; ^{1}H and ^{13}C NMR (500 and 125 MHz, respectively, acetone-d_6) see Table S4; ESIMS *m/z* 609 $[M + Na]^+$, *m/z* 1195 $[2M + Na]^+$, HRESIMS *m/z* 609.3389 $[M + Na]^+$ (calcd for $[C_{34}H_{50}NaO_8]^+$, 609.3398).

Structural elucidation of 2 and 2'. The molecular formula $C_{34}H_{50}O_8$ of **2** or **2'** was established by HR-ESIMS at *m/z* 609.3387 or 609.3389 ($[M + Na]^+$), ^{13}C and DEPT spectra. The structural elucidations of **2** and **2'** were carried out on a mixture, which was formed by rapid conversion from **2** to **2'** during sample dryness and NMR signals collection. The ^{1}H and ^{13}C NMR spectra both showed the coexistence of **2** and **2'** with a ratio of around 2 to 1 suggested on the base of the integration values in the ^{1}H NMR spectrum. Most of the signals in the ^{1}H and ^{13}C spectra were well separated, which made it possible to elucidate the structures of **2** and **2'** based on a detailed analysis of the NMR spectra. The ^{1}H and ^{13}C NMR spectra of **2** (the major) show a high similarity with those of **1** or **1'**, indicating the presence of the 16-membered lactone moiety and the *tetra*-substituted aromatic ring. The HMBC correlations from H-1, H-19 to C-1 prove the linkage of the 16-membered lactone via an ester carbonyl (C-1). The HMBC cross peaks from H-25 to the *di*-oxygenated

quaternary carbon (δ_C 98.3, C-21) establish the pyran ring from C-21 to C-25 via O-25, which was further confirmed by the obvious magnetic inequivalence of two geminally coupled protons of H_2-22 (δ_H 1.90, H-22a; δ_H 1.71, H-22b). Detailed analysis of the 1D and 2D NMR spectra determined the structure of to be **2**, a hemiacetal product with spiral ring-open form (Table S4).

The well separated signals of NMR resonance facilitated the elucidation of **2'**, minor compound in the mixture. Careful analyses of the well separated signals of **2'** in the 1D and 2D NMR spectra established the structure of **2'**, which is same as **2** in the 16-membered lactone moiety and the *tetra*-substituted aromatic ring (Table S4). The absence of HMBC correlation from H-25 to C-21 reveals the loss of the pyran ring from C-21 to C-25. The obvious magnetic inequivalence of two geminally coupled protons of H_2-18 (δ_H 0.76, H-18a; δ_H 2.01, H-18b) and H_2-20 (δ_H 1.49, H-20a; δ_H 2.04, H-20b) indicate the presence of a pyran ring from C-17 to C-21 via O-17. The pyran ring from C-17 to C-21 is also suggested by the apparent up-shield shift of carbon signals at C-18 (δ_C 43.3 in **2**, δ_C 38.4 in **2'**) and C-20 (δ_C 48.5 in **2**, δ_C 41.7 in **2'**), respectively. Meanwhile, the apparent down-shield shift of carbon signals at C-25 (δ_C 71.7 in **2**, δ_C 76.6 in **2'**) indicates the ring-open of the pyran ring from C-21 to C-25. A LC-MS analysis of NMR sample confirmed the coexistence of **2** and **2'**.

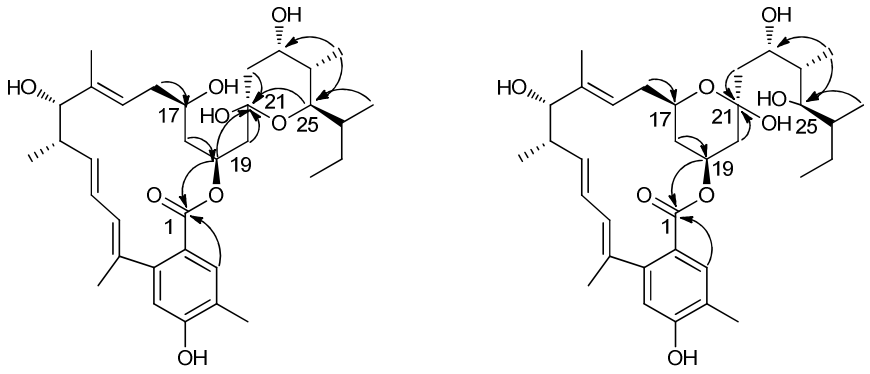

Key HMBC correlations of compound 2 (left) and 2' (right)

2.3. Physico-Chemical Properties of 3 and 3'.

Compound 3. ESIMS *m/z* 627 $[M + Na]^+$, *m/z* 1131 $[2M + Na]^+$, HRESIMS *m/z* 627.3491 $[M + Na]^+$ (calcd for $[C_{34}H_{52}NaO_9]^+$, 627.3503).

Compound 3'. ESIMS *m/z* 627 $[M + Na]^+$, *m/z* 1131 $[2M + Na]^+$, HRESIMS *m/z* 627.3493 $[M + Na]^+$ (calcd for $[C_{34}H_{52}NaO_9]^+$, 627.3503).

2.4. Physico-Chemical Properties and Structural Elucidations of 4 and 4'.

Compound 4. white amorphorous powder; $[\alpha]_D^{23}$ +41.8 (*c* 0.62, MeOH); UV (MeOH) λ_{max} (log ε) 244 nm (4.54); ^1H and ^{13}C NMR (400 and 100 MHz, respectively, acetone-d_6 and methanol-d_4) see Table S5 and Table S6; ESIMS *m/z* 611 $[M + Na]^+$, *m/z* 1199 $[2M + Na]^+$, HRESIMS *m/z* 611.3572 $[M + Na]^+$ (calcd for $[C_{34}H_{52}NaO_8]^+$, 611.3554).

Compound 4'. white amorphorous powder; $[\alpha]_D^{23}$ +31.9 (*c* 0.34, MeOH); UV (MeOH) λ_{max} (log ε) 243 nm (4.51); ^1H and ^{13}C NMR (400 and 100 MHz, respectively, acetone-d_6 and methanol-d_4) see Table S5 and Table S6; ESIMS *m/z* 611 $[M + Na]^+$, *m/z* 1199 $[2M + Na]^+$, HRESIMS *m/z* 611.3580 $[M + Na]^+$ (calcd for $[C_{34}H_{52}NaO_8]^+$, 611.3554).

Structural elucidation of 4 and 4'. The molecular formula $C_{34}H_{52}O_8$ of compounds **4** and **4'** were established by HRESIMS, ^{13}C NMR and DEPT spectra, showing the increase of two mass units in comparison with those of **2** and **2'**. The structures of **4** and **4'** were deduced by comparison of their NMR spectroscopic data with those of compounds **1** and **1'**. The ^{13}C NMR spectrum of **4** indicated the absence of a typical spiro carbon, which was usually at around 100 ppm. Instead, an additional oxymethine carbon (δ_C 70.3, C-21) was observed. This suggests the absence of a 6,6-spiroacetal ring in **4**. On the basis of detailed analysis of the 1D and 2D NMR spectroscopic data, the ^1H and ^{13}C signals of **4** were assigned (Table S5). The structure of **4** was similar to those of **1** or **1'** with a only exception for the 6,6-spiroacetal ring, which was replaced by a linear polyols chain attached at C-19. Similarly, the structure of **4'** was established based on the analyses of its NMR spectroscopic data (Table S5), which displayed the same planar structure as **4**.

The relative configurations at positions of C-17, C-19, C-23, and C-25 in **4** and **4'** were assigned according to the comparison with those of **1** and **1'**. However, the relative configurations at the

position of C-21 could not be assigned by analyzing the NOESY spectra. The ^{13}C chemical shifts of **4** and **4'** recollected in MeOD facilitated the assignment of the relative configurations at C-21 by comparing with Kishi's Universal NMR Database (Table S6)[7]. The 1,3,5-triol system was assigned as *syn*/*syn* in **4** and *anti*/*anti* in **4'** between C-19/C-21 and C-21/C-23 by comparison of the δ_C values at C-21 with the characteristic values of the central carbon of a 1,3,5-triol model system. Thus the relative configurations at C-21 were assigned as (*R*) for **4** and (*S*) for **4'**, respectively.

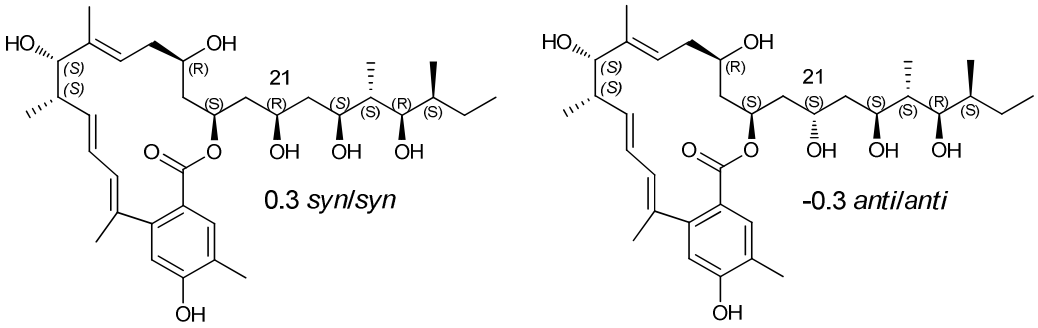

Assignment of the relative configurations of C-21 in 4 (left) and 4' (right). *Δδ* values between **4**, **4'** and the model system are shown, respectively.

2.5. Physico-Chemical Properties and Structural Elucidations of 5.

Compound 5. white amorphorous powder; $[\alpha]_D^{23}$ +28.5 (*c* 0.26, MeOH); UV (MeOH) λ_{max} (log ε) 243 nm (4.25), 206 nm (4.10); ^1H and ^{13}C NMR (500 and 125 MHz, respectively, acetone-d_6) see Table S7; ESIMS *m/z* 651 $[M + Na]^+$, *m/z* 1279 $[2M + Na]^+$, HRESIMS *m/z* 651.3897 $[M + Na]^+$ (calcd for $[C_{37}H_{56}NaO_8]^+$, 651.3867).

Structural elucidation of 5. The molecular formula of **5** was established as $C_{37}H_{56}O_8$ by HRESIMS together with ^{13}C NMR and DEPT spectroscopic data. The ^1H and ^{13}C NMR spectra of **5** are similar to those of compound **2**, except for the presence of three additional -OCH_3 groups. The locations of methoxy groups at C-5, C-17, and C-23 were suggested by the HMBC correlations between 5-OCH_3 and C-5, between 17-OCH_3 and C-17, and between 23-OCH_3 and C-23. The planar structure of **5** was further determined by detailed analyses of its 1D and 2D NMR data (Table S7). The relative configurations of **5** were deduced by NOESY spectrum analyses. The α-orientation of H-17 and H-

19 was proved by their NOE correlations. The NOE effects between 21-OH and 23-OCH_3, and between 21-OH and H-25 indicated the α-orientation of 21-OH, which was further confirmed by the β- orientation of H-23 and H_b-22 showing NOE correlations between H-23 and H_b-22, and by the α-orientation of H-25 showing NOE correlation between 24-OCH_3 and H-25.

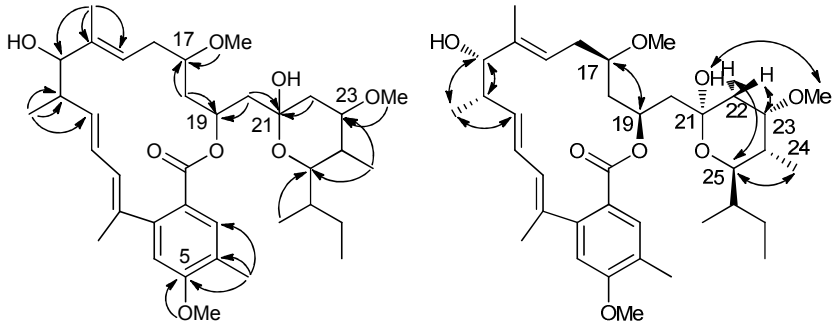

Key HMBC (left) and NOESY (right) correlations of compound 5

2.6. Physico-Chemical Properties and Structural Elucidations of 6 and 6'.

Compound 6. white amorphorous powder; $[\alpha]_D^{23}$ -76.8 (*c* 0.33, MeOH); UV (MeOH) λ_{max} (log ε) 240 nm (4.63); ^1H and ^{13}C NMR (500 and 125 MHz, respectively, acetone-d_6) see Table S8; ESIMS *m/z* 657 $[M + Na]^+$, *m/z* 1291 $[2M + Na]^+$, HRESIMS *m/z* 657.3748 $[M + Na]^+$ (calcd for $[C_{34}H_{54}N_2NaO_9]^+$, 657.3722).

Compound 6'. white amorphorous powder; $[\alpha]_D^{23}$ -71.2 (*c* 0.22, MeOH); UV (MeOH) λ_{max} (log ε) 240 nm (4.61); ^1H and ^{13}C NMR (500 and 125 MHz, respectively, acetone-d_6) see Table S8; ESIMS *m/z* 657 $[M + Na]^+$, *m/z* 1291 $[2M + Na]^+$, HRESIMS *m/z* 657.3738 $[M + Na]^+$ (calcd for $[C_{34}H_{54}N_2NaO_9]^+$, 657.3722).

Structural elucidation of 6 and 6'. The molecular formula $C_{34}H_{54}N_2O_9$ of compound **6** and **6'** was determined by analyses of their HRESIMS, ^{13}C NMR and DEPT data. The ^{13}C spectrum of **6** indicates the presence of two oxime carbons (δ_C 154.1, C-5; δ_C 157.4, C-21). Their locations are suggested by the HMBC correlations from H_3-4Me to C-5, and from H_2-20, H_2-22 to C-21. The absence of two aromatic singlet protons in the lower field of ^1H spectrum reveals the lack of aromatic ring. The COSY correlation

between H-2 and H-3 and the HMBC cross peaks between H_2-6 and C-2, C-4, C-5, C-7 suggest a six-membered ring from C-2 to C-7. The loss of the spiro carbon (δ_C at around 100 ppm, C-21) in the ^{13}C spectrum suggested the opening of the spiro-bicyclic ring, similar to that in **4** and **4'**. A detailed analysis of 1D and 2D NMR spectra established the planar structure of compound **6** (Table S8). The relative configuration of **6** was deduced by analyzing NOESY spectrum and by comparing with the known configurations of natural AVEs. The planar structure of **6'** is the same with that of **6** based on detailed analysis of its NMR data (Table S8). Compounds **6** and **6'** appear to be ketoxime stereoisomers. The configurations of oximes at C-5 and C-21 of **6** and **6'** were established on the base of the *syn-anti* α-carbon difference[8]. The ketoximes at C-5 of **6** and **6'** are not isomeric due to the effect of a quaternary α-carbon (C-4) and the steric interference between the oxime OH and 4-methyl. The oxime OHs at C-5 of **6** and **6'** were indicated to be *anti* to the C-4 based on the carbon shifts of $\Delta_{\alpha\text{-syn}}$ (-16.6 for **6**, -16.4 for **6'**, C-6, compared with C-6 of **7**) and $\Delta_{\alpha\text{-anti}}$ (-3.0 ppm for **6**, -3.0 ppm for **6'**, C-4, compared with C-4 of **7**). The ketoximes at C-21 of **6** and **6'** appear to be stereoisomeric. Because the up-field shifts effect for the α-*syn* carbon could be greater than that for α-*anti* carbon, the oxime OH at C-21 of **6** was indicated to be *anti* to C-20 (δ_C 41.5 ppm) and *syn* to C-22 (δ_C 34.9 ppm). In contrast, the oxime OH at C-21 of **6'** was indicated to be *syn* to C-20 (δ_C 33.3 ppm) and *anti* to C-22 (δ_C 39.7 ppm). Thus, the relative configurations of oxime at C-21 were assigned as (*E*) for **6** and (*Z*) for **6'**.

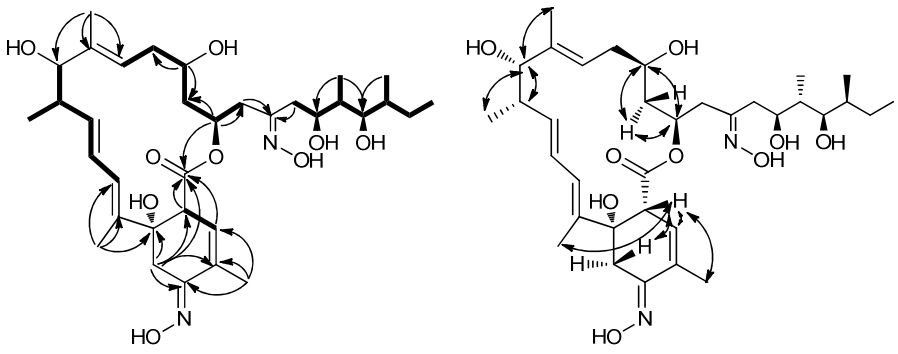

COSY, Key NOESY and HMBC correlations of compound 6

2.7. Physico-Chemical Properties and Structural Elucidations of 7 and 7'.

Compound 7. white amorphorous powder; $[\alpha]_D^{23}$ 33.1 (*c* 1.32, MeOH); UV (MeOH) λ_{max} (log ε) 239 nm (4.13); ^{1}H and ^{13}C NMR (500 and 125 MHz, respectively, acetone-d_6) see Table S9; ESIMS *m/z* 609 $[M + Na]^+$, *m/z* 1195 $[2M + Na]^+$, HRESIMS *m/z* 609.3421 $[M + Na]^+$ (calcd for $[C_{34}H_{50}NaO_8]^+$, 609.3398).

Compound 7'. white amorphorous powder; $[\alpha]_D^{28}$ 53.6 (*c* 0.32, $CHCl_3$); UV (MeOH) λ_{max} (log ε) 242 nm (4.40); ^{1}H and ^{13}C NMR (500 and 125 MHz, respectively, acetone-d_6) see Table S9; ESIMS *m/z* 609 $[M + Na]^+$, *m/z* 1195 $[2M + Na]^+$, HRESIMS *m/z* 609.3416 $[M + Na]^+$ (calcd for $[C_{34}H_{50}NaO_8]^+$, 609.3398).

Structural elucidation of 7 and 7'. Compounds **7** and **7'** have a same molecular weight of 586 (609 $[M + Na]^+$). Their formulae were determined to be $C_{34}H_{50}O_8$ by their HRESIMS. The ^{13}C spectrum of **7** indicates the presence of a ketone carbon (δ_C 197.1, C-5). Its location at C-5 is suggested by the HMBC correlations between H_3-4Me, H_2-6 and C-5. The COSY correlation between H-2 and H-3 and the HMBC cross peaks between H_2-6 and C-2 and C-7 further indicates a six-membered ring from C-2 to C-7. By detailed analysis of the NMR experiments and by comparison its ^{13}C chemical shifts with those of **1** and **1'**, the planar structure of **7** was elucidated (Table S9). In a similar way, the planar structure of **7'** was also established (Table S9). Compounds **7** and **7'** were shown with a same planar structure.

The relative configurations of **7** and **7'** were assigned by their NOESY spectra and by the comparison of their ^{13}C data with those of **1** and **1'**. In the NOESY spectrum of **7** the NOE effects between H-17 and H-22b and between H-19 and H-22a indicate the C21-C22 single bond was a α-orientation. While the NOE correlation between H-20b and H-25 suggests that the C21-O25 single bond has a β-orientation. In the NOESY spectrum of **7'**, the NOE effects between H-17 and H-25, H-27, and H_3-28 indicate that C21-O25 single bond has a α-orientation. The β-orientation of C21-C22 single bond is suggested by NOE correlations between H-20b and H-22a, and between H-23 and H-22a. Thus, the absolute configurations at C-21 of **7** and **7'** was assigned as (*S*) and (*R*), respectively. Compound **7'** was further confirmed to be the 6,8a-seco-6,8a-deoxy-5-oxo-avermectin

B2a aglycone, which have been previously isolated from a mutant strain *S. avermectinius* MA 5218[9]. Compound **7** was assigned as (21S)- 6,8a-seco-6,8a-deoxy-5-oxo-avermectin B2a aglycone.

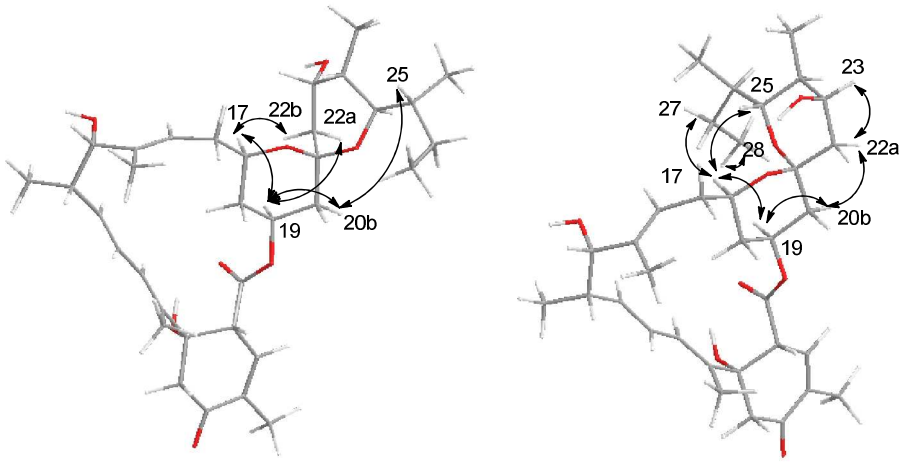

Key NOESY correlations of compound 7 (left) and 7' (right)

2.8. Physico-Chemical Properties and Structural Elucidations of 8.

Compound 8. white amorphorous powder; $[\alpha]_D^{23}$ 41.5 (*c* 0.72, $CHCl_3$); UV (MeOH) λ_{max} (log ε) 239 nm (4.33); ^1H and ^{13}C NMR (400 and 100 MHz, respectively, acetone-d_6) see Table S10; ESIMS *m/z* 569 $[M + H]^+$, *m/z* 1159 $[2M + Na]^+$, HRESIMS *m/z* 569.3456 $[M + H]^+$ (calcd for $[C_{34}H_{49}O_7]^+$, 569.3473).

Structural elucidation of 8. The formula of compound **8** was established to be $C_{34}H_{48}O_7$ by HRESIMS, ^{13}C NMR and DEPT spectra. The ^{13}C NMR spectrum of compound **8** was similar to that of **7** except two additional sp^2 carbons in the lower field (δ_C 135.9, C-22; δ_C 129.5, C-23), which suggest the presence of a C22-C23 double-bond. The structure of compound **8** was elucidated by detailed analysis of its 1D and 2D NMR spectra and by comparison with the NMR data of natural "1" type AVEs (Table S10)[4]. In the NOESY spectrum of **8**, the NOE correlations between H-17 and H-25, H_2-27, and H_3-28 indicate a α-orientation of the C21-O25 single bond. The β-orientation of C21-C22 single bond is suggested by NOE correlations between H-20b and H-23. Compound **8** was further confirmed to be the 6,8a-seco-6,8a-deoxy-5-oxo-avermectin Bla aglycone, which has

previously been isolated from mutant K2057 (aveD aveE X)[6] and proved to be a biosynthetic intermediate of AVE-A1a and AVE-B1a by feeding experiments[9b].

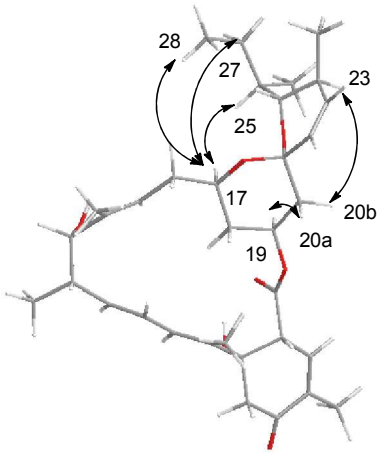

Key NOESY correlations of compound 8

3. Supplementary Tables

Table S1. Bacterial strains and plasmids

Strain/Plasmid	Characteristic(s)	Sources/Reference
E. coli		
DH5α	Host for general cloning	Invitrogen
ET12567/pUZ8002	Donor strain for conjugation between *E.coli* and *Streptomyces*	[10]
Rosetta	Host for gene expression	Novagen
VL2001	recombinant *E. coli* strain for *meiC* expression	This study
S. avermectinius		
ATCC 31267	Wild type strain, avermectin producing	ATCC
VL1001	*ΔaveD* mutant, G79L, producing only "B" components	This study
VL1002	*ΔaveDC* double mutant	This study
VL1003	VL1002 derivative carrying *meiC* in trans	This study
VL1004	*ΔaveDCE* triple mutant	This study
VL1005	ATCC 31267 derivative for site-specific mutation of AveA1-M2-DH	This study
VL1006	VL1002 derivative carrying *aveC* in trans	This study
VL1008	*ΔaveDE* double mutant	This study
S. lividans		
TK 24	Host for gene expression, wide type	[1]
VL1007	TK 24 derivative carrying pVL1012 for *aveC* expression	This study
VL1009	TK 24 derivative carrying pSET152	This study
S. nanchangensis		
NS3226	Wild type strain, meilingmycins producing	[11]
Plasmids		
pMD19-T	*E. coli* subcloning vector	Takara

pKC1139	*E.coli-Streptomyces* shuttle vector for gene inactivation, temperature sensitive replication in *Streptomyces*	[1]
pOJ260	*E.coli-Streptomyces* shuttle vector for gene inactivation, non-replicating in *Streptomyces*	NRRLB-14785
pSET152	*E.coli-Streptomyces* shuttle vector	[1]
pQ8	Protein expression vector, encoding His-MBP-His tag	[12]
pWHM79	pGEM-3zf derivative carrying a 0.5 kb fragment containing the *PermE** promoter	[13]
pAGe-2	Erythromycin resistance cassette containing plasmid	[14]
pVL1001	pMD-19T derivative containing partial *aveD* fragment	This study
pVL1002	pMD-19T derivative containing partial *aveD* fragment	This study
pVL1003	pKC1139 derivative containing EcoRI-HindIII fragment of pVL1001 and XbaI-HindIII fragment of pVL1002，construct for *aveD* site-specific mutation	This study
pVL1004	pMD-19T derivative containing partial *aveC* fragment	This study
pVL1005	pMD-19T derivative containing partial *aveE* fragment	This study
pVL1006	pKC1139 derivative containing EcoRI-PstI fragment of pVL1004, PstI-BglII erythromycin resistance cassette and BglII-XbaI fragment of pVL1005, construct for *aveC* and *aveE* deletion in VL1001	This study
pVL1007	pMD-19T derivative containing partial *aveC* fragment	This study
pVL1008	pKC1139 derivative containing EcoRI-PstI fragment of pVL1004 and PstI-XbaI fragment of pVL1007, construct for *aveC* in-frame deletion in VL1001	This study
pVL1009	pMD-19T derivative containing *meiC* fragment	This study
pVL1010	pSET152 derivative containing EcoRI-BamHI fragment of *PermE** and BamHI-XbaI fragment of pVL1009, construct for *meiC* heterologous complementation in	This study

	VL1002	
pVL1011	pMD-19T derivative containing *aveC* fragment	This study
pVL1012	pSET152 derivative containing EcoRI-BamHI fragment of *PermE** and BamHI-XbaI fragment of pVL1011, construct for *aveC* complementation in VL1002	This study
pVL1013	pMD-19T derivative containing partial *aveA1-M2-DH* fragment	This study
pVL1014	pMD-19T derivative containing partial *aveA1-M2-DH* fragment	This study
pVL1015	pKC1139 derivative containing HindIII-KpnI fragment of pVL1013 and KpnI-BamHI fragment of pVL1014，construct for AveA1-M2-DH site-sepecific mutation in ATCC 31267	This study
pVL1016	pOJ260 derivative containing partial *aveE* fragment	This study
pVL1017	pOJ260 derivative containing partial *aveE* fragment	This study
pVL1018	pOJ260 derivative containing EcoRI-XbaI fragment of pVL1016, XbaI-XbaI fragment of erythromycin resistance gene and XbaI-HindIII fragment of pVL1017，construct for *aveE* deletion in VL1001	This study
pVL1019	pQ8 derivative containing *meiC* fragment	This study

Table S2. Primers used in this study.

Primers	Sequences
aveD-L-for	5’- TAT GAA TTC CCT CGT CGA GGT GGC CGA G -3’ (EcoRI site underlined)
aveD-L-rev	5’- TTA AAG CTT ACC GCA GCC GAC GTC CAG G -3’ (HindIII site underlined)
aveD-R-for	5’- TTA AAG CTT AAG CCG GCG GTG CGG CTC G -3’ (HindIII site underlined)
aveD-R-rev	5’- TTA TCT AGA TCC TCA CCC TTT CCC CCG GC -3’ (XbaI site underlined)
aveD-gt-for	5’- CCC CGC CGT CCA TCC TCT G -3’
aveD-gt-rev	5’- TAC CGC GGC CGC ACT CAC G -3’
aveCE-L-for	5’- TTA GAA TTC CAT CAC GCT GCT GGA CTT CG -3’ (EcoRI site underlined)
aveCE-L-rev	5’- ACG CCT GCA GGG CCA GAA ACA G -3’ (PstI site underlined)
aveCE-R-for	5’-TAT AGA TCT CGC CGA TGC ATT TGT AGG TGC C-3’ (BglII site underlined)
aveCE-R-rev	5’- TTA TCT AGA GTT CCG GTC TGC ATC CCA TG -3’ (XbaI site underlined)
aveCE-gt-for	5’- TGC TGT TTC TGG CCC TGC AG -3’
aveCE-gt-rev	5’- GCG CTC GGC ACC TAC AAA TG -3’
aveC-R-for	5’- TAT CTG CAG GTG AAT GCC GTG ATG TTC CTC -3’ (PstI site underlined)
aveC-R-rev	5’- TAT TCT AGA TGC TCT CCT CCA CCA CAT CCT C -3’ (XbaI site underlined)
meiC-c-for	5’- TAT GGA TCC CTG CGC AAT AGG CTC ACC AC -3’ (BamHI site underlined)
meiC-c-rev	5’- TAT TCT AGA CGG GAG GTG TCT ACA AGT GC -3’ (XbaI site

	underlined)
aveC-c-for	5’- TAT GGA TCC AGA TGG ACA TCG ACG ACC TG -3’ (BamHI site underlined)
aveC-c-rev	5’- TAT TCT AGA CCT TCT CCG TCT CCT CCG ACC -3’ (XbaI site underlined)
DH2-L-for	5’-CTT AAG CTT CCC CTC CTC ACC CAA AAC GAC AAC-3’(HindIII site underlined)
DH2-L-rev	5’- CAC GGT ACC GCC GAC GGC CCC GTC AGC CAG CCA C -3’ (KpnI site underlined)
DH2-R-for	5’- GGG GCC GTC GGC GGT ACC GTG CTG GGC GCC ACC -3’(KpnI site underlined)
DH2-R-rev	5’-CTT GGA TCC ACC CCG GGT CAC CAC CAC CAG CCG -3’ (BamHI site underlined)
DH2-gt-for	5’- CCT CAC CCA CCA CAA CCT CCC CAA CC-3’
DH2-gt-rev	5’- CGG CTG GAC CAC ACC ATC CAG CAA CG-3’
aveE-L-for	5’- TT GAA TTC TGG GAA GAG GGC ACA GGG AT -3’ (EcoRI site underlined)
aveE-L-rev	5’- TGC TCT AGA ATC GCT GAA CCG AGG AGT G -3’ (XbaI site underlined)
aveE-R-for	5’- TGC TCT AGA CGA TAC GGC TAC GAG GAT GGG -3’ (XbaI site underlined)
aveE-R-rev	5’- CCC AAG CTT GGC TGA GGA GGA TGG TGT G -3’ (HindIII site underlined)
ermE-S	5’- TGC TCT AGA GCA GTA GGC GGC GAA CTC C -3’ (XbaI site underlined)
ermE-A	5’- TGC TCT AGA GGC TTT CCT ACA CCA CGT T -3’ (XbaI site underlined)
aveE-gt-for	5’- CAT TCC GTT CTC GTC TCC AA -3’

aveE-gt-rev	5’- AAG CCC AGA AAC CAC TCC GAG -3’

Table S3. ^{1}H and ^{13}C NMR spectroscopic data for 1 and 1'[a]

	1			1'		
position	δ_H (mult., J in Hz)	δ_C	mutl.	δ_H (mult., J in Hz)	δ_C	mutl.
1		169.7	C		169.4	C
2		123.9	C		123.8	C
3	7.25 (1H, s)	132.6	CH	7.30 (1H, s)	132.9	CH
4		123.8	C		123.7	C
4-Me	2.16 (3H, s)	15.7	CH_3	2.16 (3H, s)	15.7	CH_3
5		158.0	C		158.2	C
5-OH	8.61 (1H, s)			8.67 (1H, s)		
6	6.69 (1H, s)	114.7	CH	6.17 (1H, s)	114.8	CH
7		144.7	C		145.2	C
8		135.5	C		135.7	C
8-Me	2.03 (3H, s)	18.4	CH_3	2.02 (3H, s)	18.5	CH_3
9	5.59 (1H, d, 8.0)	129.5	CH	5.59 (1H, d, 10.0)	129.3	CH
10	6.18 (1H, dd, 12.0, 8.0)	127.6	CH	6.20 (1H, dd, 15.2, 10.0)	127.7	CH
11	5.46 (1H, dd, 12.0, 8.0)	136.6	CH	5.48 (1H, dd, 24.8, 10.0)	136.6	CH
12	2.58 (1H, m)	41.9	CH	2.60 (1H, m)	41.9	CH
12-Me	1.14 (3H, d, 5.6)	19.3	CH_3	1.14 (3H, d, 6.8)	19.3	CH_3
13	3.94 (1H, brs)	79.4	CH	3.95 (1H, brs)	79.4	CH
13-OH	3.74 (1H, d, 4.0)			3.80 (1H, d, 5.6)		
14		139.1	C		139.8	C
14-Me	1.59 (3H, s)	15.4	CH_3	1.61 (3H, s)	15.3	CH_3
15	5.31 (1H, brd)	118.3	CH	5.32 (1H, m)	117.9	CH
16a	2.26 (2H, m)	35.2	CH_2	2.32 (1H, m)	34.3	CH_2
16b				2.29 (1H, m)		
17	3.71 (1H, m)	70.5	CH	3.85 (1H, m)	69.9	CH
18a	0.76 (1H, q, 9.6)	37.9	CH_2	1.93 (1H, m)	37.4	CH_2

18b	1.86 (1H, brd, 9.6)			0.76(1H, q, 12.4)		
19	5.18 (1H, m)	69.4	CH	5.34 (1H, m)	67.6	CH
20a	1.23 (1H, m)	40.7	CH_2	1.86 (1H, m)	42.1	CH_2
20b	2.83 (1H, dd, 9.3, 3.6)			1.42 (1H, m)		
21		100.4	C		100.8	C
22a	1.57 (1H, d, 2.0)	40.1	CH_2	1.86 (1H, m)	42.3	CH_2
22b	2.27 (1H, m)			1.68 (1H, dd, 14.0, 3.2)		
23	4.00 (1H, m)	69.1	CH	3.65 (1H, dd, 10.0, 3.0)	70.4	CH
23-OH	3.92 (1H, d, 2.8)			3.37 (1H, d, 10.0)		
24	1.71 (1H, m)	36.8	CH	1.58 (1H, m)	36.7	CH
24-Me	0.84 (3H, d, 4.0)	13.5	CH_3	0.84 (3H, d, 8.0)	14.2	CH_3
25	3.65 (1H, dd, 7.6, 1.2)	74.7	CH	3.61 (1H, d, 12.0)	71.7	CH
26	1.46 (1H, m)	36.3	CH	1.53 (3H, m)	36.2	CH
26-Me	0.83 (3H, d, 4.0)	13.0	CH_3	0.86 (3H, d, 8.0)	12.2	CH_3
27a	1.26 (1H, m)	27.8	CH_2	1.41 (1H, m)	28.2	CH_2
27b	1.42 (1H, m)			1.54 (1H, m)		
28	0.84 (3H, t, 4.0)	12.4	CH_3	0.95(3H, t, 7.2)	12.8	CH_3

[a]In acetone-d_6, 400 MHz for ^{1}H and 100 MHz for ^{13}C NMR; Chemical shifts are reported in ppm; All signals are determined by ^{1}H-^{1}H COSY, HSQC, HMBC, and NOESY correlations.

Table S4. ^{1}H and ^{13}C NMR spectroscopic data for 2 and 2'[a]

	2 (major)			2' (minor)		
position	δ_H (mult., J in Hz)	δ_C	mutl.	δ_H (mult., J in Hz)	δ_C	mutl.
1		170.9	C		171.3	C
2		123.1	C		123.0	C
3	7.44 (1H, s)	133.8	CH	7.31 (1H, d, 1.0)	133.0	CH
4		124.1	C		124.4	C
4-Me	2.17 (3H, s)	15.8	CH_3	2.17 (1H, s)	15.7	CH_3
5		159.4	C		159.0	C
5-OH						
6	6.56 (1H, s)	115.1	CH	6.59 (1H, d, 4.3)	114.8	CH
7		146.9	C		145.9	C
8		137.1	C		136.5	C
8-Me	2.05 (3H, s)	18.9	CH_3	2.06 (3H, s)	18.5	CH_3
9	5.60 (1H, d, 10.8)	129.4	CH	5.60 (1H, d, 10.8)	129.4	CH
10	6.16 (1H, dd, 15.1, 10.8)	127.8	CH	6.22 (1H, dd, 15.0, 10.9)	128.3	CH
11	5.51 (1H, dd, 15.1, 9.8)	136.5	CH	5.45 (1H, dd, 15.0, 10.0)	136.1	CH
12	2.49 (1H, m)	41.8	CH	2.64 (1H, m)	42.1	CH
12-Me	1.18 (3H, d, 6.9)	19.1	CH_3	1.18 (3H, d, 6.9)	19.1	CH_3
13	3.92 (1H, brs)	79.8	CH	3.96 (1H, s)	80.1	CH
13-OH						
14		139.3	C		139.4	C
14-Me	1.59 (3H, s)	15.5	CH_3	1.64 (3H, s)	15.3	CH_3
15	5.33 (1H, m)	120.3	CH	5.30 (1H, m)	118.7	CH
16	2.25 (2H, m)	38.7	CH_2	2.35 (2H, m)	34.6	CH_2
17	3.65 (1H, m)	70.5	CH	4.10 (1H, m)	69.8	CH
18a	1.73 (1H, m)	43.3	CH_2	0.76 (1H, m)	38.4	CH_2

18b	1.49 (1H, m)			2.01 (1H, m)		
19	5.41 (1H, m)	71.0	CH	5.42 (1H, m)	69.3	CH
20a	2.05 (1H, m)	48.5	CH_2	1.49 (1H, m)	41.7	CH_2
20b	1.91 (1H, m)			2.04 (1H, m)		
21		98.3	C		100.1	C
22a	1.90 (1H, m)	40.9	CH_2	1.73 (2H, m)	41.8	CH_2
22b	1.71 (1H, m)					
23	3.82 (1H, m)	71.7	CH	4.41 (1H, ddd, 10.3, 4.7, 1.8)	70.6	CH
23-OH						
24	1.55 (1H, m)	36.9	CH	1.89 (1H, m)	43.0	CH
24-Me	0.84 (3H, d, 6.7)	12.6	CH_3	0.80 (3H, d, 7.0)	11.3	CH_3
25	3.81 (1H, m)	71.7	CH	3.34 (1H, m)	76.6	CH
26	1.49 (1H, m)	36.4	CH	1.50 (1H, m)	38.1	CH
26-Me	0.86 (3H, d, 7.4 Hz)	14.2	CH_3	0.84 (3H, d, 6.7)	12.2	CH_3
27a	1.41(1H, m)	28.1	CH_2	1.30 (1H, m)	28.2	CH_2
27b	1.30 (1H, m)			1.46 (1H, m)		
28	0.87 (3H, t, 7.5)	12.8	CH_3	0.92 (3H, t, 7.4)	12.3	CH_3

[a]In methnal-*d*4, 500 MHz for ^{1}H and 125 MHz for ^{13}C NMR; Chemical shifts are reported in ppm; All signals are determined by ^{1}H-^{1}H COSY, HSQC, HMBC, and NOESY correlations.

Table S5. ^{1}H and ^{13}C NMR spectroscopic data for 4 and 4' in acetone-d_6[a]

	4			4'		
position	δ_H (mult., J in Hz)	δ_C	mutl.	δ_H (mult., J in Hz)	δ_C	mutl.
1		169.2	C		169.9	C
2		122.9	C		122.3	C
3	7.51 (1H, s)	134.0	CH	7.56 (1H, s)	134.3	CH
4		123.7	C		123.7	C
4-Me	2.20 (3H, s)	15.5	CH_3	2.19 (3H, s)	15.8	CH_3
5		158.8	C		159.1	C
5-OH						
6	6.68 (1H, s)	115.3	CH	6.67 (1H, s)	115.3	CH
7		146.6	C		147.0	C
8		136.5	C		136.6	C
8-Me	2.05 (3H, s)	19.1	CH_3	2.01 (3H, s)	19.2	CH_3
9	5.61 (1H, d, 11.0)	128.9		5.61 (1H, d, 12.0)	128.8	
10	6.19 (1H, dd, 15.0, 11.0)	127.3		6.18 (1H, dd, 12.0, 8.5)	127.2	
11	5.56 (1H, dd, 15.0, 9.6)	136.7		5.57 (1H, dd, 15.0, 10.5)	136.8	
12	2.51 (1H, m)	41.7		2.49 (1H, m)	41.7	
12-Me	1.18 (3H, d, 6.8)	19.4	CH_3	1.18 (3H, d, 7.0)	19.4	CH_3
13	3.95 (1H, m)	79.2		3.94 (1H, m)	79.2	
13-OH						
14		139.0			139.0	
14-Me	1.60 (3H, s)	15.4	CH_3	1.58 (3H, s)	15.5	CH_3
15	5.40 (1H, m)	120.1	CH	5.39 (1H, m)	120.2	CH
16	2.24 (2H, m)	38.8	CH_2	2.22 (2H, m)	38.8	CH_2
17	3.69 (1H, m)	70.3	CH	3.62 (1H, t, 9.5)	70.0	CH
18a	1.80 (1H, m)	41.6	CH_2	1.83 (1H, dd, 14.0, 5.5)	42.8	CH_2

18b	1.53 (1H, m)			1.42 (1H, m)		
19	5.31 (1H, m)	71.9	CH	5.37 (1H, d, 11.5)	71.9	CH
20a	1.95 (1H, m)	44.4	CH_2	1.98 (1H, d, 11.5)	45.3	CH_2
20b	1.87 (1H, m)			1.67 (1H, m)		
21	3.92 (1H, m)	70.3	CH	3.89 (1H, t, 9.0)	65.9	CH
22a	1.84 (1H, m)	40.0	CH_2	1.61 (1H, m)	41.3	CH_2
22b	1.39 (1H, m)			1.44 (1H, m)		
23	3.98 (1H, m)	76.7	CH	3.98 (1H, m)	73.3	CH
23-OH						
24	1.66 (1H, m)	42.8	CH	1.66 (1H, m)	42.2	CH
24-Me	0.75 (3H, d, 6.8)	12.4	CH_3	0.71 (3H, d, 6.5)	12.7	CH_3
25	3.45 (1H, d, 8.4)	77.5	CH	3.44 (1H, d, 9.5)	77.8	CH
26	1.49 (1H, m)	37.9	CH	1.47 (1H, m)	37.8	CH
26-Me	0.84 (3H, d, 6.4)	12.4	CH_3	0.81 (3H, d, 6.5)	12.4	CH_3
27a	1.44 (1H, m)	27.9	CH_2	1.43 (1H, m)	27.9	CH_2
27b	1.31 (1H, m)			1.29 (1H, m)		
28	0.90 (3H, t, 6.8)	12.5	CH_3	0.88 (3H, t, 6.5)	12.4	CH_3

[a]In acetone-d_6, 400 MHz for ^{1}H and 100 MHz for ^{13}C NMR; Chemical shifts are reported in ppm; All signals are determined by ^{1}H-^{1}H COSY, HSQC, HMBC, and NOESY correlations.

Table S6. ^{13}C NMR spectroscopic data for 4 and 4' in methnol-d_4[a]

	4	4'
position	δ_C	δ_C
1	170.7	171.3
2	122.4	122.5
3	134.1	134.1
4	124.2	124.2
4-Me	15.7	15.7
5	159.6	159.5
6	115.2	115.1
7	147.1	147.0
8	136.3	136.7
8-Me	19.1	18.9
9	129.1	129.3
10	127.9	127.9
11	137.1	137.0
12	41.9	41.8
12-Me	19.2	19.1
13	79.9	79.8
14	139.2	139.2
14-Me	15.5	15.5
15	120.2	120.2
16	38.8	38.8
17	70.1	70.7
18	41.9	43.1
19	72.4	71.2
20	44.2	45.7
21	70.7	66.0

22	38.9	40.6
23	74.5	72.4
24	43.0	42.7
24-Me	12.2	12.4
25	77.0	77.0
26	38.0	38.0
26-Me	11.4	11.6
27	28.2	28.2
28	12.4	12.2

[a]100 MHz; Chemical shifts are reported in ppm

Table S7. ^{1}H and ^{13}C NMR spectroscopic data for 5[a]

position	δ_H (mult., J in Hz)	δ_C	mult.	HMBC (H→C)	NOESY
1		168.3	C		
2		123.9	C		
3	7.54 (1H, s）	133.0	CH	C-1, 5, 7, 4-Me	4-Me
4		125.1	C		
4-Me	2.17 (1H, s）	15.9	CH_3	C-3, 4, 5	3, 21-OH
5		160.5	C		
5-OMe	3.89 (3H, s)	55.9	CH_3	C-5	6
6	6.73 (1H, s)	110.7	CH	C-2, 4, 5, 8	5-OMe, 8-Me
7		146.8	C		
8		137.0	C		
8-Me	2.07 (3H, s)	19.3	CH_3	C-7, 8, 9	6, 10
9	5.65 (1H, d, 11.0)	128.9	CH	C-7, 11, 8-Me	10, 11
10	6.22 (1H, dd, 15.0, 11.0)	127.2	CH	C-8, 9, 12	8-Me, 11, 12
11	5.59 (1H, dd, 15.0, 11.0)	136.7	CH	C-9, 8-Me	9, 12-Me
12	2.50 (1H, m)	41.7	CH	12-Me	11, 13, 12-Me
12-Me	1.19 (3H, d, 6.9)	19.3	CH_3	C-11, 12, 13	11, 12, 13
13	3.95 (1H, brs)	79.0	CH		12, 12-Me, 14-Me
14		139.5	C		
14-Me	1.58 (3H, s)	15.3	CH_3	C-13, 14, 15	12, 13
15	5.37 (1H, dd, 11.2, 5.0)	112.0	CH	C-14-Me, 13	16, 17
16a	2.35 (1H, m)	33.7	CH_2	C17, 18	15, 19
16b	2.03 (1H, m)				
17	3.14 (1H, m)	80.0	CH	17-OMe	16, 17-OMe, 19
17-OMe	3.30 (3H, s)	56.9	CH_3	C-17	16, 17

18a	1.67 (1H, m)	41.9	CH_2	C-16,17,19, 20	19
18b	1.61 (1H, m)				
19	5.46 (1H, m)	69.8	CH	C-1, 17, 21	17, 18, 20
20a	1.97 (1H, dd, 14.4, 4.6)	47.9	CH_2		
20b	1.80 (1H, dd, 14.4, 7.4)			C-18,19, 21,22	19
21		97.2	C		
21-OH	5.14 (1H, s)			C-20, 21, 22	23-OMe, 25
22a	2.19 (1H, m)	35.8	CH_2	C23, 24	
22b	1.61 (1H, m)				
23	3.51 (1H, dd, 5.6, 2.8)	81.9	CH		22b
23-OMe	3.42 (3H, s)	58.1	CH_3	C-23	21-OH, 22b, 23
24	1.63 (1H, m)	36.4	CH		
24-Me	0.87 (3H, d, 5.4)	13.8	CH_3	C-23, 25	
25	3.72(1H, d, 11.0)	70.5	CH	C-27, 26-Me	21-OH
26	1.49 (1H, m)	35.8	CH	26-Me	
26-Me	0.86 (3H, d, 5.4)	12.8	CH_3	C-25	25
27a	1.42 (1H, m)	27.6	CH_2	C-28, 25, 26	28
27b	1.31 (1H, m)				
28	0.84 (3H, d, 5.0)	12.3	CH_3	C-27	27

[a]In acetone-d_6, 500 MHz for ^{1}H and 125 MHz for ^{13}C NMR; Chemical shifts are reported in ppm; All signals are determined by ^{1}H-^{1}H COSY, HSQC, HMBC, and NOESY correlations.

Table S8. ^{1}H and ^{13}C NMR spectroscopic data for 6 and 6'[a]

	6			6'		
position	δ_H (mult., *J* in Hz)	δ_C	mutl.	δ_H (mult., *J* in Hz)	δ_C	mutl.
1		175.5	C		175.1	C
2	3.67 (1H, t, 2.0)	48.7	C	3.74 (1H, t, 2.0)	48.7	C
3	5.64 (1H, brs)	125.7	CH	5.72 (1H, br s)	125.9	CH
4		132.9	C		133.0	C
4-Me	1.83 (3H, s)	17.7	CH_3	1.84 (3H, s)	17.7	CH_3
5		154.1	C		154.1	C
5-NOH	10.03 (1H, s)			10.05 (1H, s)		
6a	2.99 (1H, d, 16.9)	33.2	CH	2.98 (1H, d, 16.8)	33.5	CH
6b	2.36 (1H, dd, 15.9, 6.5)			2.39 (1H, d, 16.8)		
7		75.8	C		76.0	C
8		138.1	C		138.2	C
8-Me	1.81 (3H, s)	14.14	CH_3	1.82 (3H, s)	14.2	CH_3
9	6.30 (1H, d, 10.9)	125.9	CH	6.31 (1H, d, 11.0)	125.9	CH
10	6.08 (1H, dd, 15.1, 11.0)	127.3	CH	6.08 (1H, dd, 15.0, 11.0)	127.3	CH
11	5.53 (1H, m)	136.8	CH	5.53 (1H, dd, 13.6, 8.5)	136.9	CH
12	2.44 (1H, m)	41.8	CH	2.45 (1H, ddd, 9.0, 6.7, 2.0)	41.8	CH
12-Me	1.19 (3H, d, 6.8)	18.7	CH_3	1.19 (3H, d, 6.8)	18.8	CH_3
13	3.95 (1H, m)	79.4	CH	3.95 (1H, br s)	79.4	CH
13-OH	3.56 (1H, d, 4.6)			3.57 (1H, d, 4.3)		
14		137.2	C		137.4	C
14-Me	1.55 (3H, s)	15.1	CH_3	1.56 (3H, s)	15.2	CH_3
15	5.58 (1H, m)	121.3	CH	5.54 (1H, dd, 11.0, 4.0)	121.5	CH
16a	2.20 (1H, ddd, 13.5,	37.2	CH_2	2.23 (1H, m)	37.4	CH_2

	11.5, 4.5)					
16b	1.94 (1H, m)			1.97 (1H, m)		
17	3.35 (1H, m)	69.0	CH	3.34 (1H, br s)	69.1	CH
18a	1.63 (1H, m)	43.2	CH_2	1.64 (1H, ddd, 14.1, 7.8, 2.2)	43.3	CH_2
18b	1.53 (1H, m)			1.56 (1H, m)		
19	5.47 (1H, m)	71.3	CH	5.55 (1H, m)	71.9	CH
20a	2.81 (1H, m)	41.5	CH_2	2.92 (1H, dd, 13.6, 3.8)	34.9	CH_2
20b	2.56 (1H, dd, 15.4, 9.7)			2.76 (1H, dd, 13.5, 9.3)		
21		157.4	C		157.2	C
21-NOH	9.88 (1H, s)			9.87 (1H, s)		
22a	2.78 (1H, dd, 15.4, 2.5)	33.3	CH_2	2.55 (1H, dd, 15.7, 2.4)	39.7	CH_2
22b	2.33 (1H, m)			2.31 (1H, dd, 15.7, 9.5)		
23	4.12 (1H, t, 7.1)	73.5	CH	4.13 (1H, t, 2.0)	72.9	CH
23-OH	4.41 (1H, brs)			4.31 (1H, br s)		
24	1.72 (1H, m)	43.2	CH	1.75 (1H, dt, 9.2, 6.8)	42.2	CH
24-Me	0.85 (3H, d, 6.8)	12.4	CH_3	0.81 (3H, d, 6.9)	12.4	CH_3
25	3.51 (1H, m)	77.5	CH	3.46 (1H, d, 9.4)	77.1	CH
26	1.52 (1H, m)	37.8	CH	1.51 (1H, m)	37.7	CH
26-Me	0.85 (3H, d, 6.8)	12.3	CH_3	0.83 (3H, d, 6.6)	12.4	CH_3
27a	1.46 (1H, m)	27.9	CH_2	1.45 (1H, m)	27.9	CH_2
27b	1.31 (1H, m)			1.31 (1H, m)		
28	0.90 (3H, t, 7.4)	12.4	CH_3	0.89 (3H, t, 7.4)	12.4	CH_3

[a]In acetone-d_6, 500 MHz for ^{1}H and 125 MHz for ^{13}C NMR; Chemical shifts are reported in ppm; All signals are determined by ^{1}H-^{1}H COSY, HSQC, HMBC, and NOESY correlations.

Table S9. ^{1}H and ^{13}C NMR spectroscopic data for 7 and 7'[a]

	7			7'		
position	δ_H (mult., J in Hz)	δ_C	mutl.	δ_H (mult., J in Hz)	δ_C	mutl.
1		172.0	C		171.8	C
2	3.95 (1H, d, 4.8)	49.2	C	3.94 (1H, m)	49.3	C
3	6.59 (1H, m)	138.9	CH	6.59 (1H, m)	139.0	CH
4		136.0	C		135.9	C
4-Me	1.77 (3H, dd, 2.4, 1.5)	15.7	CH_3	1.76 (3H, dd, 2.4, 1.5)	15.7	CH_3
5		197.1	C		197.1	C
6a	3.00 (1H, d, 16.0)	48.8	CH	2.99 (1H, d, 16.1)	48.9	CH
6b	2.24 (1H, d, 16.0)		CH	2.24 (1H, d, 16.1)		CH
7		80.4	C		80.5	C
8		137.5	C		137.7	C
8-Me	1.86 (3H, s)	14.3	CH_3	1.86 (3H, s)	14.3	CH_3
9	6.21 (1H, dd, 14.0, 8.0)	125.8	CH	6.22 (1H, dd, 24.0, 10.1)	125.8	CH
10	6.19 (1H, dd, 14.0, 8.0)	127.0	CH	6.19 (1H, dd, 24.4, 10.1)	127.1	CH
11	5.57 (1H, dd, 14.2, 10.2)	137.1	CH	5.59 (1H, dd, 14.3, 10.2)	137.1	CH
12	2.56 (1H, m)	41.6	CH	2.59 (1H, m)	41.7	CH
12-Me	1.18 (3H, d, 6.8)	19.6	CH_3	1.18 (3H, d, 6.8)	19.7	CH_3
13	3.96 (1H, m)	79.2	CH	3.96 (1H, m)	79.2	CH
13-OH				3.84 (1H, d, 5.2)		
14		139.4	C		140.1	C
14-Me	1.61 (3H, s)	15.2	CH_3	1.63 (3H, s)	15.1	CH_3
15	5.33 (1H, m)	118.0	CH	5.34 (1H, dd, 9.6, 2.9)	117.5	CH
16	2.26 (1H, m)	35.8	CH_2	2.33 (2H, m)	34.9	CH_2
17	3.83 (1H, m)	70.3	CH	3.78 (1H, m)	69.7	CH
18a	1.73 (1H, m)	37.0	CH_2	1.83 (1H, m)	36.7	CH_2

18b	0.80 (1H, m)			0.86 (1H, q, 11.0)		
19	4.99 (1H, m)	70.0	CH	5.16 (1H, m)	68.3	CH
20a	2.92 (1H, dd, 6.8, 1.6)	40.5	CH_2	2.01 (1H, m)	41.9	CH_2
20b	1.34 (1H, m)			1.44 (1H, m)		
21		100.0	C		100.5	C
22a	2.23 (1H, m)	40.1	CH_2	1.92 (1H, dd, 14.1, 2.9)	42.2	CH_2
22b	1.60 (1H, m)			1.73 (1H, dd, 14.1, 3.5)		
23	4.02 (1H, m)	68.9	CH	3.69 (1H, m)	70.2	CH
23-OH				3.35 (1H, d, 10.0)		
24	1.71 (1H, m)	36.6	CH	1.62 (5H, m)	36.6	CH
24-Me	0.86 (3H, d, 8.0)	13.0	CH_3	0.87 (3H, d, 6.6)	14.1	CH_3
25	3.68 (1H, dd, 9.6, 2.6)	74.6	CH	3.61 (1H, dd, 10.7, 1.4)	71.6	CH
26	1.54 (1H, m)	36.2	CH	1.50 (1H, m)	36.0	CH
26-Me	0.88 (3H, d, 8.0)	13.4	CH_3	0.87 (3H, d, 6.9)	12.1	CH_3
27a	1.50 (1H, m)	27.7	CH_2	1.53 (1H, m)	28.1	CH_2
27b	1.34 (1H, m)			1.43 (1H, m)		
28	0.92 (3H, t, 7.4)	12.3	CH_3	0.95 (3H, t, 7.3)	12.7	CH_3

[a]In acetone-d_6, 500 MHz for ^{1}H and 125 MHz for ^{13}C NMR; Chemical shifts are reported in ppm; All signals are determined by ^{1}H-^{1}H COSY, HSQC, HMBC, and NOESY correlations.

Table S10. ^{1}H and ^{13}C NMR spectroscopic Data for 8[a]

	8		
position	δ_H (mult., J in Hz)	δ_C	mutl.
1		171.8	C
2	3.94 (1H, m)	49.3	C
3	6.59 (1H, m)	139.1	CH
4		135.8	C
4-Me	1.76 (3H, dd, 2.4, 1.5)	15.7	CH_3
5		197.1	C
6a	2.99 (1H, dd, 16.0, 1.2)	48.9	CH
6b	2.24 (1H, m)		CH
7		80.5	C
7-OH	4.08 (1H, s)		C
8		137.7	C
8-Me	1.86 (3H, s)	14.3	CH_3
9	6.23 (1H, dd, 23.0, 10.5)	125.8	CH
10	6.19 (1H, dd, 23.0, 10.5)	127.1	CH
11	5.60 (1H, dd, 14.7, 10.5)	137.1	CH
12	2.58 (1H, m)	41.7	CH
12-Me	1.18 (3H, d, 6.9)	19.7	CH_3
13	3.96 (1H, m)	79.2	CH
13-OH	3.82 (1H, d, 5.0)		
14		139.7	C
14-Me	1.61 (3H, m)	15.1	CH_3
15	5.33 (1H, m)	118.0	CH
16	2.24 (2H, m)	35.1	CH_2
17	3.86 (1H, m)	69.7	CH
18a	1.83 (1H, ddd, 11.0, 4.5,	36.9	CH_2

	2.2)		
18b	0.82 (1H, dd, 24.3, 11.0)		
19	5.20 (1H, m)	69.0	CH
20a	1.98 (1H, ddd, 11.9, 4.6,	41.6	CH_2
	2.0)		
20b	1.49 (1H, m)		
21		96.6	C
22	5.72 (1H, dd, 10.0, 2.0)	135.9	CH
23	5.56 (1H, dd, 10.0, 2.0)	129.5	CH
24	2.25 (1H, m)	31.4	CH
24-Me	0.90 (3H, d, 7.0)	16.7	CH_3
25	3.47 (1H, dd, 10.0, 1.7)	75.6	CH
26	1.64 (1H, m)	36.0	CH
26-Me	0.90 (3H, d, 7.0)	13.3	CH_3
27	1.47 (2H, m)	28.3	CH_2
28	0.94 (3H, t, 7.4)	12.3	CH_3

[a]In acetone-d_6, 400 MHz for ^{1}H and 100 MHz for ^{13}C NMR; Chemical shifts are reported in ppm; All signals are determined by ^{1}H-^{1}H COSY, HSQC, HMBC, and NOESY correlations.

Fig. S1. Alignment of the amino acid sequences of AveC, MilC, MeiC, and NemC. AveC (*NP_822115.1*) from *S. avermectinius*; MilC (*YP_004958979.1*) from *S. hygroscopicus*; MeiC (*AAM97313.1*) from *S. nanchangensis*; NemC (*BAF85840.1*) from *S. cyaneogriseus* ssp. *Noncyanogenus*.

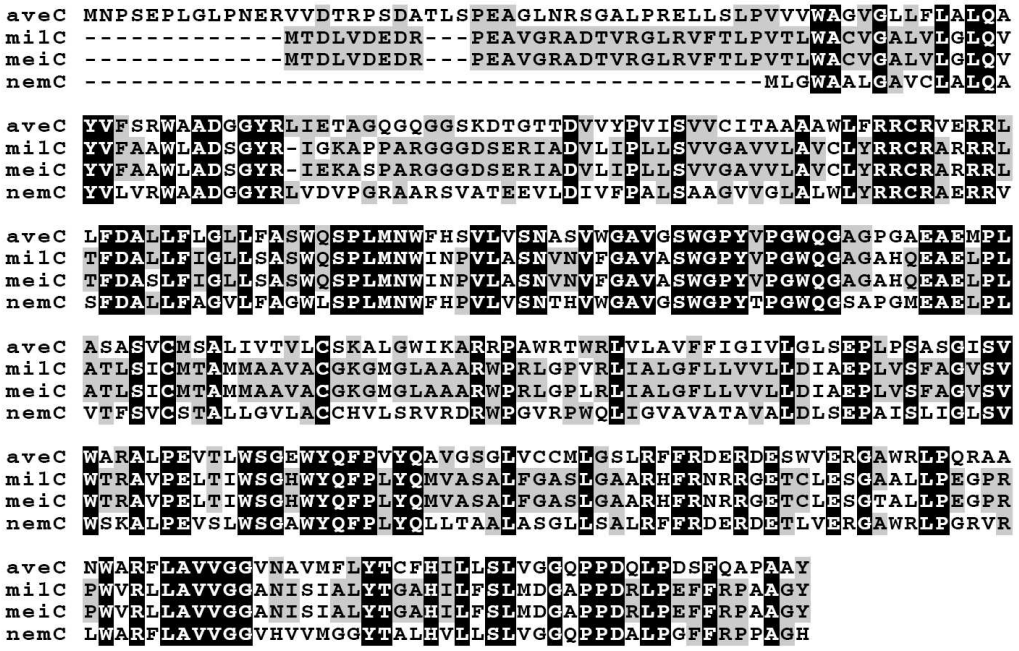

Fig. S2. Spontaneous conversions of the unstable products **2** (approx. 21.0 μM, A), **2'** (approx. 13.9 μM, B), **3** (approx. 7.2 μM, contaminated with a trace of **2'**, C) and **7** and **7'** (approx. 1.7 mM, D)**.** Each HPLC fraction was prepared from the culture broth of the *ΔaveDC* double mutant strain VL1002 by the method described in Supplementary Method. For **2**, **2'** or **3**, the conversion was performed at 4 °C. For **7** and **7'**, the conversion was carried out at 25 °C. The concentration of each compound was estimated according to a UV-absorbance curve of AVE-B2a varying in concentration.

A

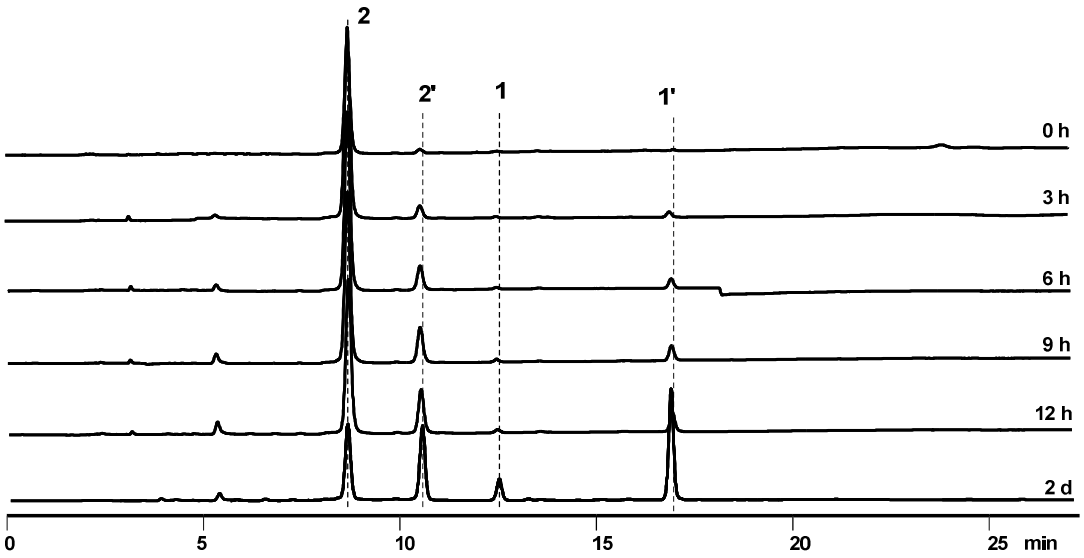

B

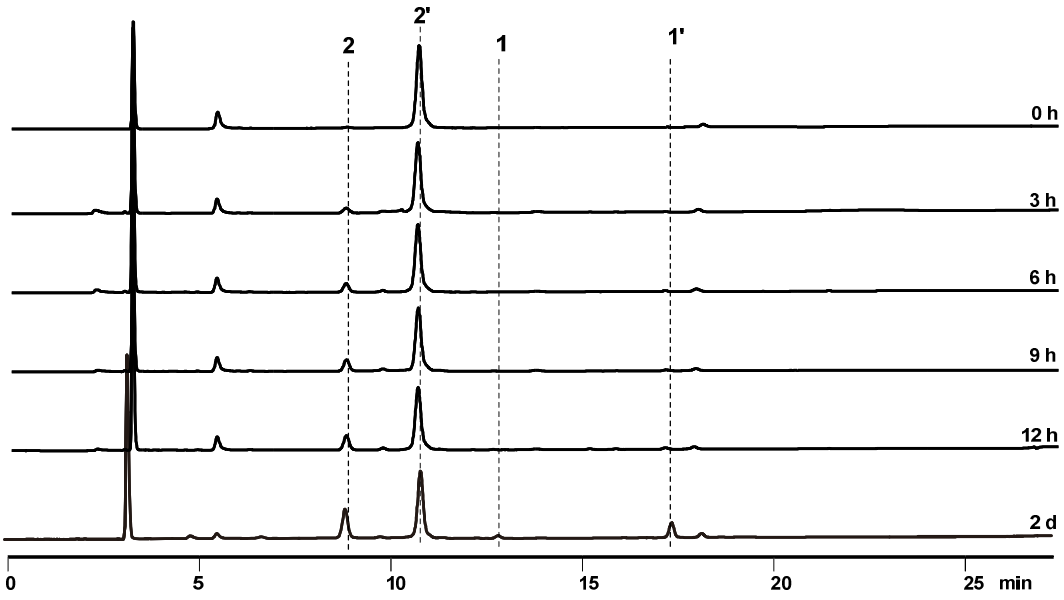

C

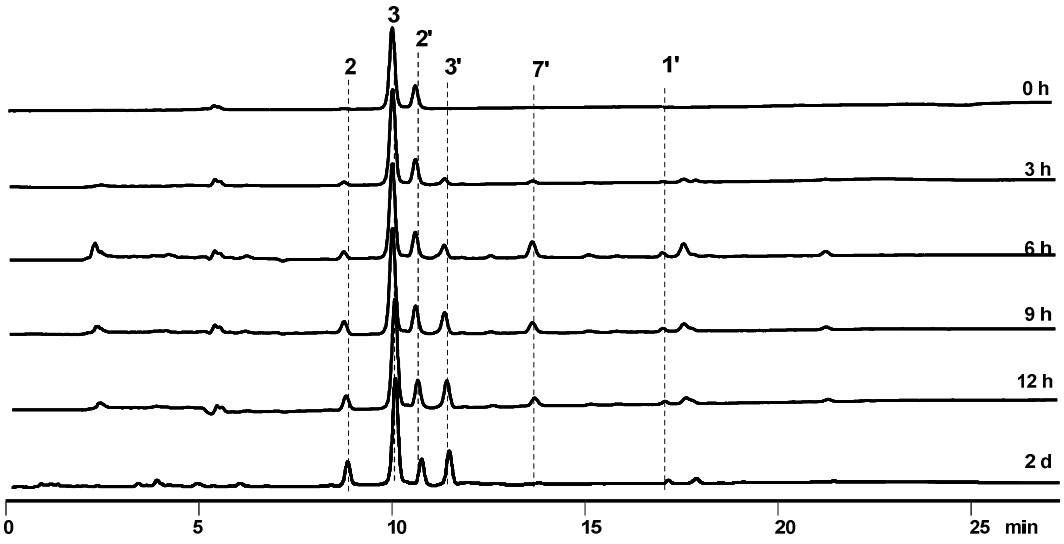
3
2'
2
3'
7'
1'
0 h
3 h
6 h
9 h
12 h
2 d
0
5
10
15
20
25 min

D

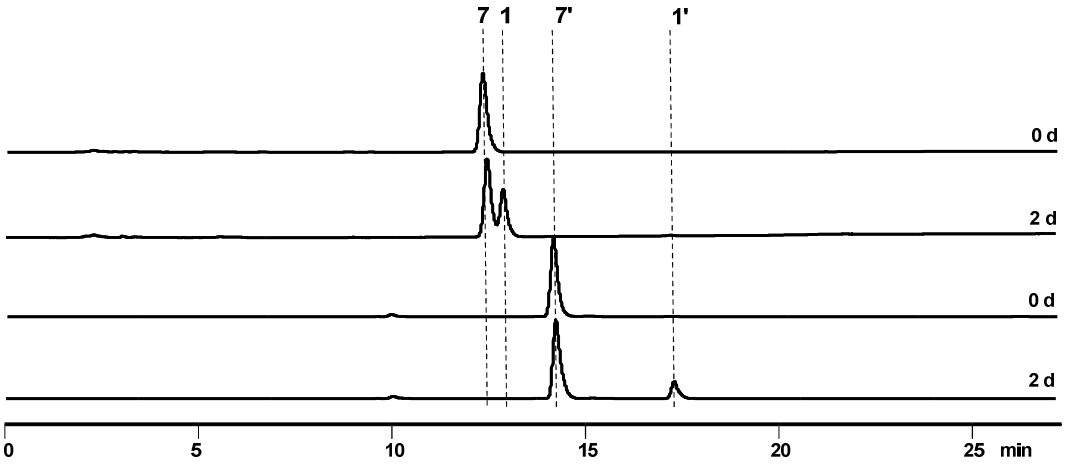
7
1
7'
1'
0 d
2 d
0 d
2 d
0
5
10
15
20
25 min

Fig. S3. SDS-PAGE analysis of the proteins in the recombinant *E. coli* strain VL2001. Lane 1, without IPTG induction; Lane 2, with IPTG induction; and Lane 3, the supernatant of lysate from lane 2.

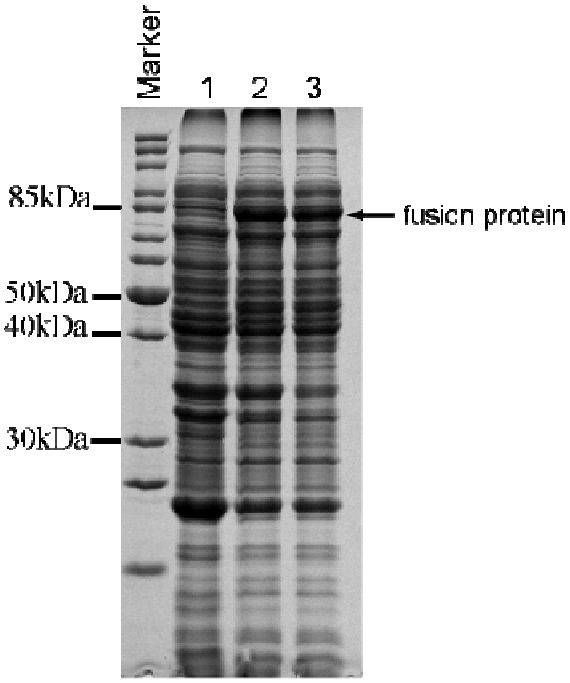

Fig. S4. Time course analysis of MBP-MeiC-catalyzed biotransformation *in vitro*, at 0.1 h, 0.5 h, and 1.0 h. (A) Cell free extract of VL2001 with MBP-MeiC production. (B) Cell free extract of VL2001 without MBP-MeiC production.

A

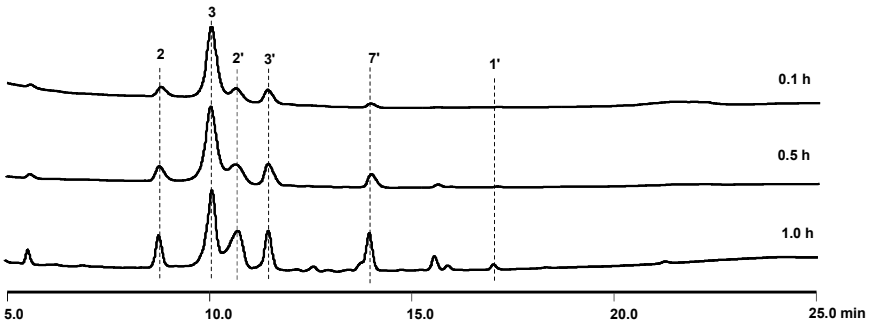

B

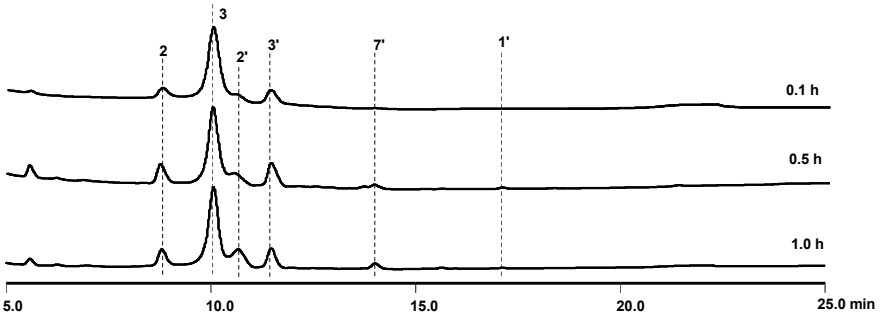

Fig. S5. Construction of *S. avermectinius* mutant strains, including VL1001 (A), VL1004 (B), VL1002 (C), VL1005 (D), and VL1008 (E), and their genotypes verification. The PCR primers are labeled with their predicted fragment sizes

A. Construction of VL1001 (top) and genotype validation with the DNA marker (Lane 1) by PCR amplification (below) of the genomic DNAs from VL1001 (Lane 2), wild type strain (Lane 3), and single crossover mutant for VL1001 generation (Lane 4). The resulting PCR products from wild type strain (Lane 5), VL1001 (Lane 6) and the single crossover mutant (Lane 7) were individually digested by HindIII.

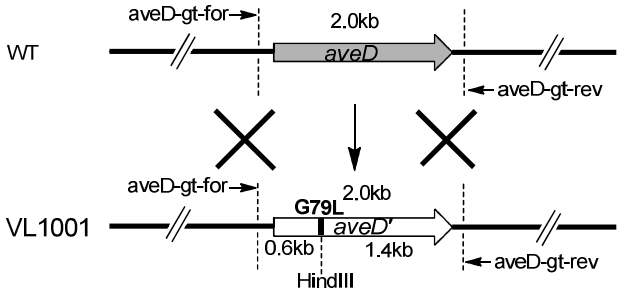

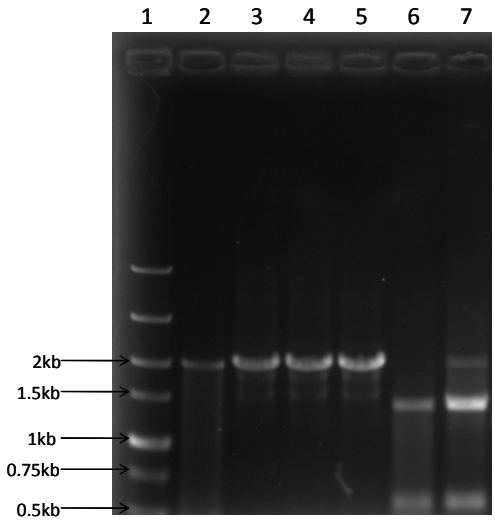

B. Construction of VL1004 (top) and genotype validation by PCR amplification (below) of the genomic DNAs from VL1001 (Lane 1), VL1004 (Lane 2), and single crossover mutant for VL1004 generation (Lane 3). Lane 5, DNA marker.

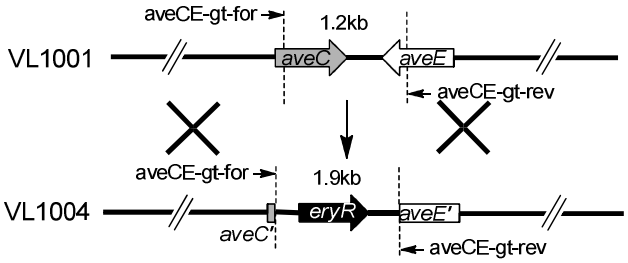

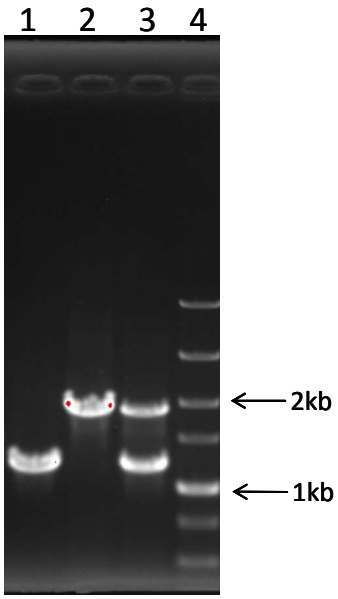

C. Construction of VL1002 (top) and genotype validation with the DNA marker (Lane 1) by PCR amplification (below) of the genomic DNAs from VL1004 (Lanes 2-3), VL1002 (Lanes 4-5), single crossover mutant for VL1002 generation (Lane 6), and wild type strain (Lane 7).

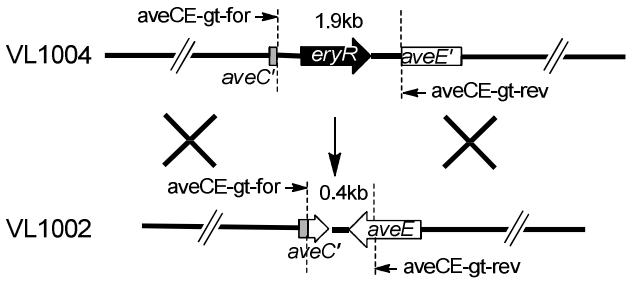

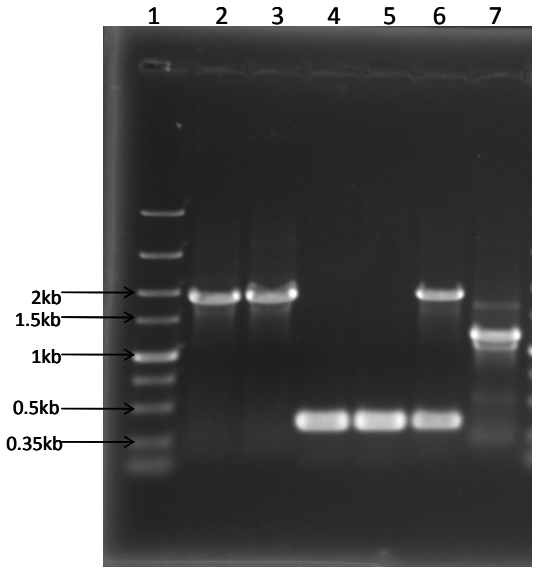

D. Construction of VL1005 (top) and genotype validation with the DNA marker (Lane 1) by PCR amplification (below) of the genomic DNAs from wild type strain (Lanes 2-3), VL1005 (Lanes 4-5), and single crossover mutant for VL1005 generation (Lane 6). The PCR products from VL1005 (Lane 8) and the single crossover mutant were individually digested by KpnI.

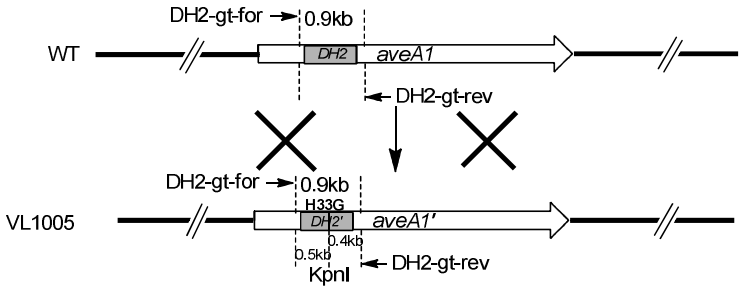

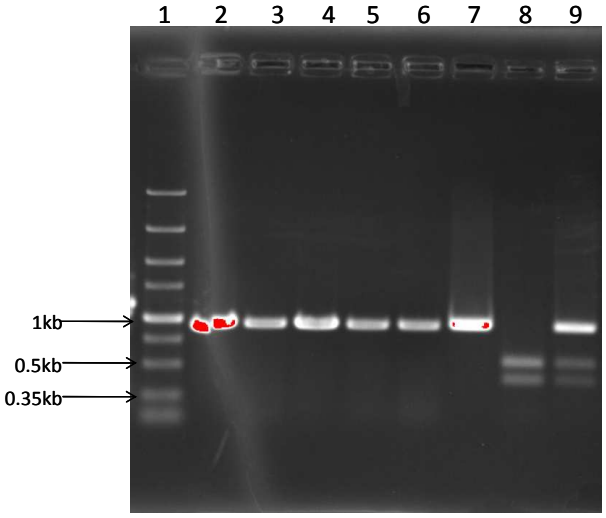

E. Construction of VL1008 (top) and genotype validation with the DNA marker (Lane 1) by PCR amplification (below) of the genomic DNAs from VL1008 (Lanes 2-3) and single crossover mutant for VL1008 generation (Lane 4). The recombinant plasmid pVL1019 (Lane 5) serves as the positive control.

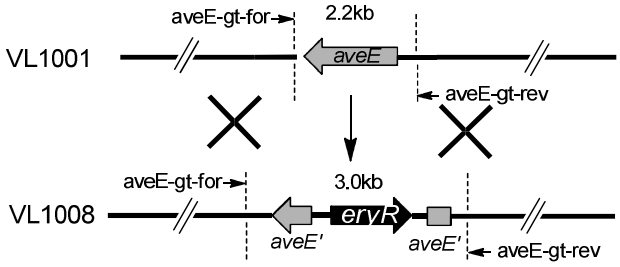

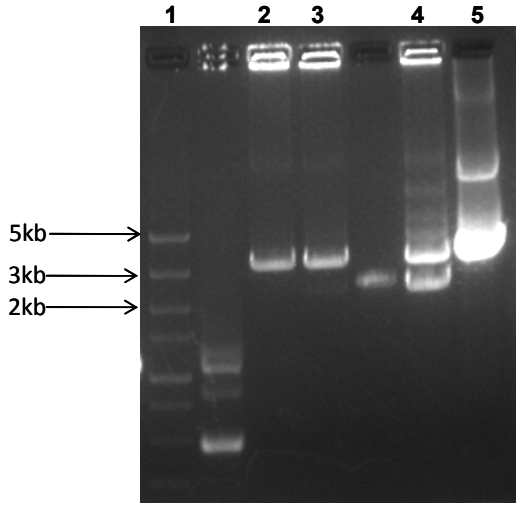

Fig. S6. NMR spectra of compound **1**. (A) ^{1}H spectrum. (B) ^{13}C spectrum. (C) HMQC spectrum. (D) HMBC spectrum. (E) NOESY spectrum.

A

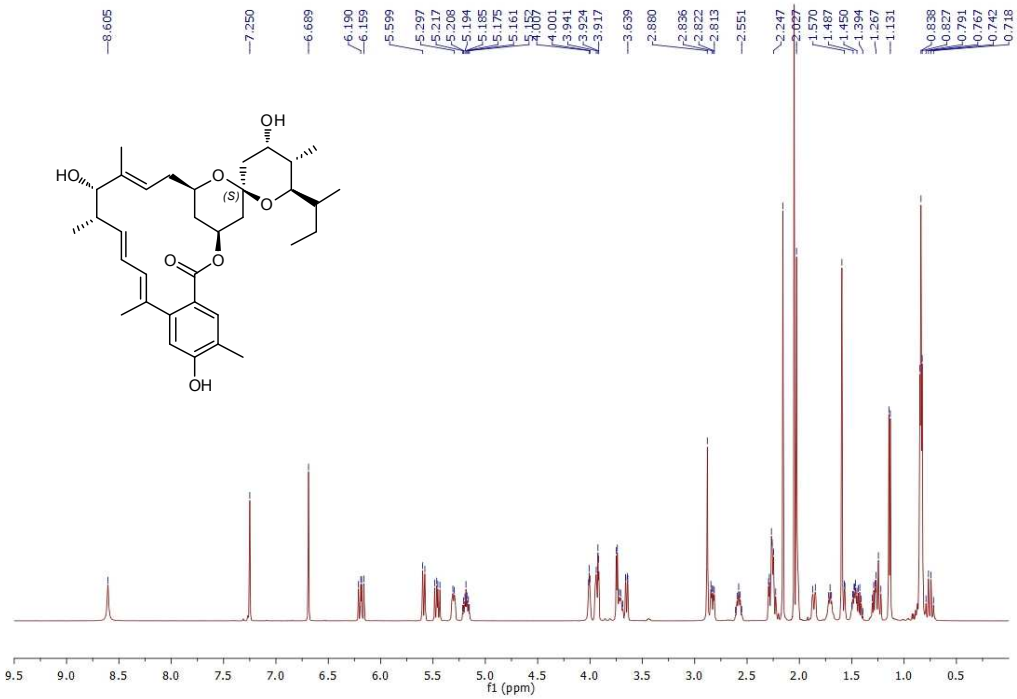

B

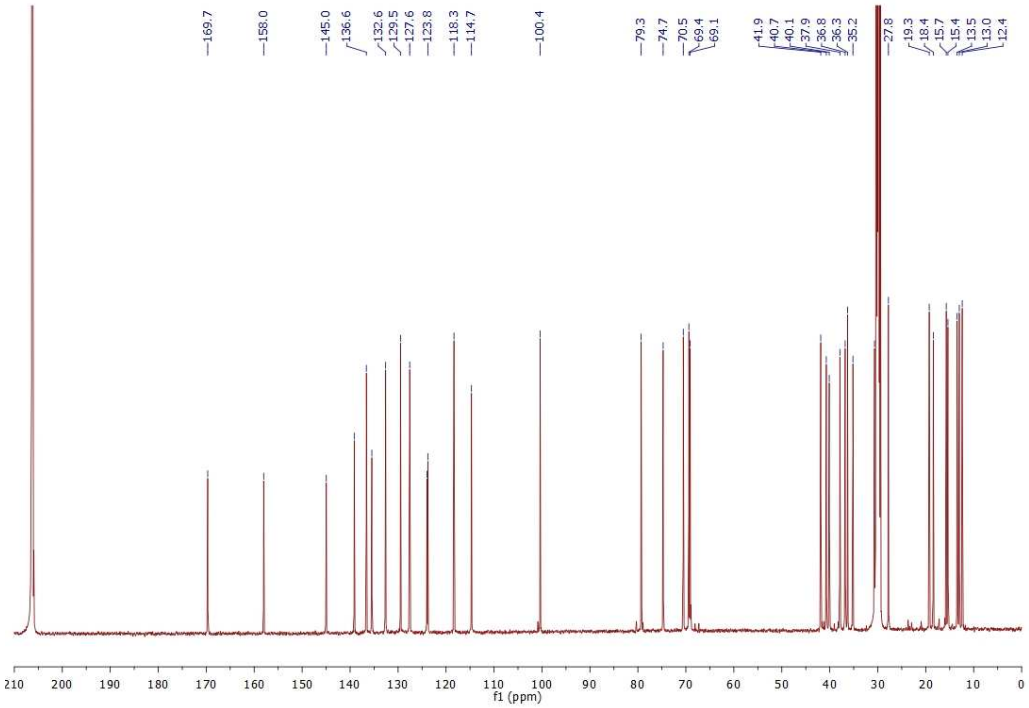

C

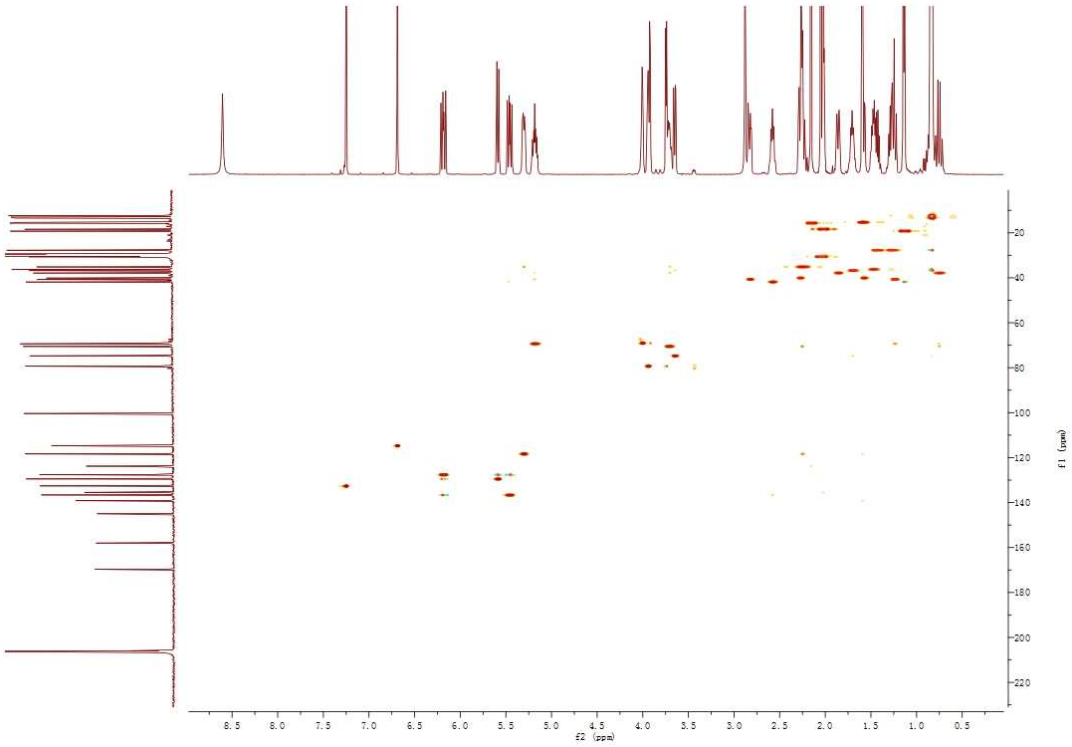

D

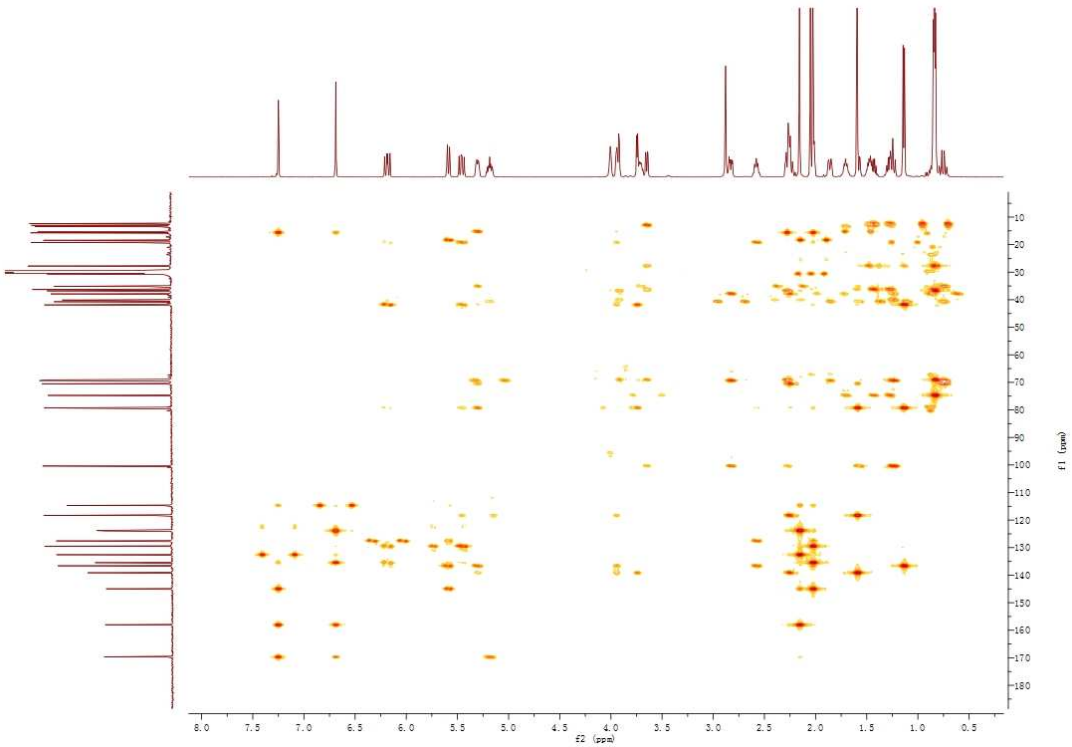

E

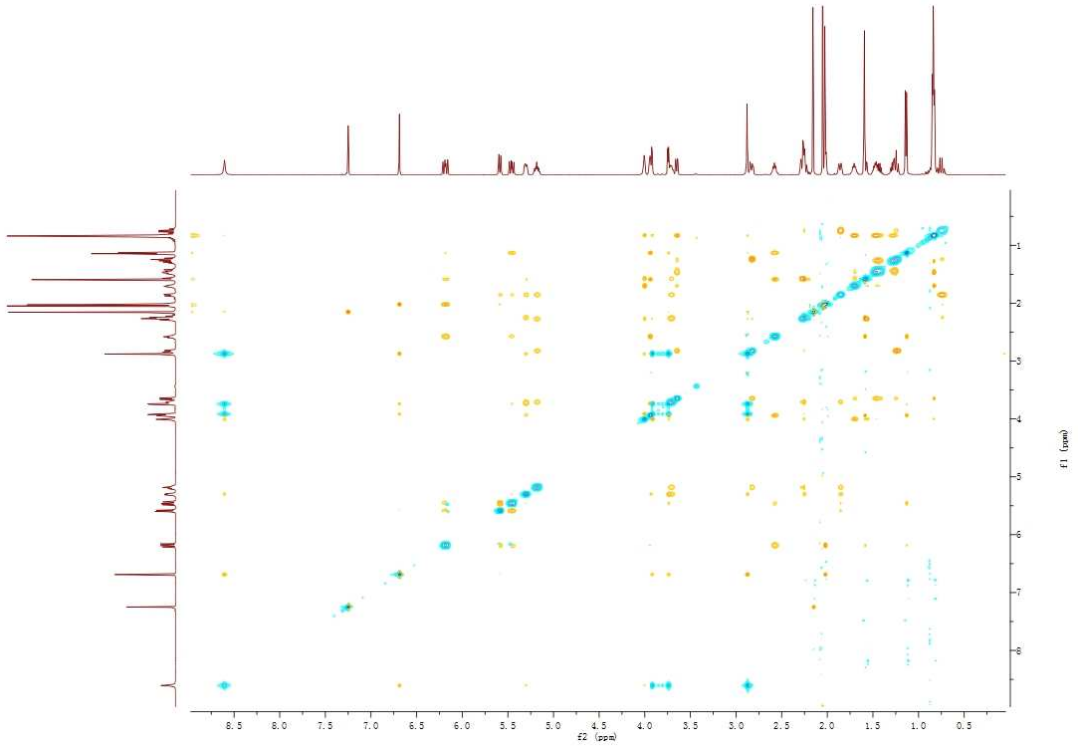

Fig. S7. NMR spectra of compound **1'**. (A) ^{1}H spectrum. (B) ^{13}C spectrum. (C) HMQC spectrum. (D) HMBC spectrum. (E) NOESY spectrum.

A

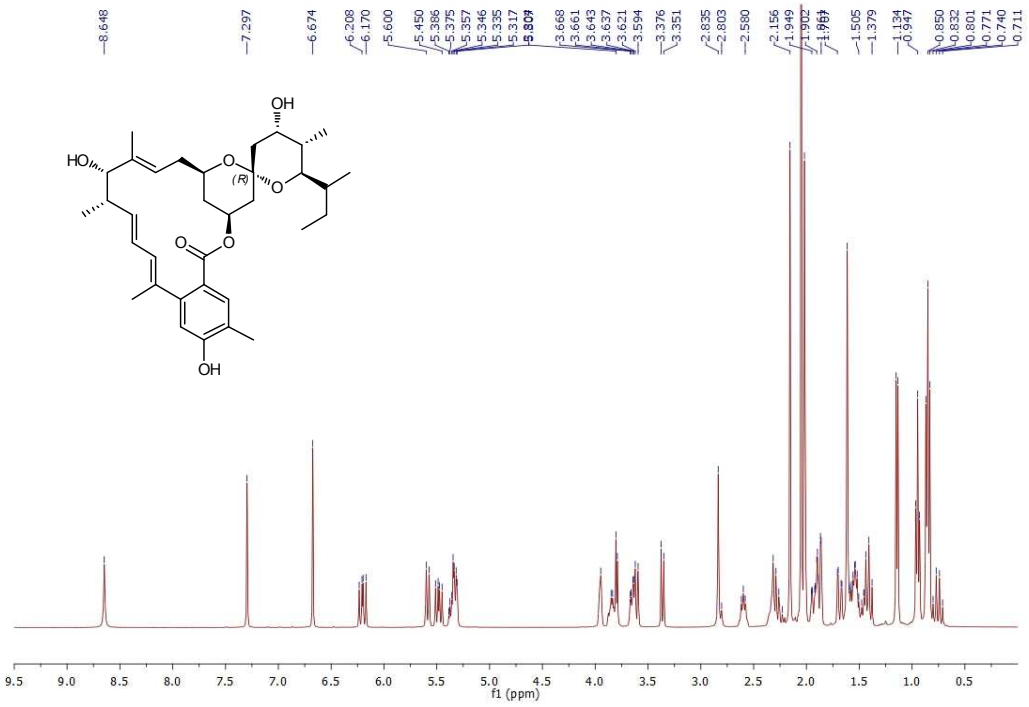

B

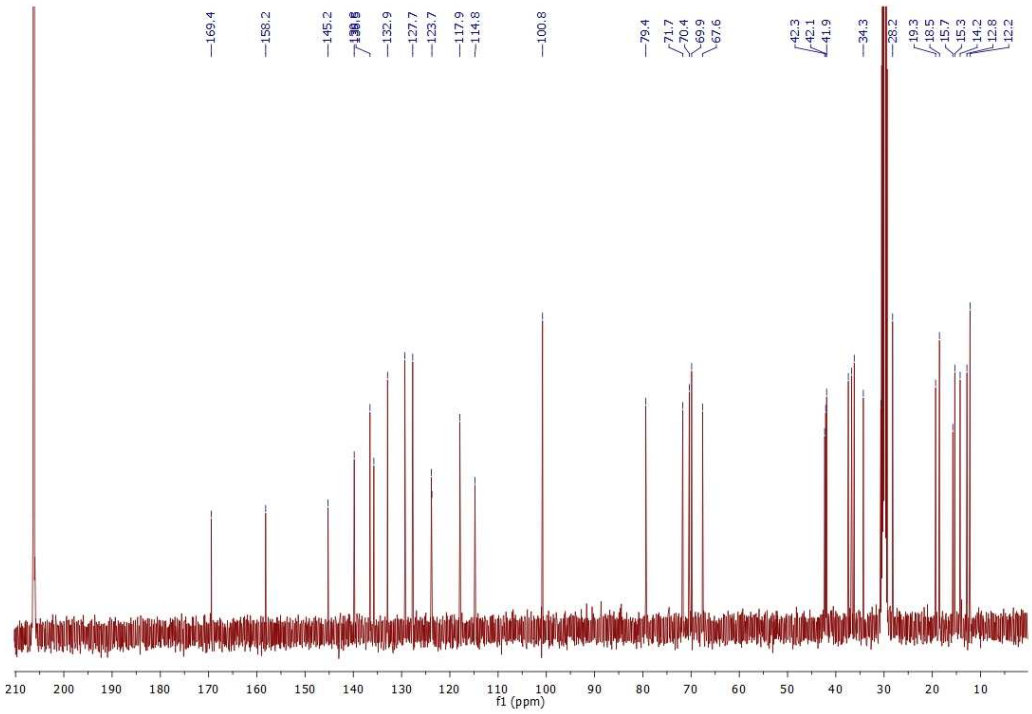

C

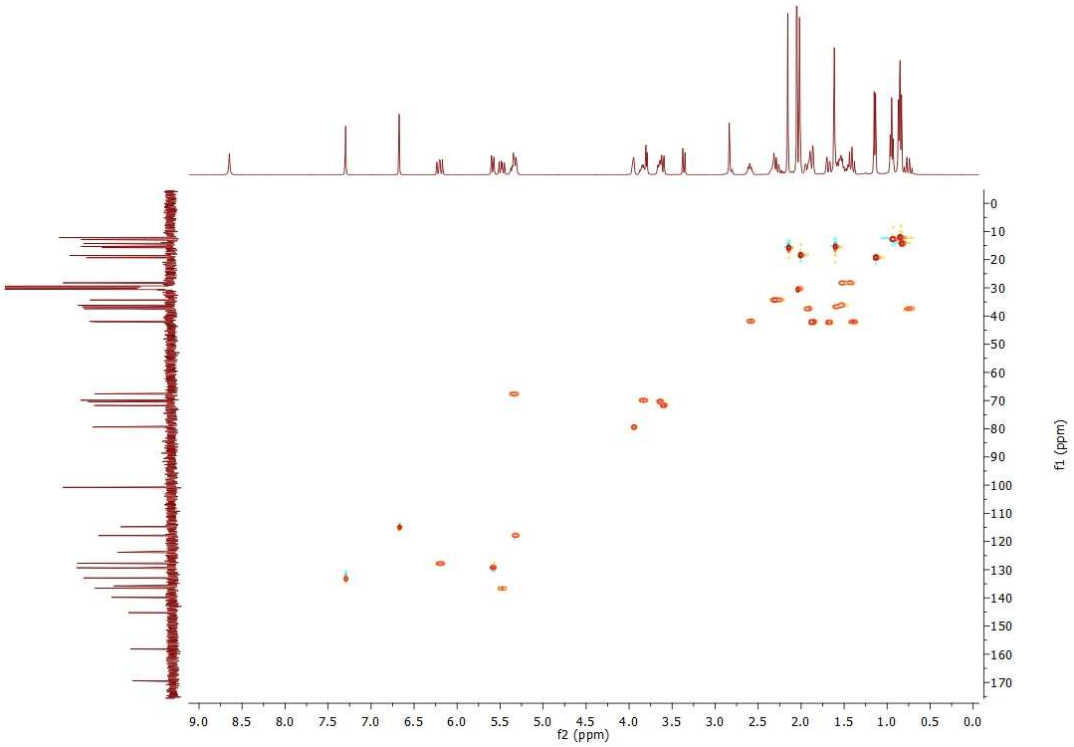

D

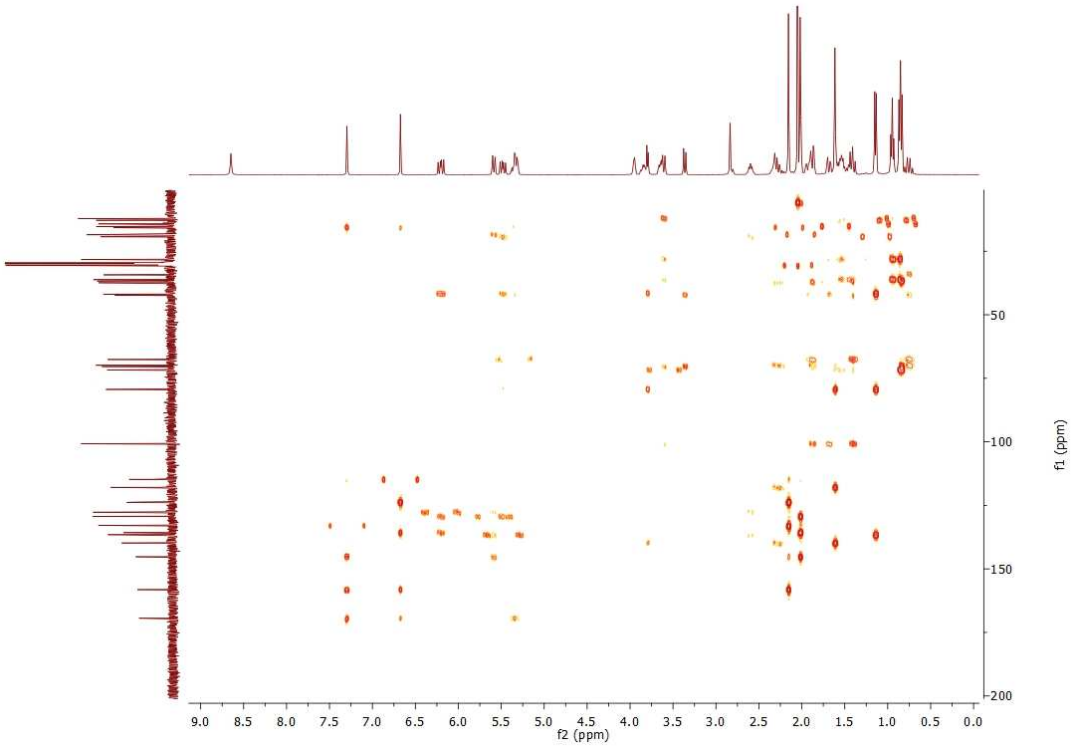

E

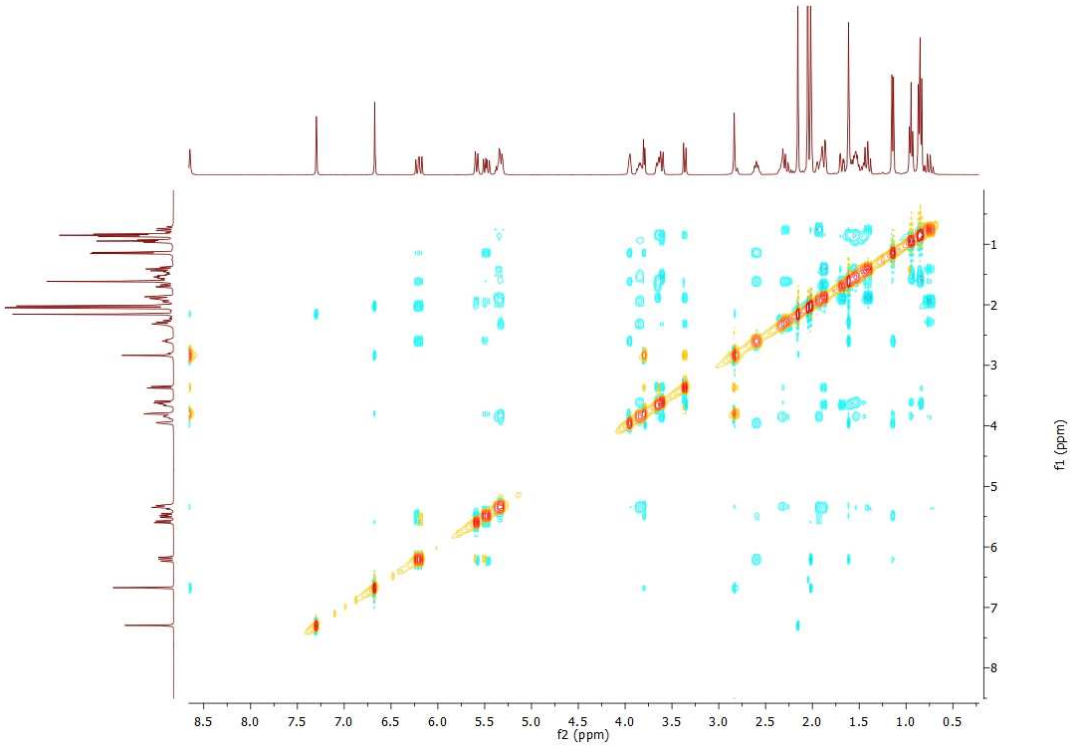
8.5
8.0
7.5
7.0
6.5
6.0
5.5
5.0
4.5
4.0
3.5
3.0
2.5
2.0
1.5
1.0
0.5
f2 (ppm)
1
2
3
4
5
6
7
8
f1 (ppm)

Fig. S8. NMR spectra of compounds **2** and **2'**. (A) ^{1}H spectrum (with a ratio around 2 : 1 according to the signal intensity shown in the chart). (B) ^{13}C spectrum (signals for 2' are labeled by asterisk). (C) HMQC spectrum. (D) HMBC spectrum. (E) NOESY spectrum.

A

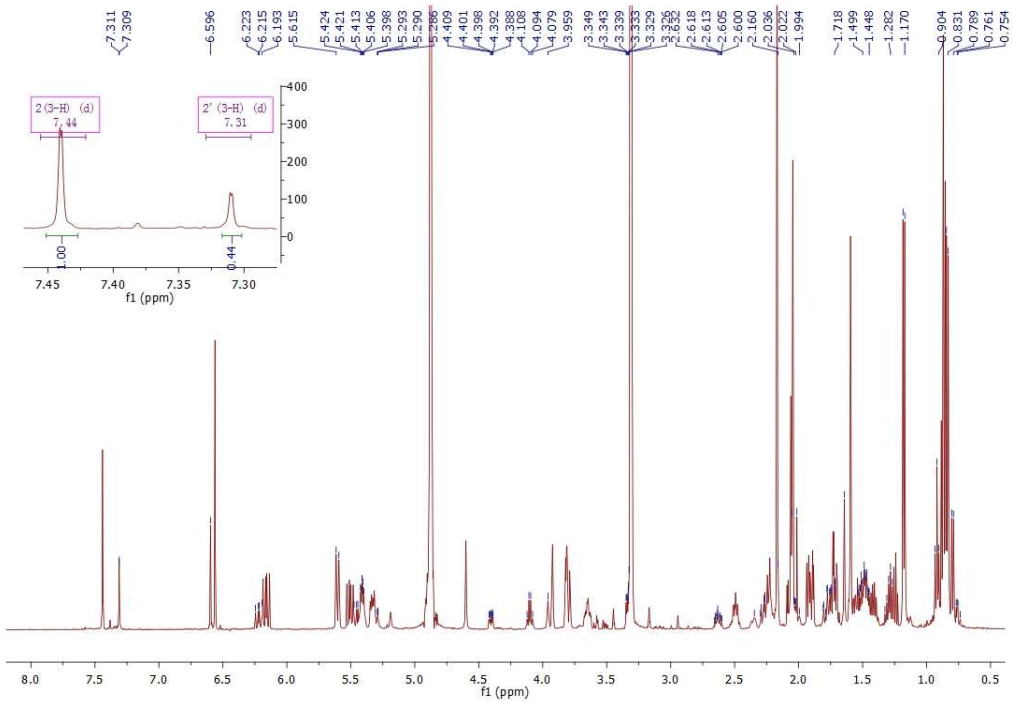

B

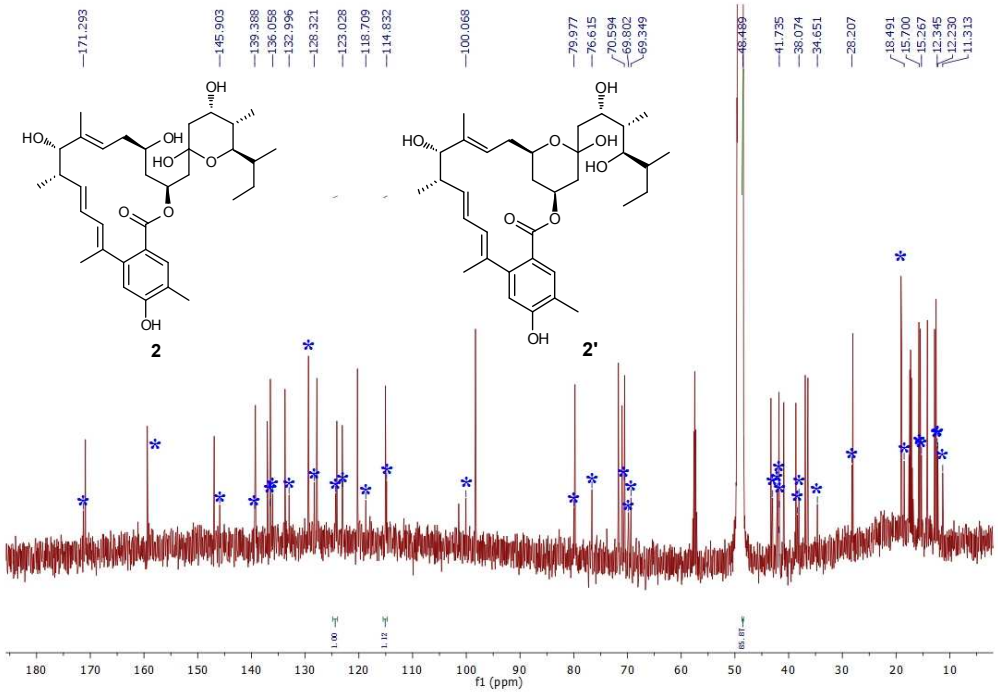

C

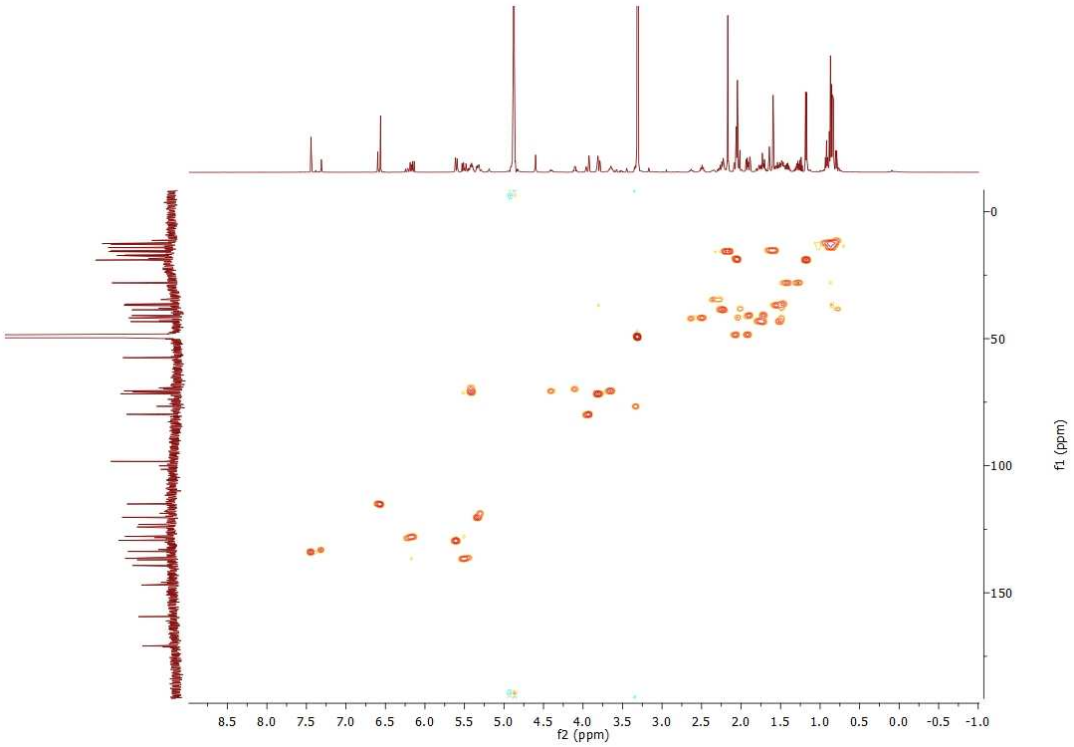
0
50
100
150
f1 (ppm)
8.5 8.0 7.5 7.0 6.5 6.0 5.5 5.0 4.5 4.0 3.5 3.0 2.5 2.0 1.5 1.0 0.5 0.0 -0.5 -1.0
f2 (ppm)

D

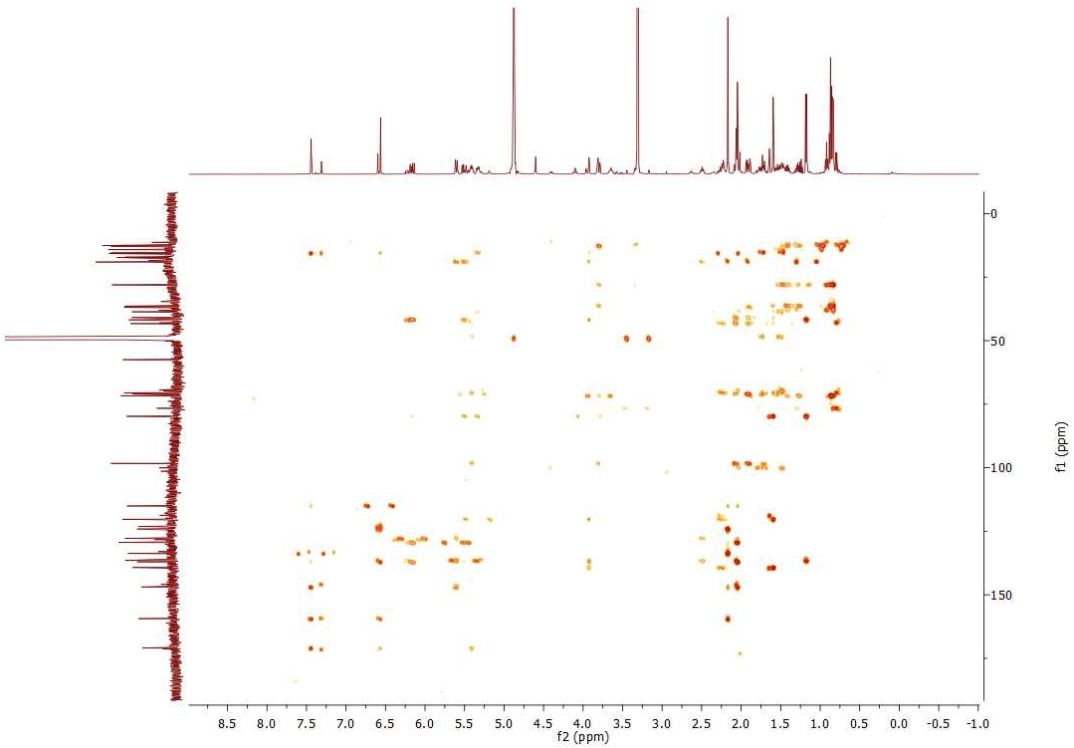
0
50
100
150
f1 (ppm)
8.5 8.0 7.5 7.0 6.5 6.0 5.5 5.0 4.5 4.0 3.5 3.0 2.5 2.0 1.5 1.0 0.5 0.0 -0.5 -1.0
f2 (ppm)

E

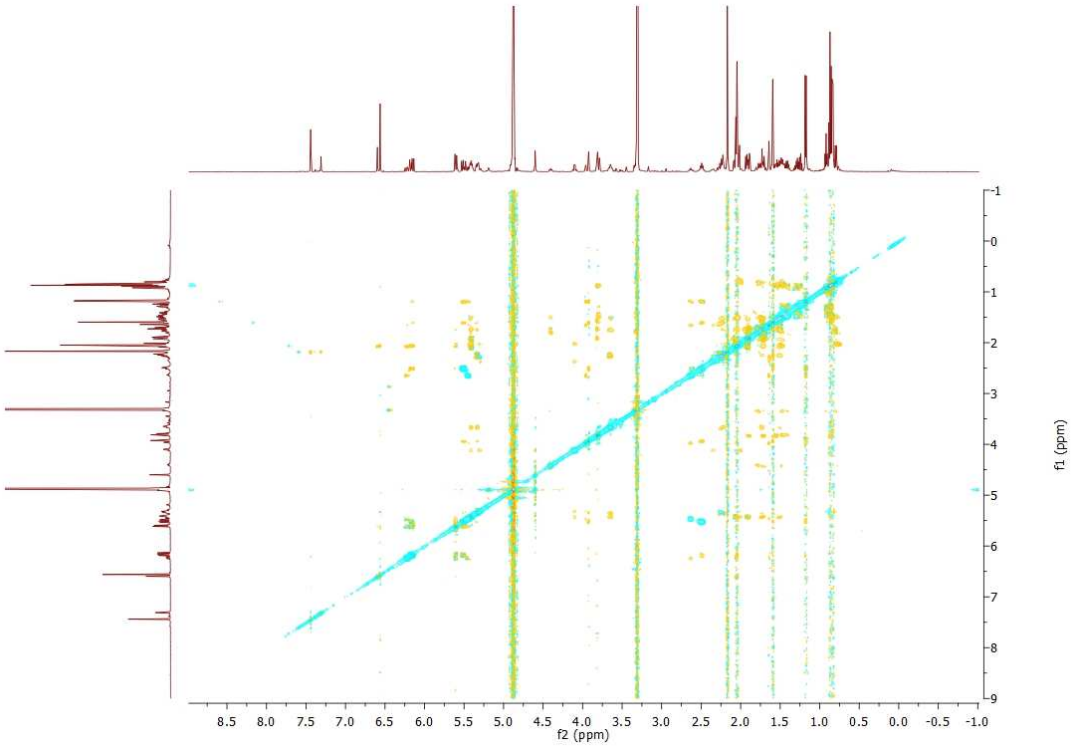

Fig. S9. NMR spectra of compound **4**. (A) ^{1}H spectrum in acetone-d_6. (B) ^{13}C spectrum in acetone-d_6. (C) ^{13}C spectrum in methanol-d_4.

A

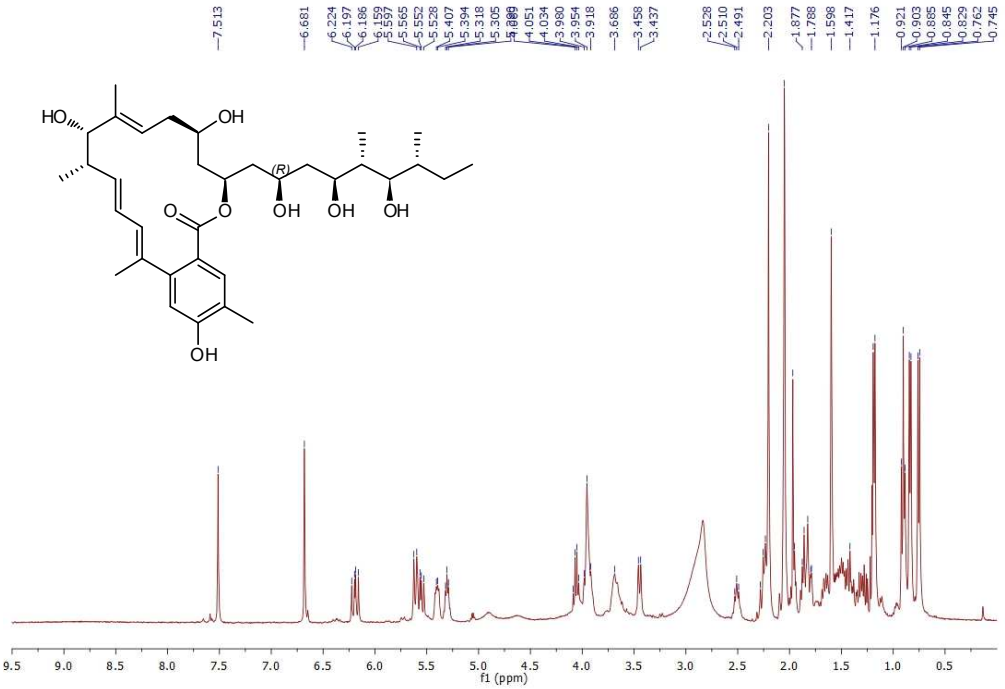

B

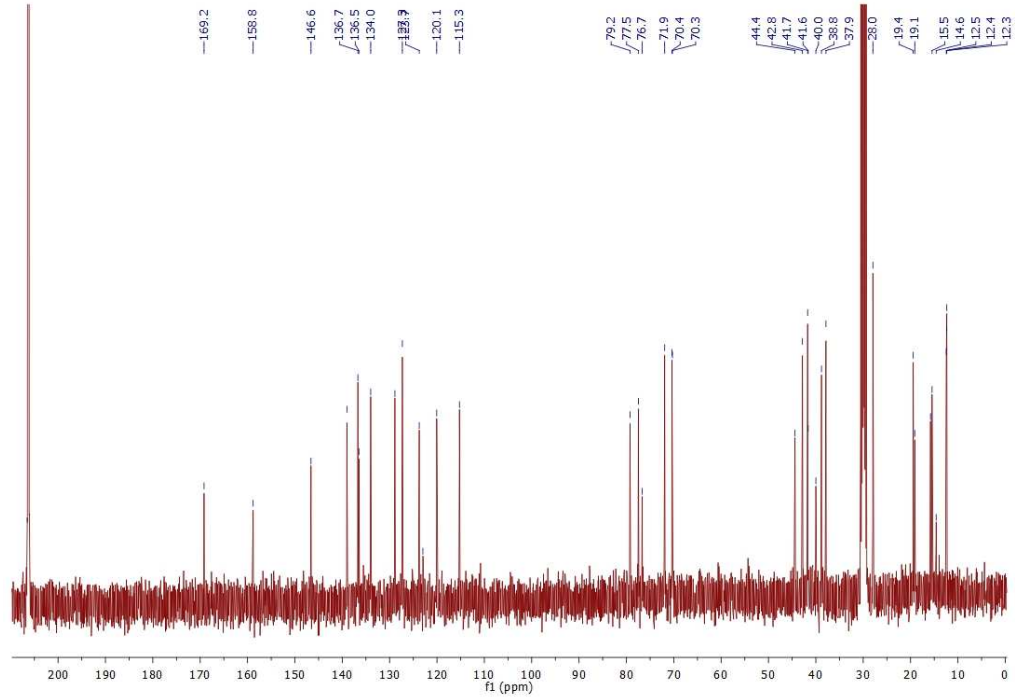

C

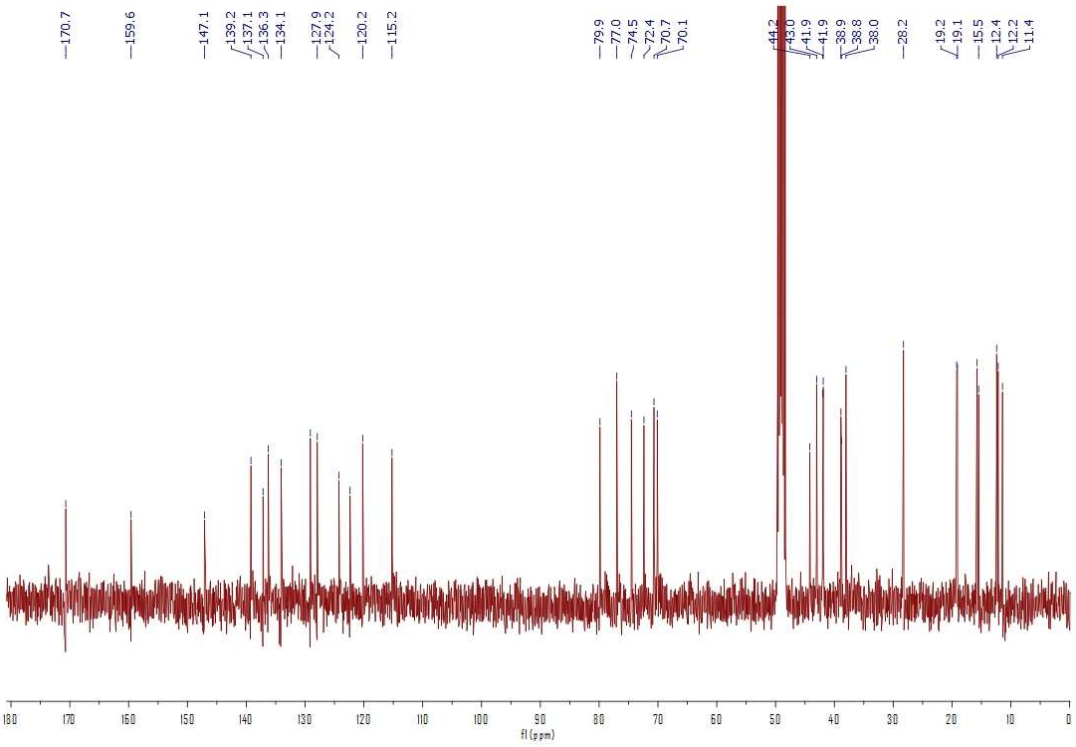
170.7
159.6
147.1
139.2
137.1
136.3
134.1
127.9
124.2
120.2
115.2
79.9
77.0
74.5
72.4
70.7
70.1
44.2
43.0
41.9
41.9
38.9
38.8
38.0
28.2
19.2
19.1
15.5
12.4
12.2
11.4
180
170
160
150
140
130
120
110
100
90
80
70
60
50
40
30
20
10
0
f1 (ppm)

Fig. S10. NMR spectra of compound **4'**. (A) ^{1}H spectrum in acetone-d_6. (B) ^{13}C spectrum in acetone-d_6. (C) ^{13}C spectrum in methanol-d_4.

A

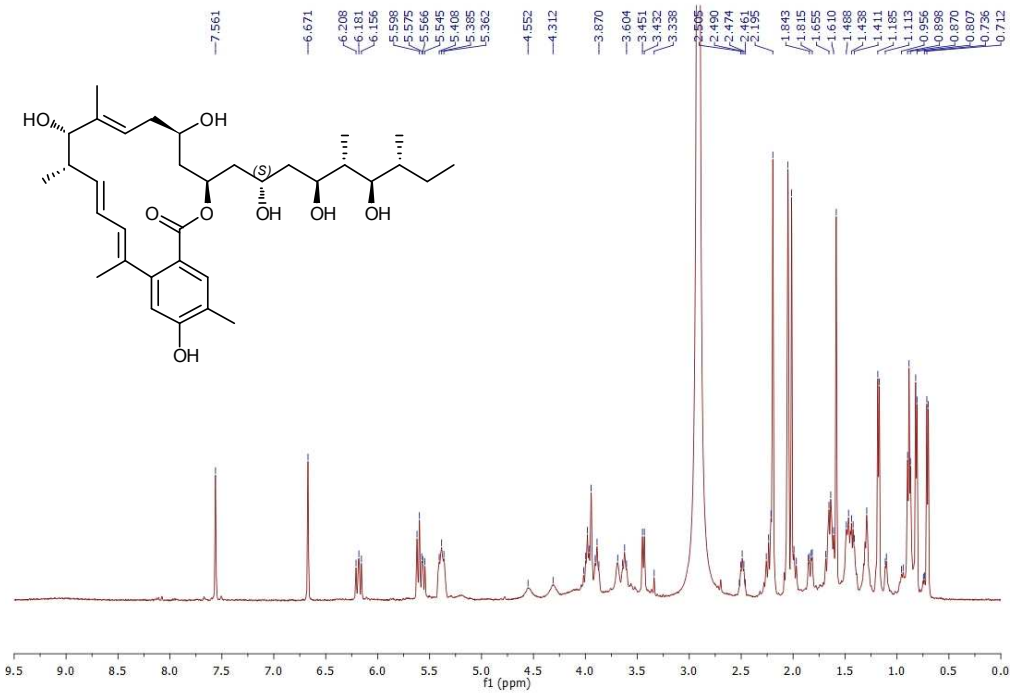

B

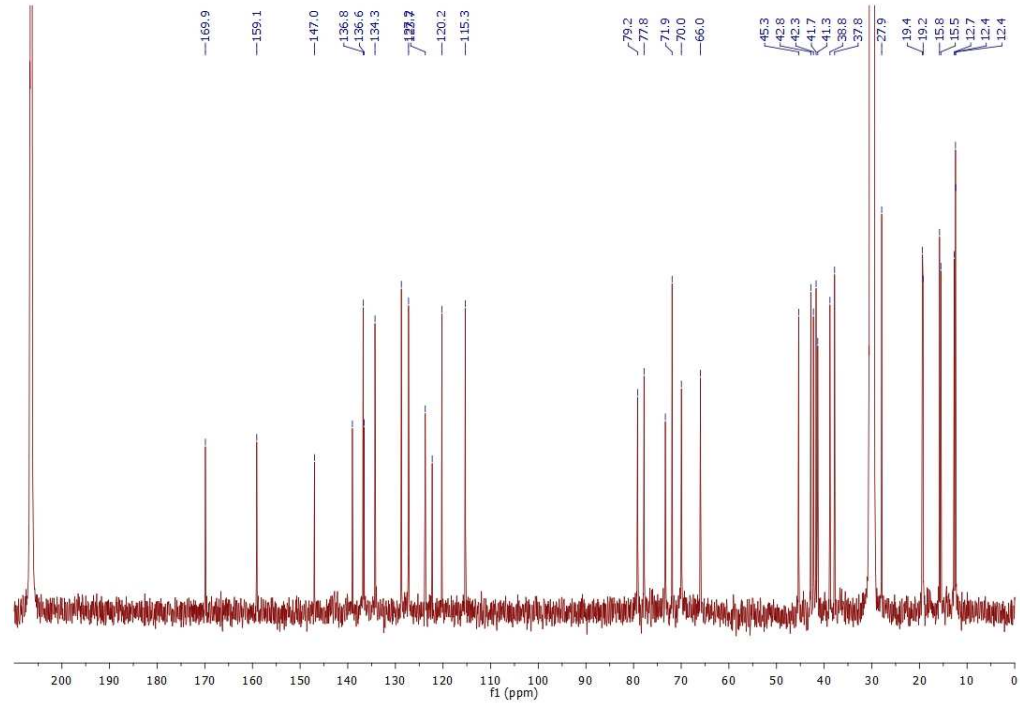

C

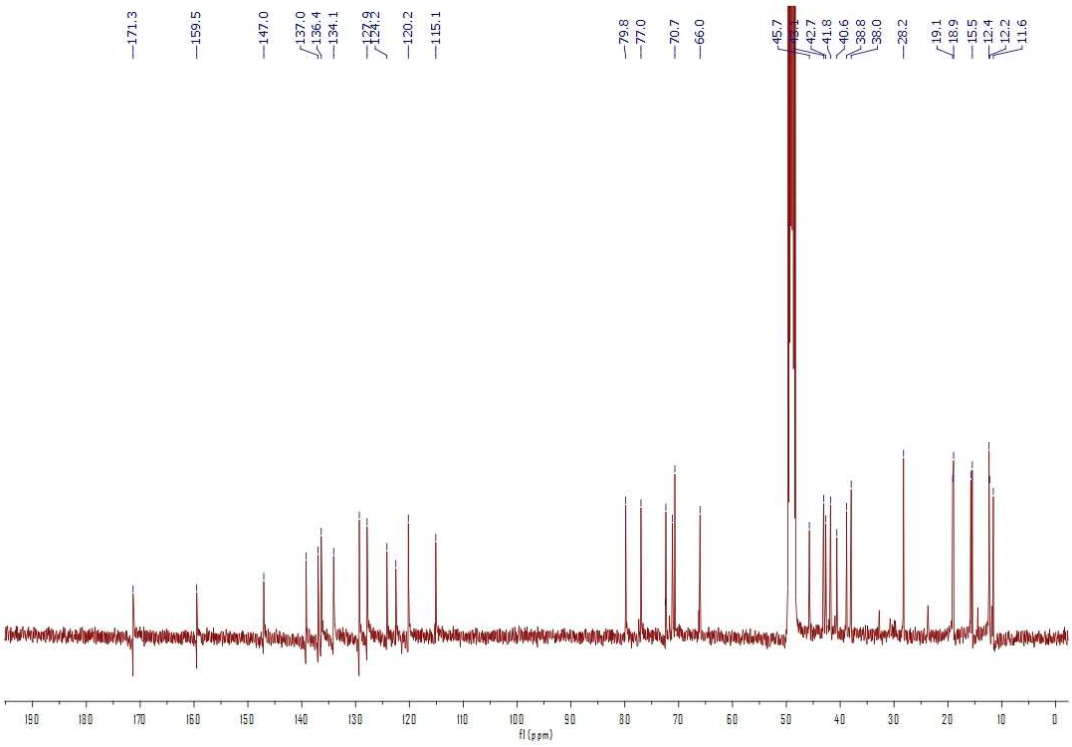
171.3
159.5
147.0
137.0
136.4
134.1
127.9
124.2
120.2
115.1
79.8
77.0
70.7
66.0
45.7
42.7
41.8
40.6
38.8
38.0
28.2
19.1
18.9
15.5
12.4
12.2
11.6
f1 (ppm)

Fig. S11. NMR spectra of compound **5**. (A) ^{1}H spectrum. (B) ^{13}C spectrum. (C) HMQC spectrum. (D) HMBC spectrum. (E) NOESY spectrum.

A

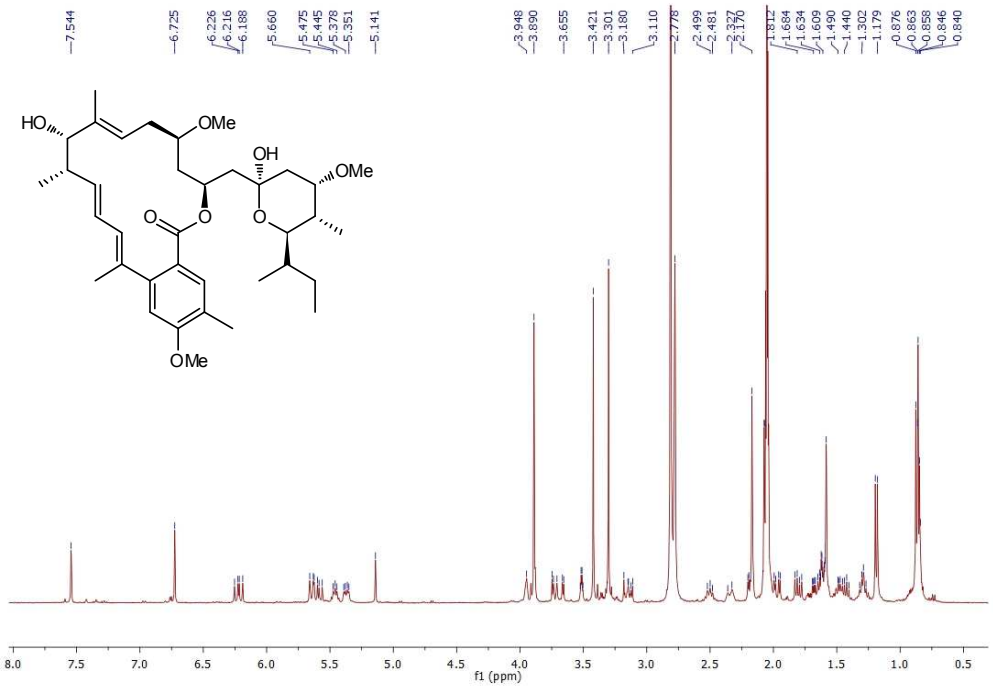

B

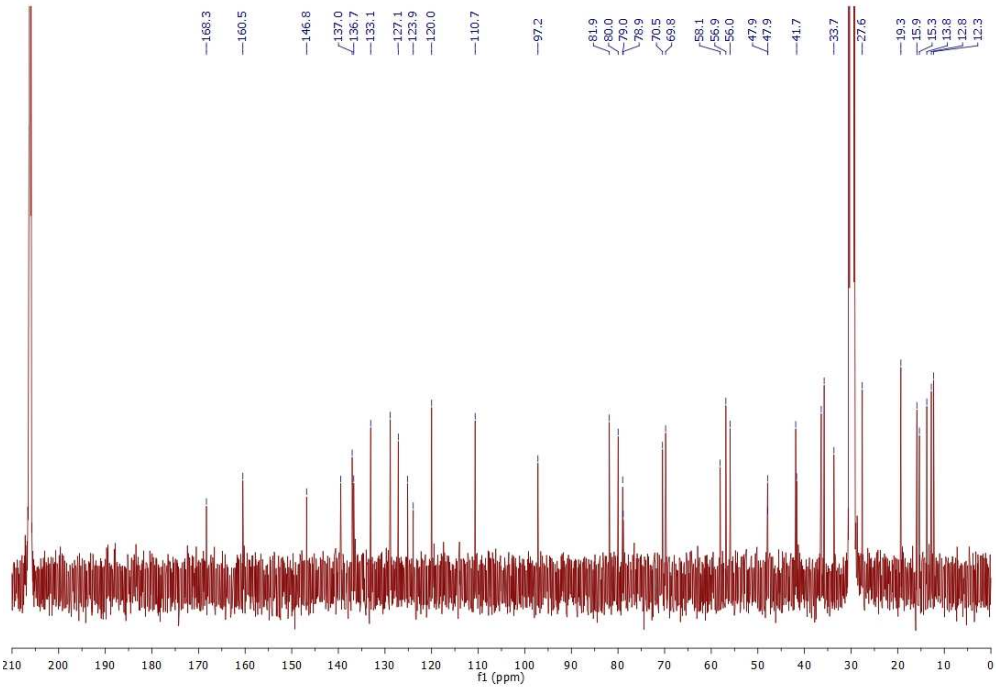

C

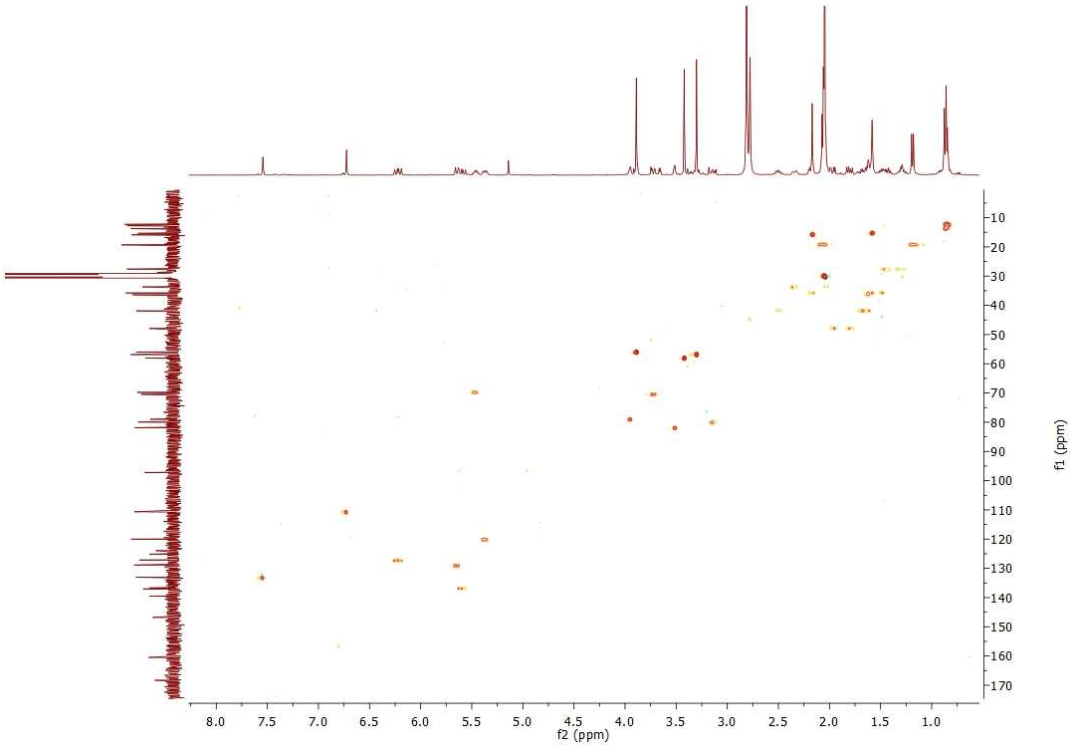

D

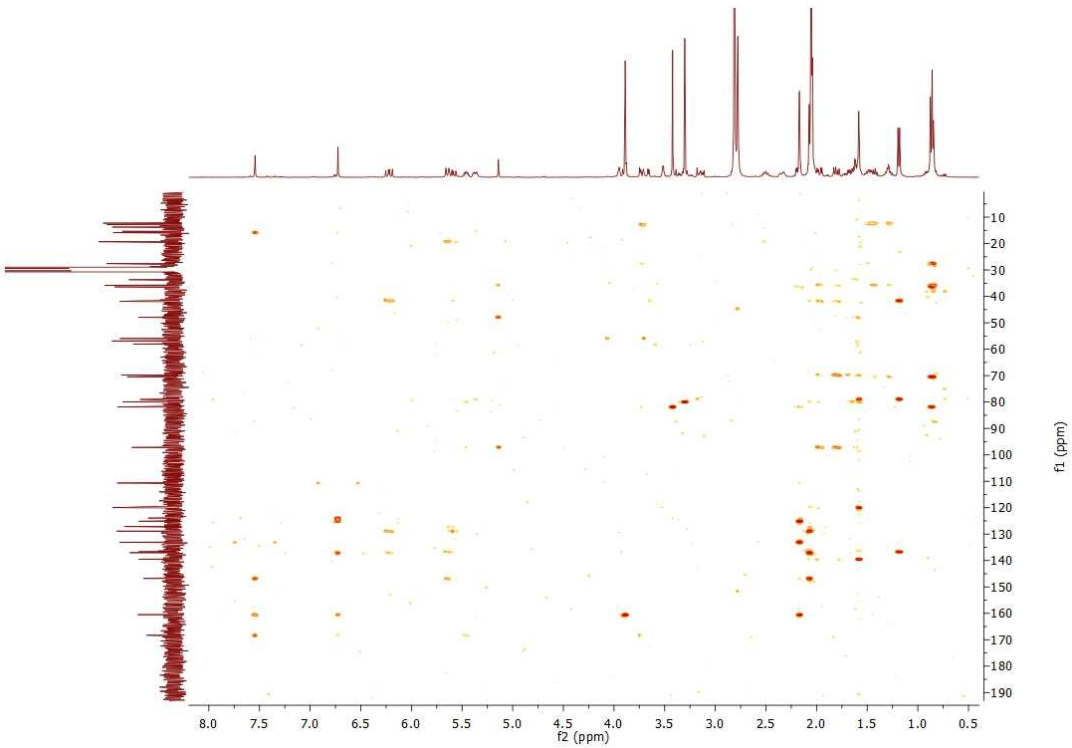

E

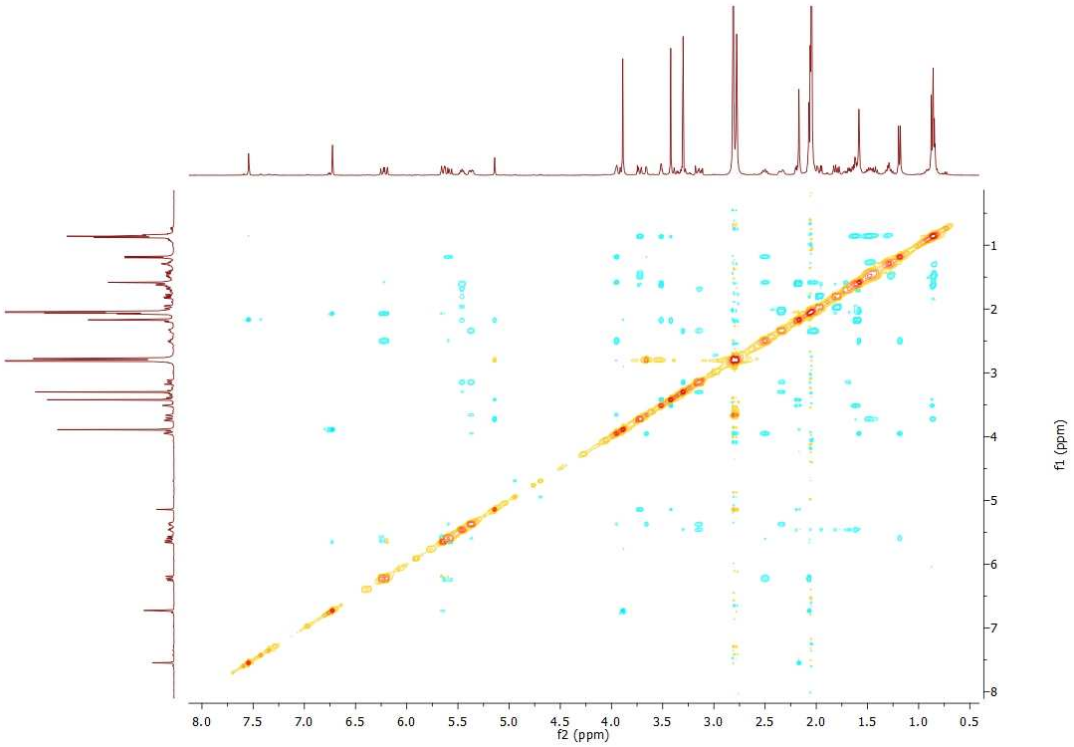
8.0
7.5
7.0
6.5
6.0
5.5
5.0
4.5
4.0
3.5
3.0
2.5
2.0
1.5
1.0
0.5
f2 (ppm)
1
2
3
4
5
6
7
8
f1 (ppm)

Fig. S12. NMR spectra of compound **6**. (A) ^{1}H spectrum. (B) ^{13}C spectrum. (C) HMQC spectrum. (D) HMBC spectrum. (E) NOESY spectrum.

A

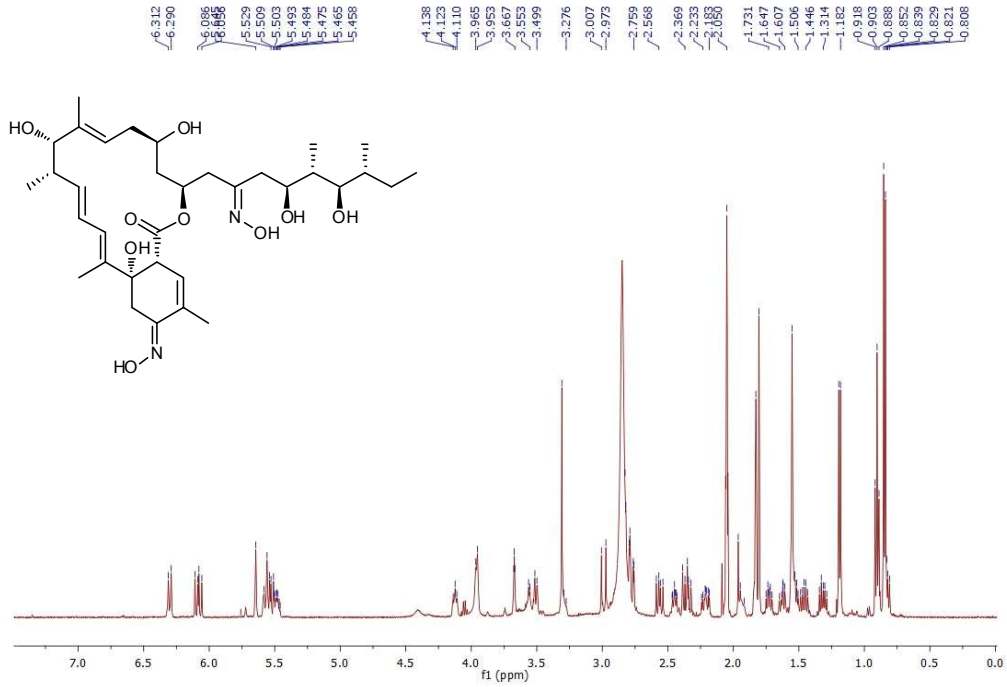

B

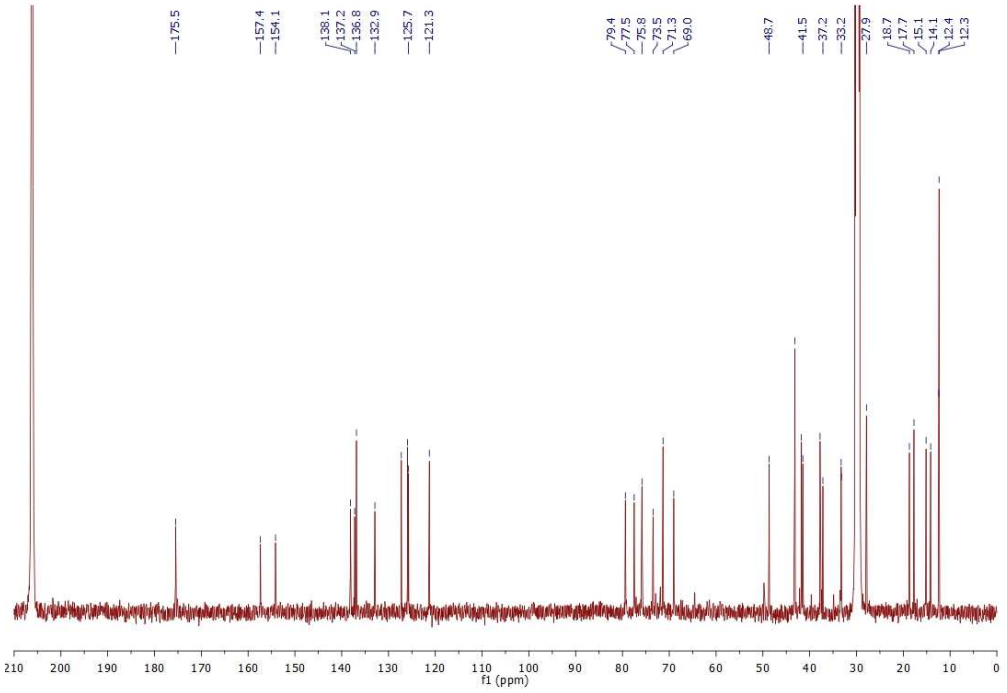

C

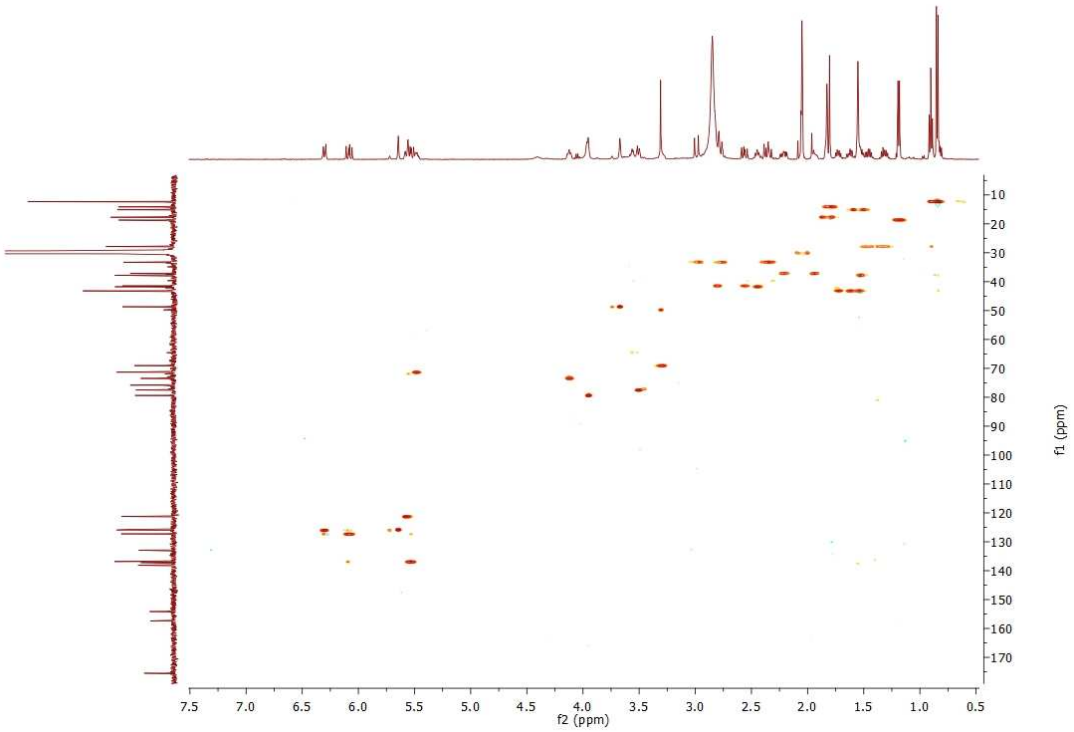

D

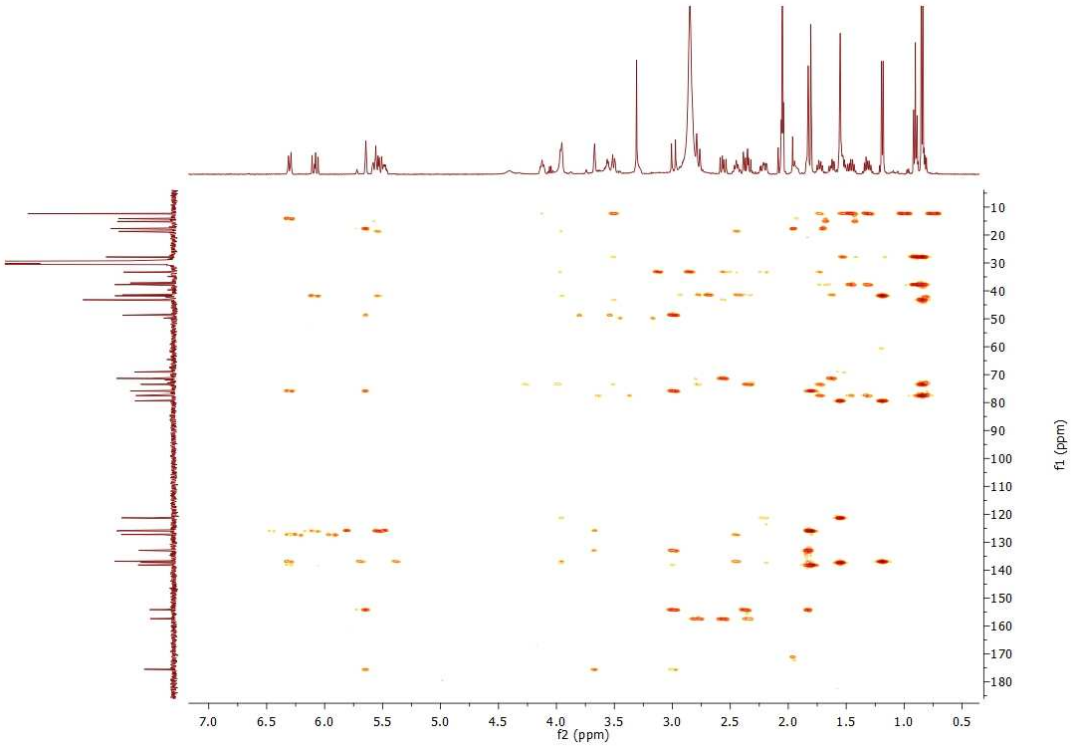

E

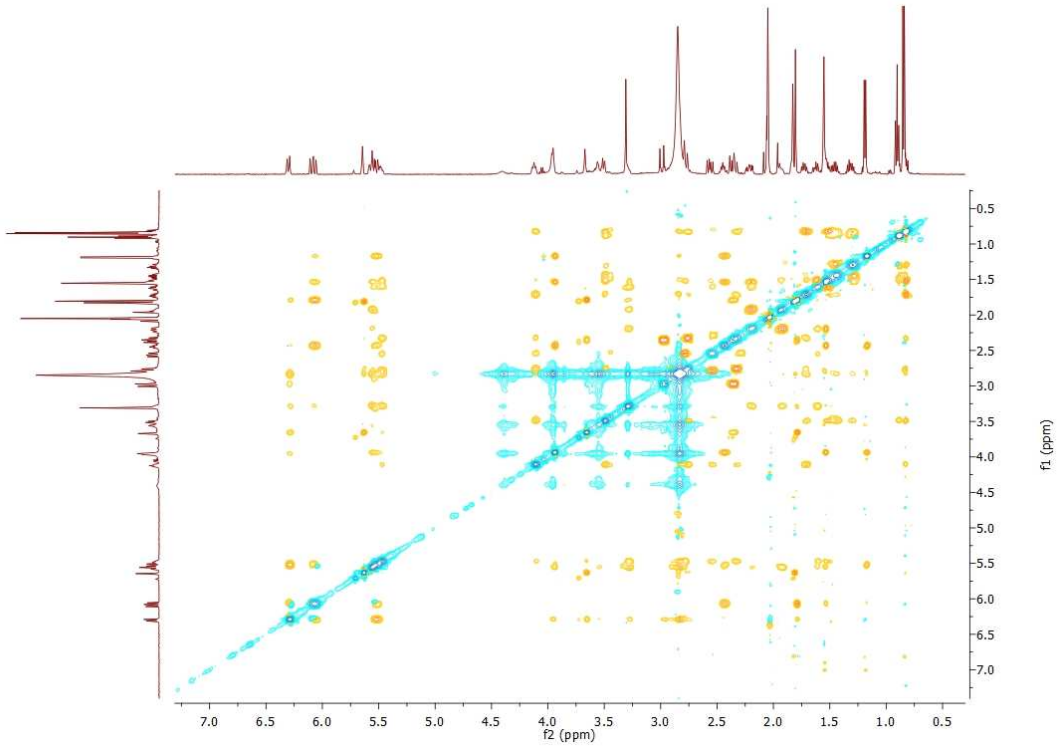

Fig. S13. NMR spectra of compound **6'**. (A) ^{1}H spectrum. (B) ^{13}C spectrum. (C) HMQC spectrum. (D) HMBC spectrum. (E) NOESY spectrum.

A

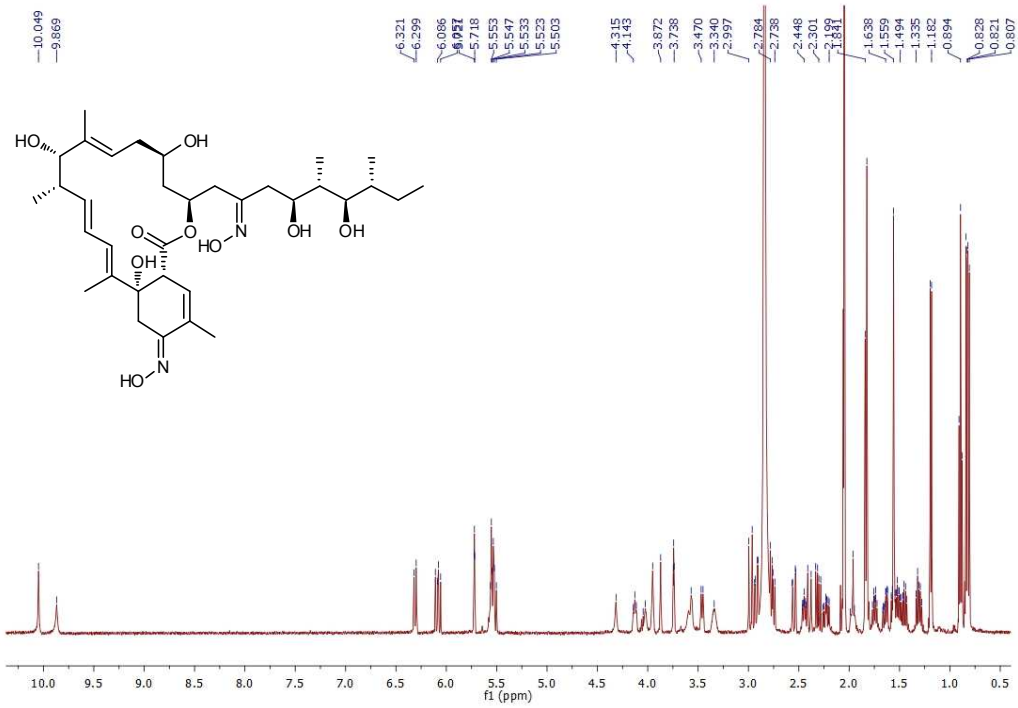

B

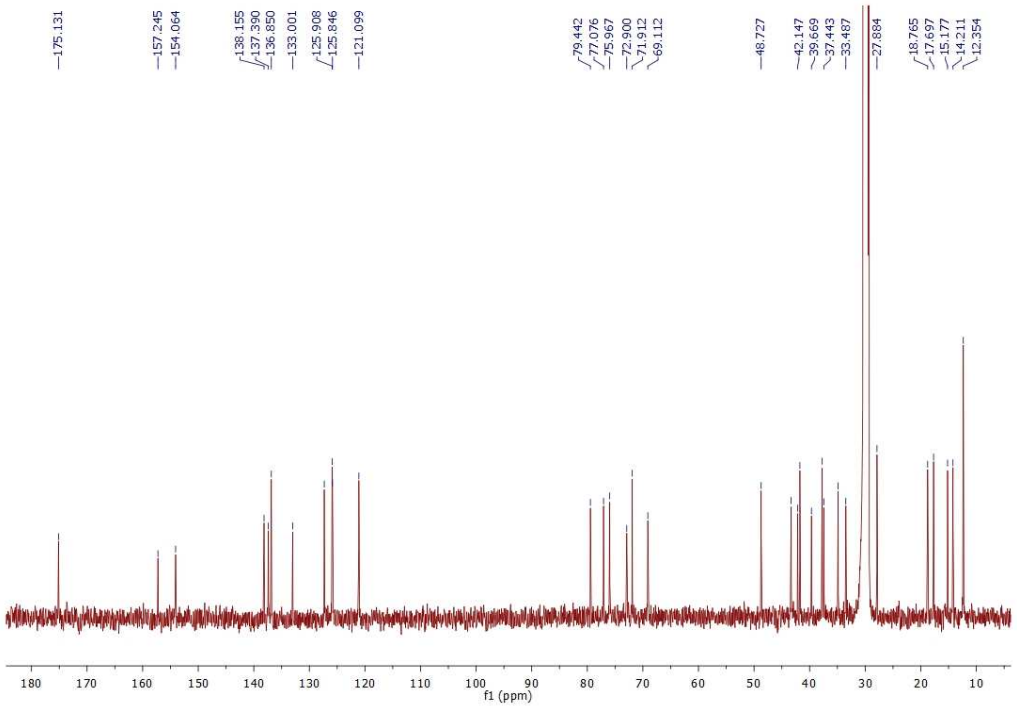

C

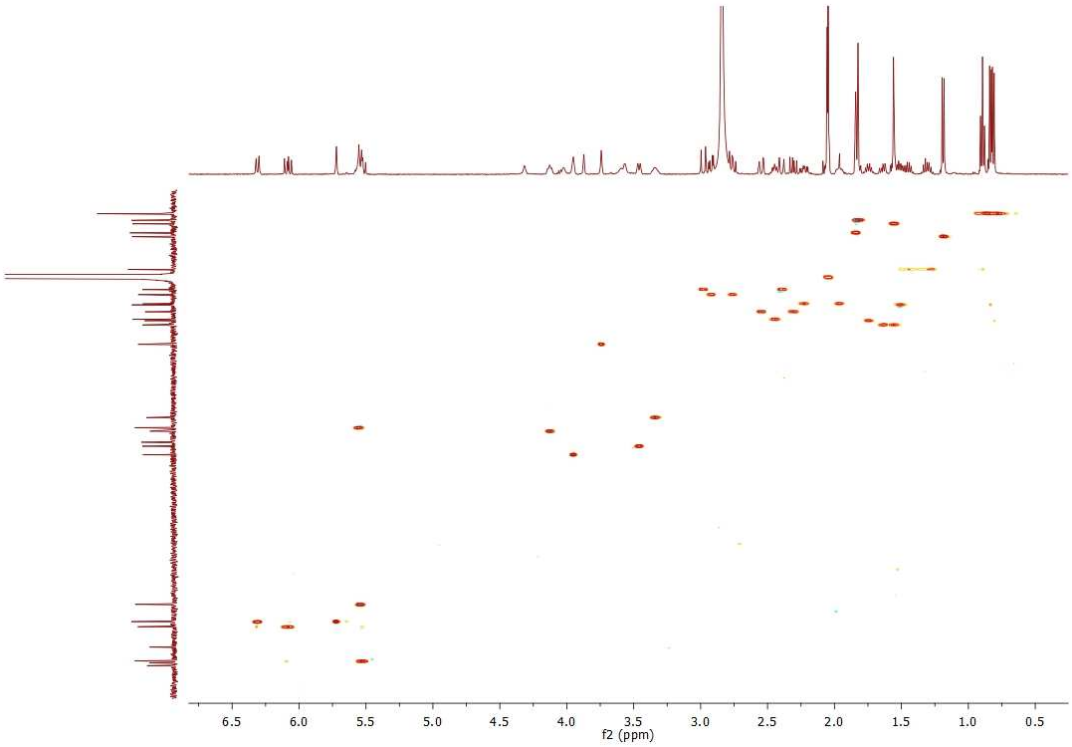
6.5
6.0
5.5
5.0
4.5
4.0
3.5
3.0
2.5
2.0
1.5
1.0
0.5
f2 (ppm)

D

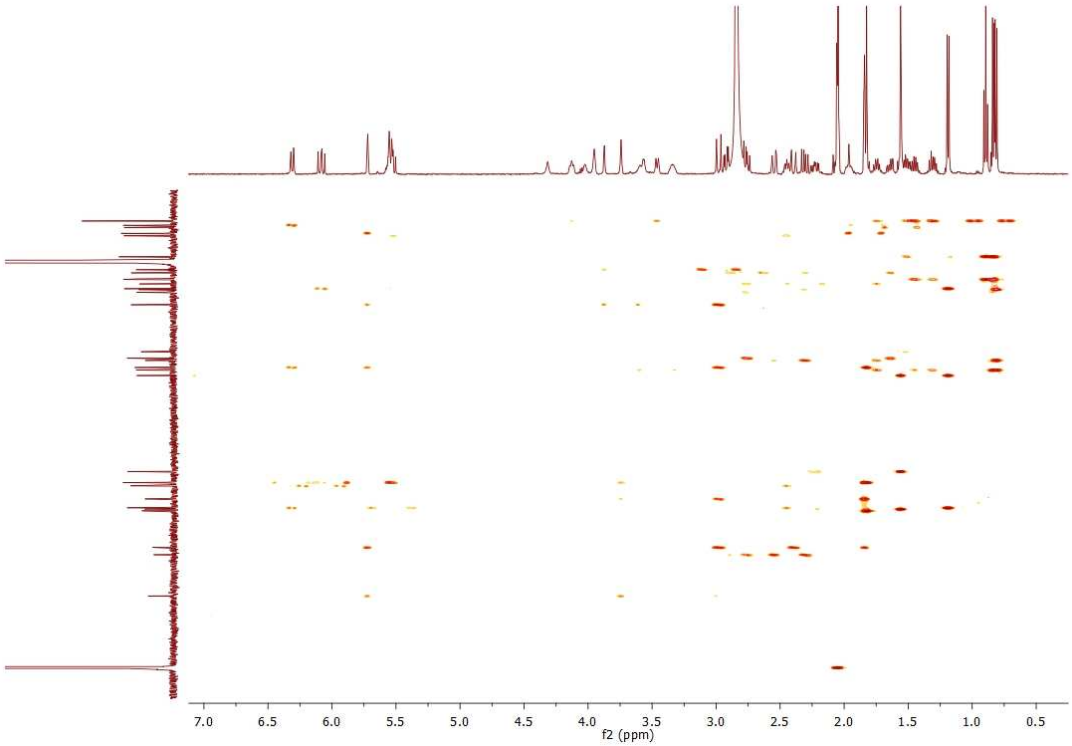
7.0
6.5
6.0
5.5
5.0
4.5
4.0
3.5
3.0
2.5
2.0
1.5
1.0
0.5
f2 (ppm)

E

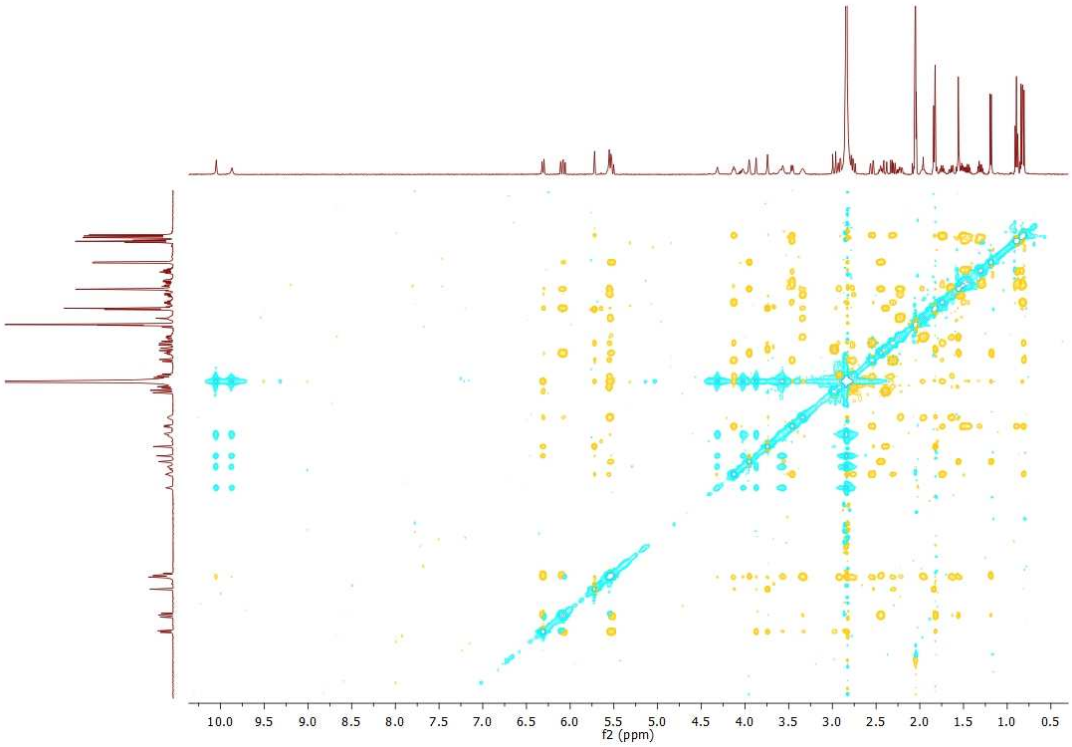

Fig. S14. NMR spectra of compound **7**. (A) ^{1}H spectrum. (B) ^{13}C spectrum. (C) HMQC spectrum. (D) HMBC spectrum. (E) NOESY spectrum.

A

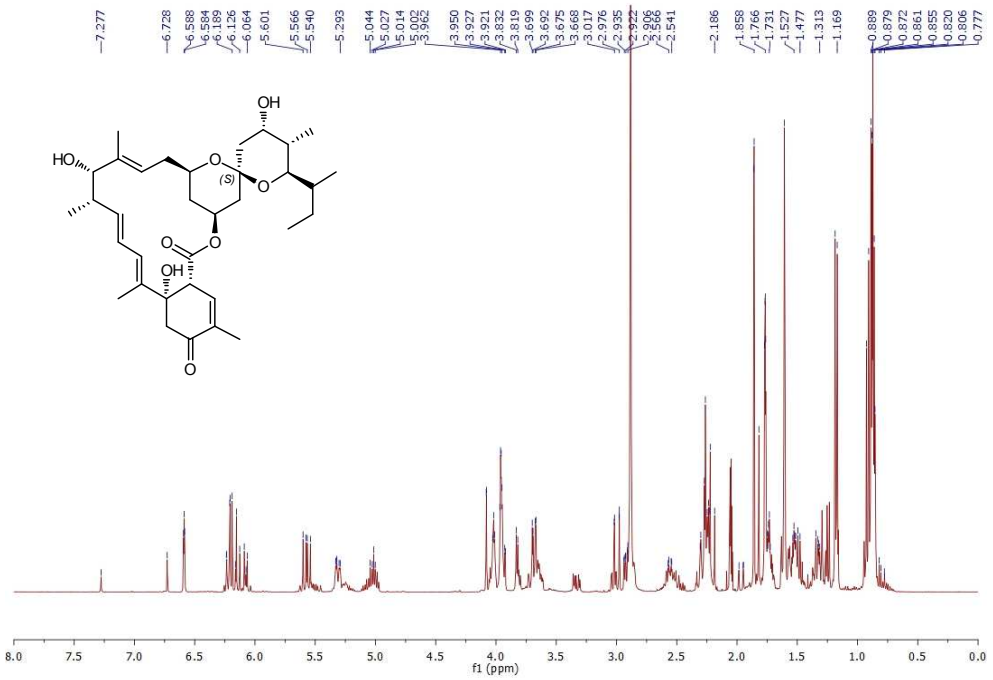

B

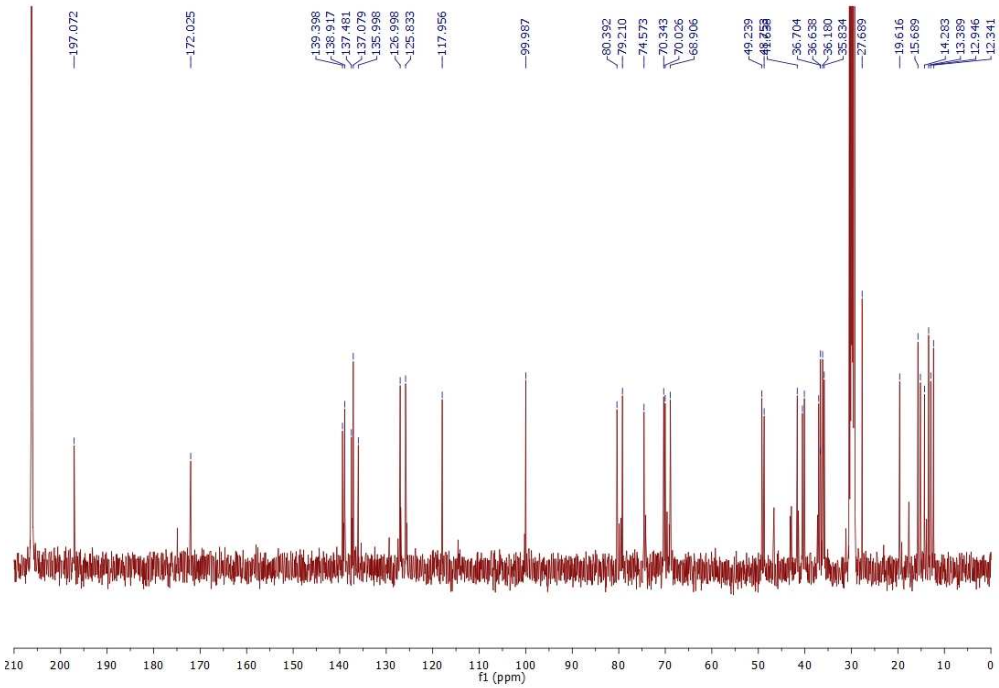

C

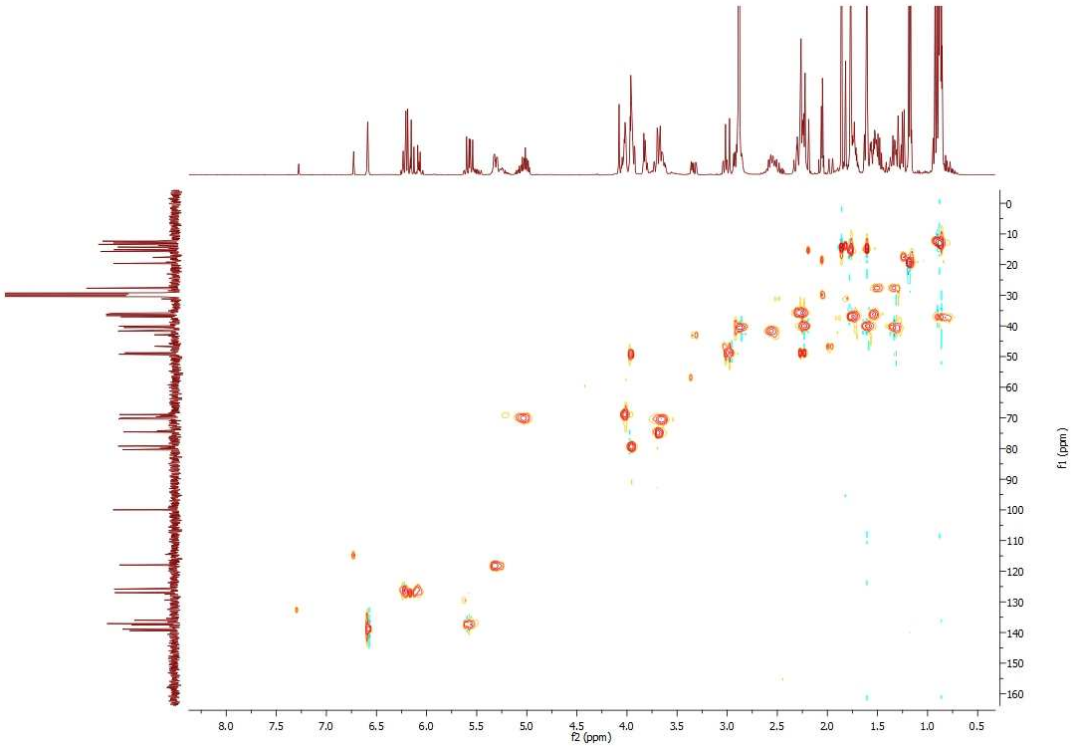

D

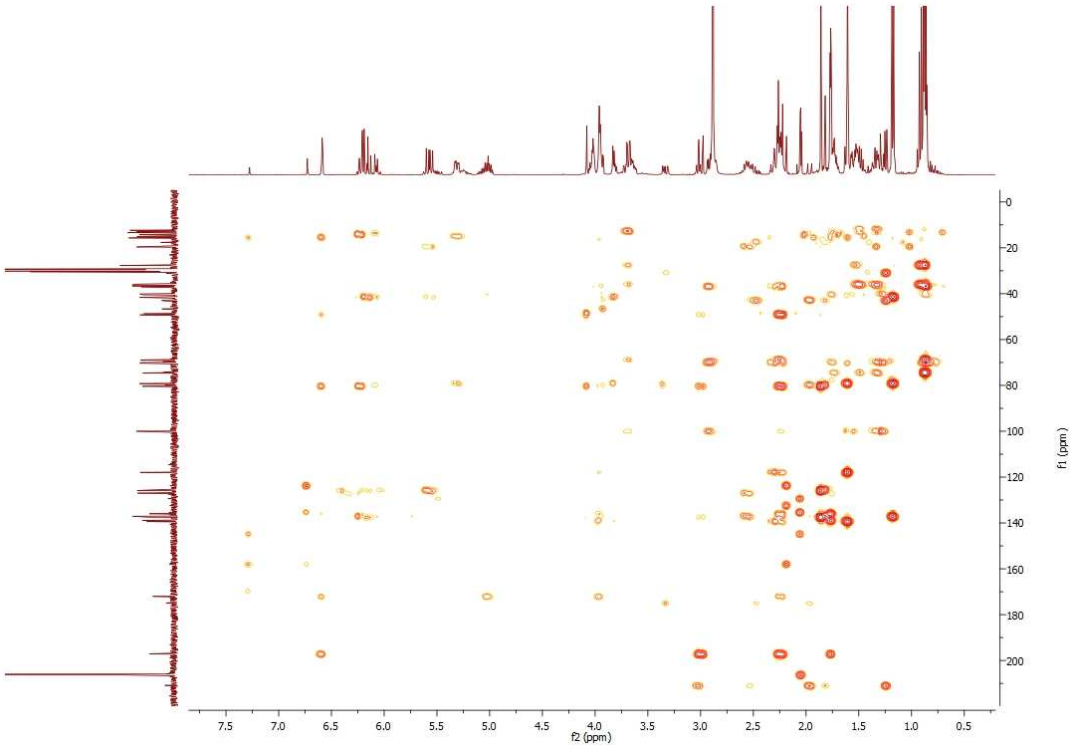

E

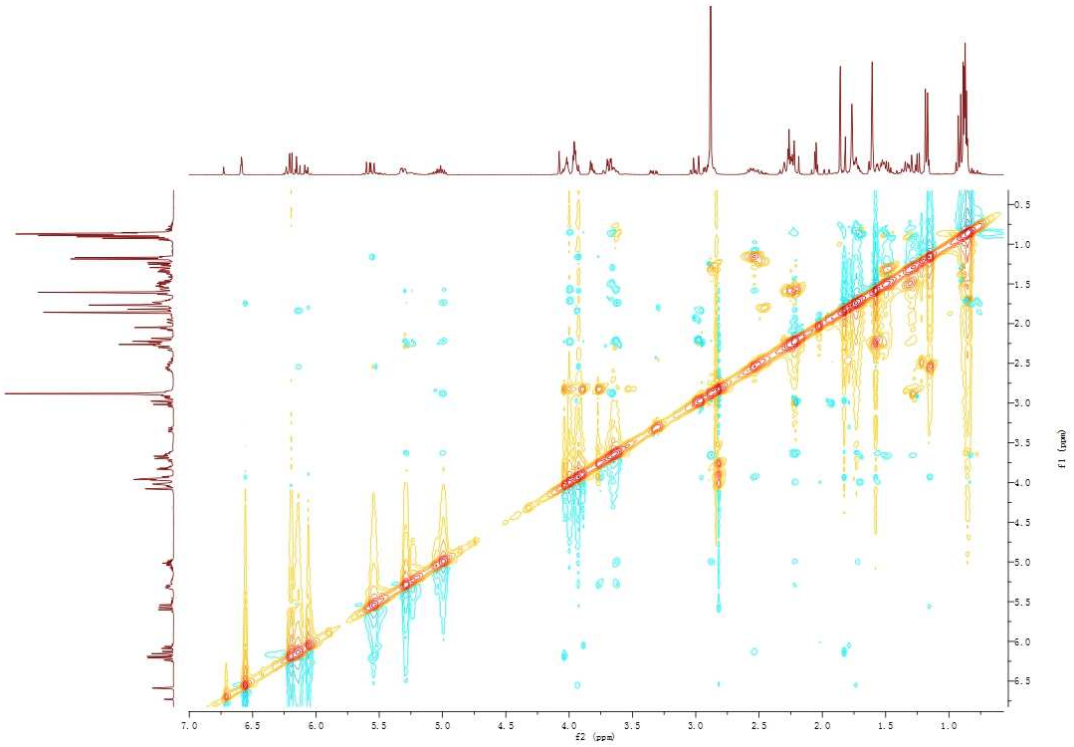
7.0
6.5
6.0
5.5
5.0
4.5
4.0
3.5
3.0
2.5
2.0
1.5
1.0
f2 (ppm)
0.5
1.0
1.5
2.0
2.5
3.0
3.5
4.0
4.5
5.0
5.5
6.0
6.5
f1 (ppm)

Fig. S15. NMR spectra of compound **7'**. (A) ^{1}H spectrum. (B) ^{13}C spectrum. (C) HMQC spectrum. (D) HMBC spectrum. (E) NOESY spectrum.

A

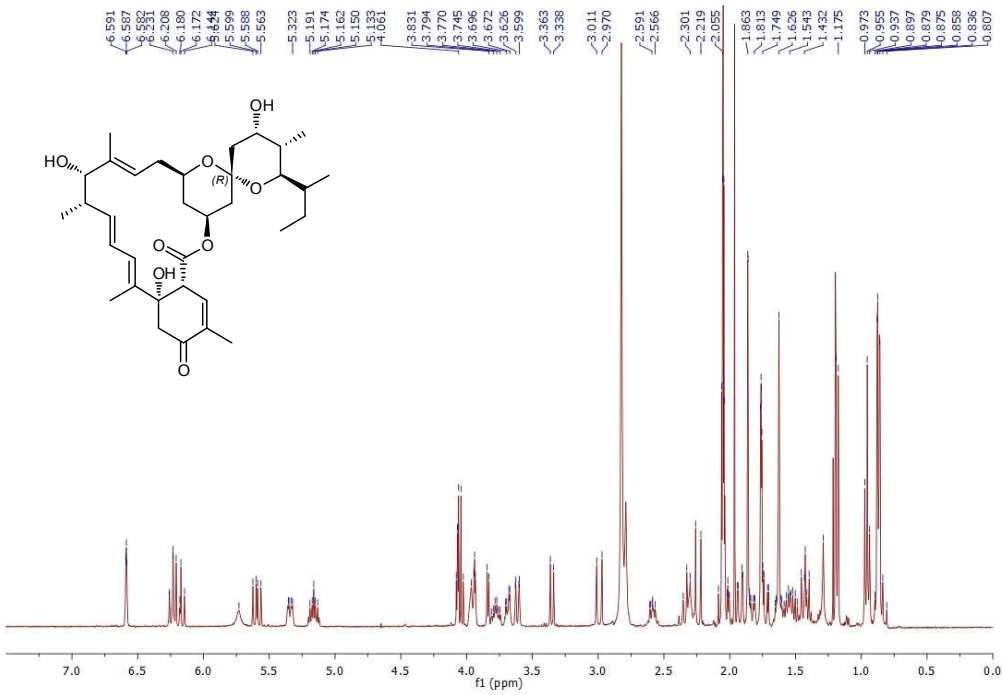

B

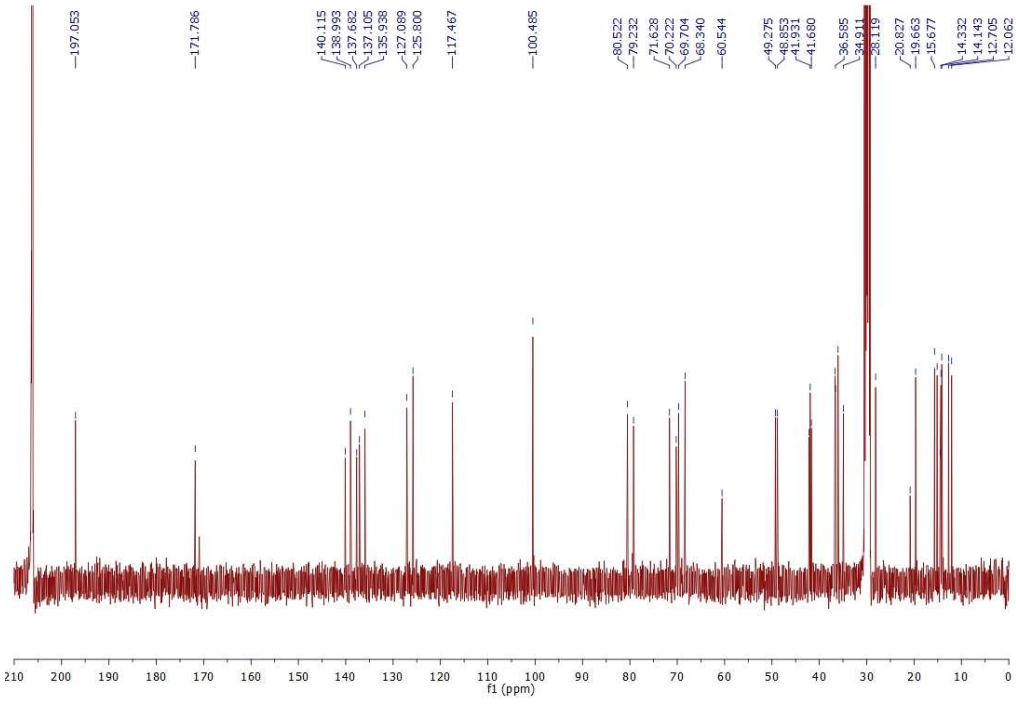

C

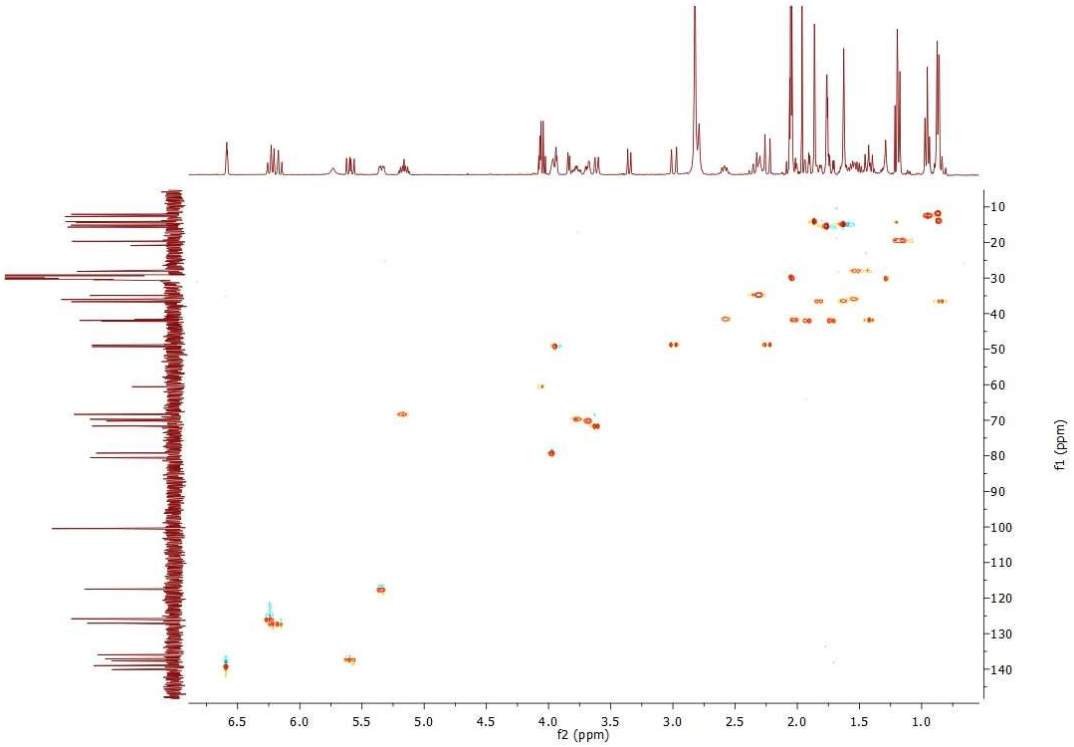

D

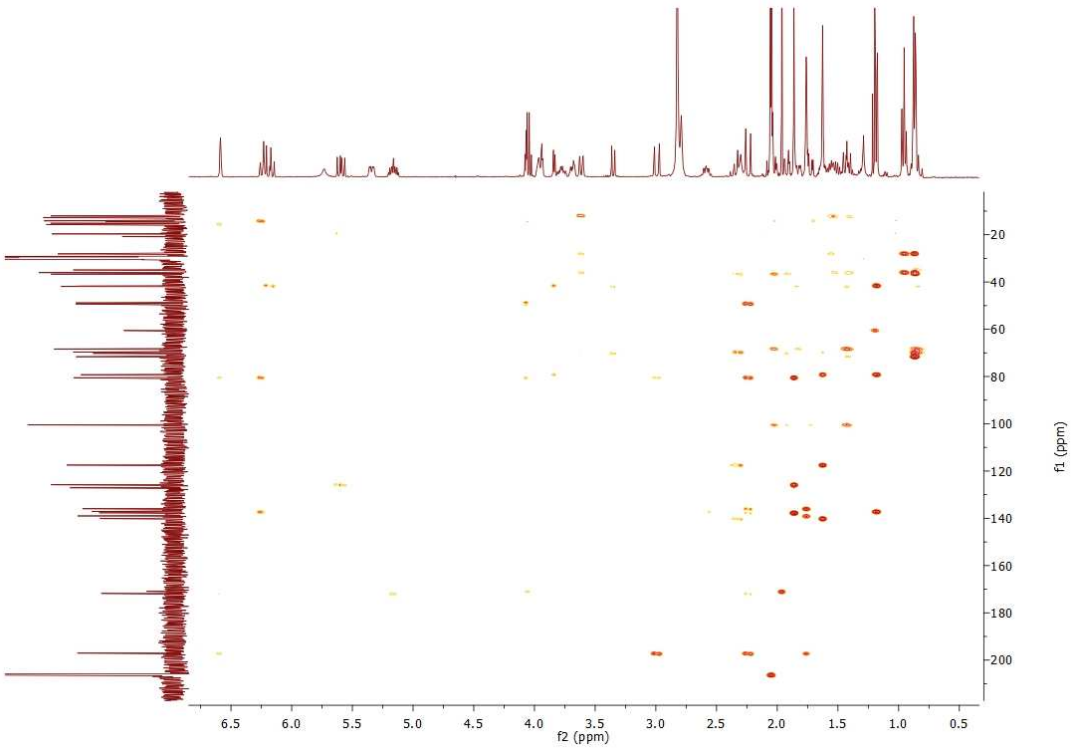

E

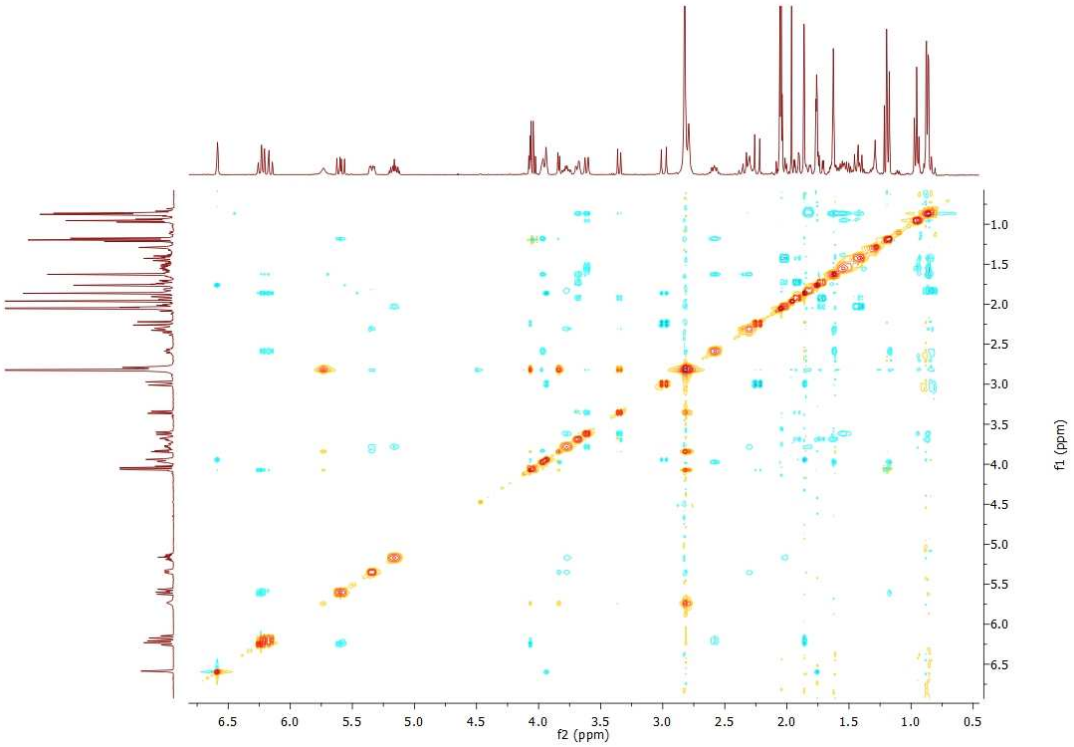

Fig. S16. NMR spectra of compound **8**. (A) ^{1}H spectrum. (B) ^{13}C spectrum. (C) HMQC spectrum. (D) NOESY spectrum.

A

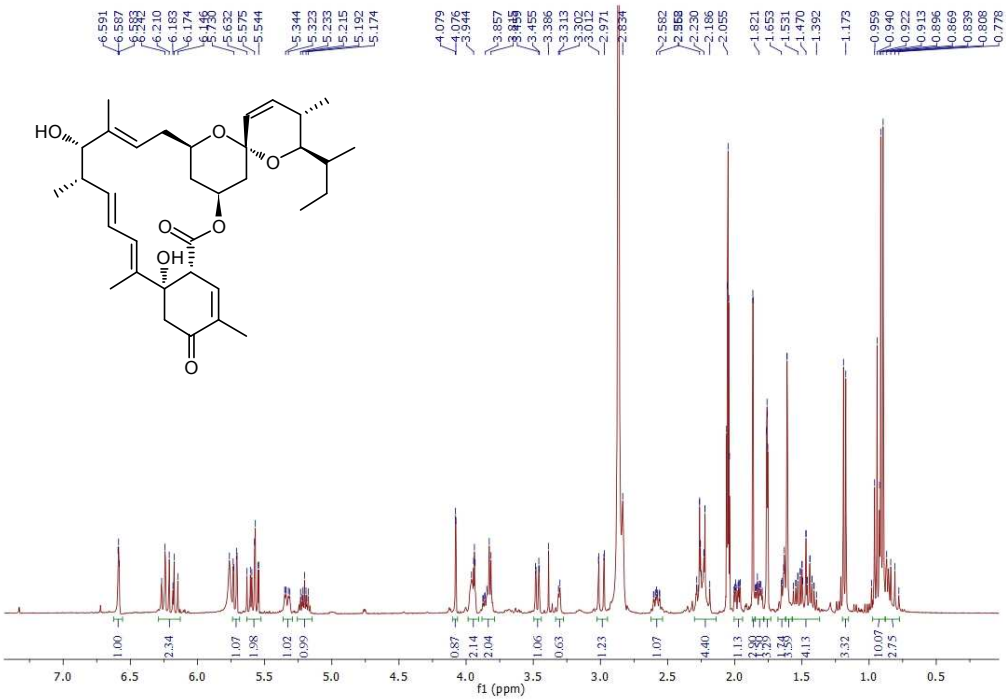

B

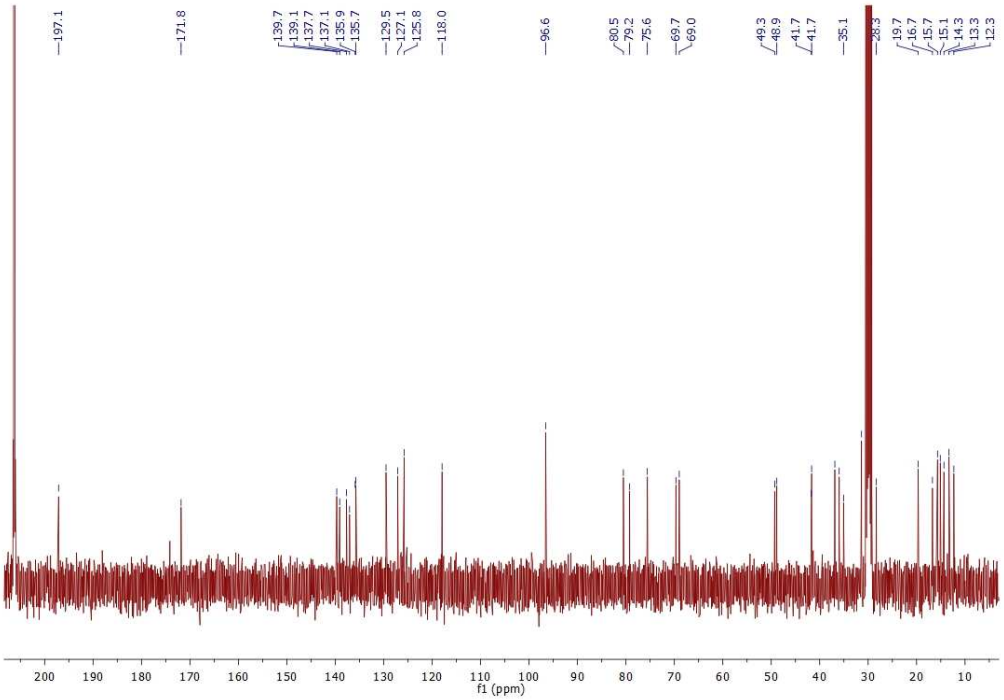

C

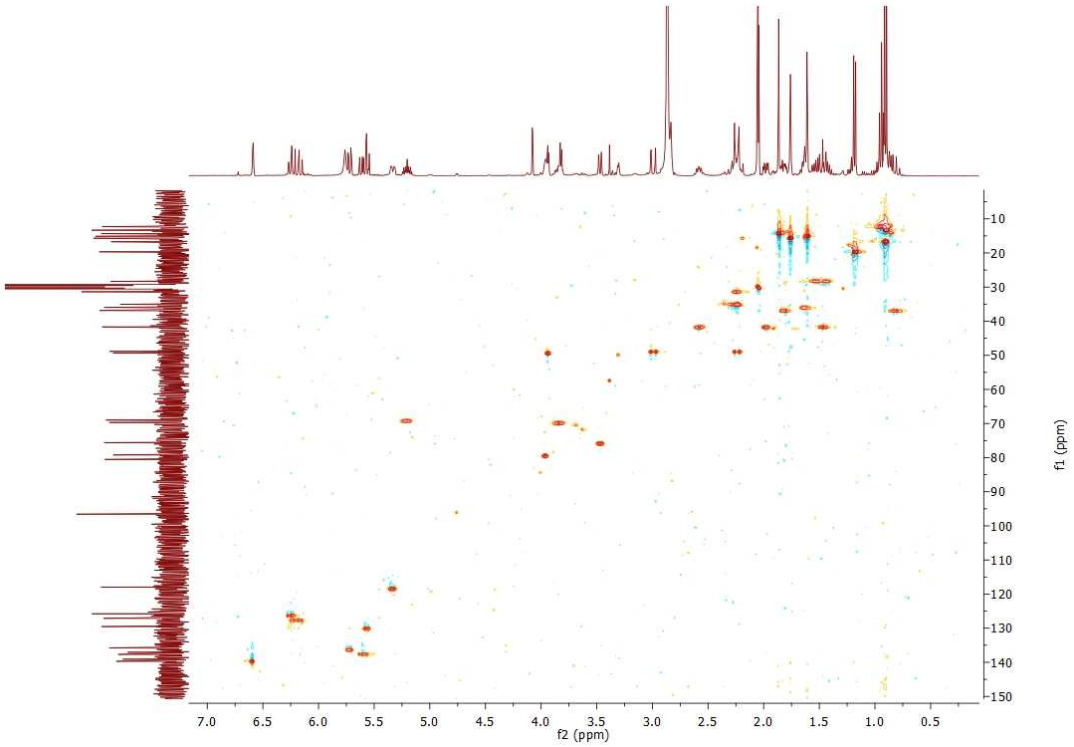

D

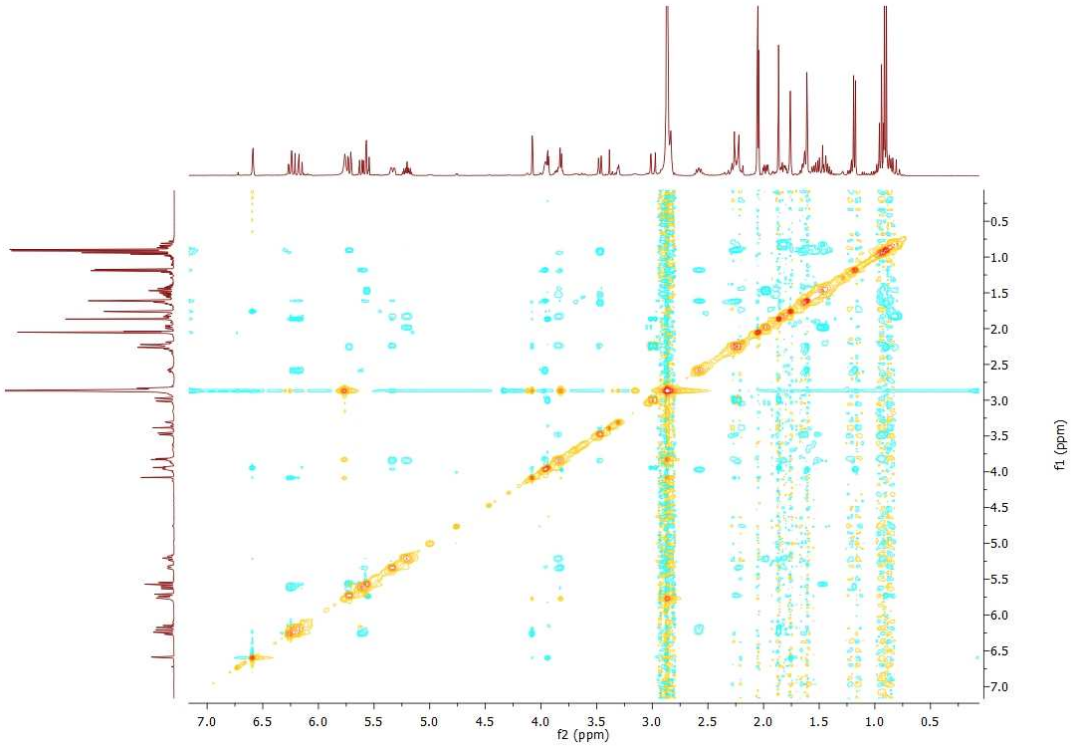

Fig. S17. Stereoisomerization between **1** and **1'**. I, 1.0 mg/mL of **1** in MeOH; II, 1.0 mg/mL of **1'** in MeOH; III, 1.0 mg/mL of **1** in MeOH incubated with 1% formic acid (v/v); and IV, 1.0 mg/mL of **1'** in MeOH incubated with 1% formic acid (v/v). The treatment with formic acid was performed at 25 °C for 2 h.

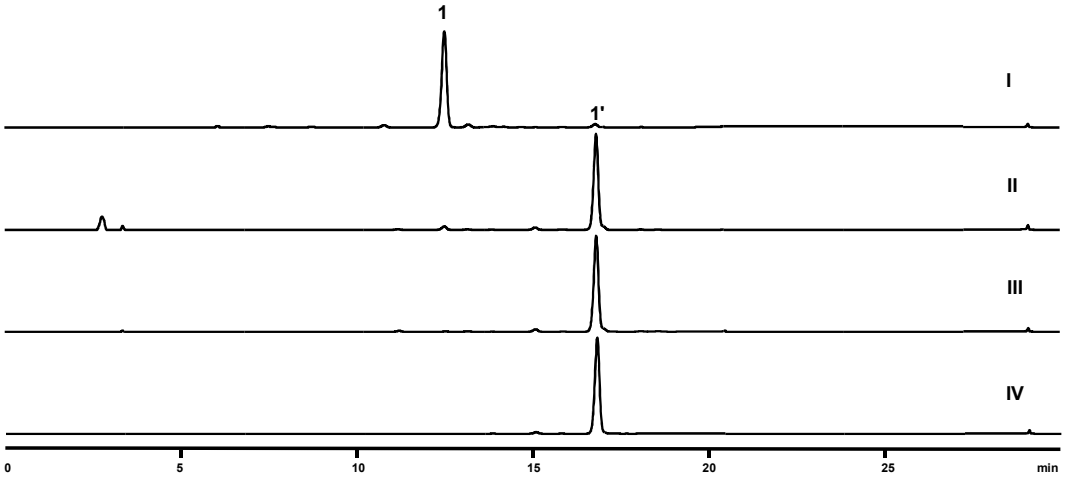

Supplementary References

(1) Kieser, T.; Bibb, M. J.; Buttner, M. J.; Chater, K. F.; Hopwood, D. A., *Practical Streptomyces Genetics*. The John Innes Foundation: Colney, Norwich, U.K., 2000.

(2) R. Blakemore, P.; J. Kocienski, P.; Morley, A.; Muir, K. *J. Chem. Soc. Perkin T. 1* **1999**, 955.

(3) Tsukamoto, Y.; Sato, K.; Mio, S.; Sugai, S.; Yanai, T.; Kitano, N.; Muramatsu, S.; Nakada, Y.; Ide, J. *Agric. Biol. Chem.* **1991**, *55*, 2615.

(4) Albers-Schoenberg, G.; Arison, B. H.; Chabala, J. C.; Douglas, A. W.; Eskola, P.; Fisher, M. H.; Lusi, A.; Mrozik, H.; Smith, J. L.; Tolman, R. L. *J. Am. Chem. Soc.* **1981**, *103*, 4216.

(5) Wang, M.; Yang, X.-H.; Wang, J.-D.; Wang, X.-J.; Chen, Z.-J.; Xiang, W.-S. *J. Antibiot.* **2009**, *62*, 587.

(6) Pang, C. H.; Matsuzaki, K.; Ikeda, H.; Tanaka, H.; Ōmura, S. *J. Antibiot.* **1995**, *48*, 59.

(7) Kobayashi, Y.; Tan, C.-H.; Kishi, Y. *Helv. Chim. Acta* **2000**, *83*, 2562.

(8) Hawkes, G. E.; Herwig, K.; Roberts, J. D. *J. Org. Chem.* **1974**, *39*, 1017.

(9) (a) Goegelman, R. T.; Gullo, V. P.; Kaplan, L., Novel C-076 compounds. United States Patent 4,373,358: 1983; (b) Chen, T. S.; Inamine, E. S. *Arch. Biochem. Biophys.* **1989**, *270*, 521.

(10) MacNeil, D. J.; Gewain, K. M.; Ruby, C. L.; Dezeny, G.; Gibbons, P. H.; MacNeil, T. *Gene* **1992**, *111*, 61.

(11) He, Y.; Sun, Y.; Liu, T.; Zhou, X.; Bai, L.; Deng, Z. *Appl. Environ. Microbiol.* **2010**, *76*, 3283.

(12) Qu, X.; Pang, B.; Zhang, Z.; Chen, M.; Wu, Z.; Zhao, Q.; Zhang, Q.; Wang, Y.; Liu, Y.; Liu, W. *J. Am. Chem. Soc.* **2012**, *134*, 9038.

(13) Shen, B.; Hutchinson, C. R. *Proc. Natl. Acad. Sci. USA* **1996**, *93*, 6600.

(14) Qu, X.; Jiang, N.; Xu, F.; Shao, L.; Tang, G.; Wilkinson, B.; Liu, W. *Mol. BioSyst.* **2011**, *7*, 852.